Summer 8-11-2015

# Photoluminescent Silicon Nanoparticles: Fluorescent Cellular Imaging Applications and Photoluminescence (PL) Behavior Study

Sheng-Kuei Chiu
*Portland State University*



Recommended Citation
Chiu, Sheng-Kuei, "Photoluminescent Silicon Nanoparticles: Fluorescent Cellular Imaging Applications and Photoluminescence (PL) Behavior Study" (2015). *Dissertations and Theses.* Paper 2455.
https://doi.org/10.15760/etd.2453

# Photoluminescent Silicon Nanoparticles: Fluorescent Cellular Imaging Applications and Photoluminescence (PL) Behavior Study

by

Sheng-Kuei Chiu

A dissertation submitted in partial fulfillment of the
requirements for the degree of

Doctor of Philosophy
in
Chemistry

Dissertation Committee:
Andrea M. Goforth, Chair
Robert Strongin
Shankar Rananavare
Erik Johansson
Jun Jiao

Portland State University
2015

## Abstract

Molecular fluorophores and semiconductor quantum dots (QDs) have been used as cellular imaging agents for biomedical research, but each class has challenges associated with their use, including poor photostability or toxicity. Silicon is a semiconductor material that is inexpensive and relatively environmental benign in comparison to heavy metal-containing quantum dots. Thus, red-emitting silicon nanoparticles (Si NPs) are desirable to prepare for cellular imaging application to be used in place of more toxic QDs. However, Si NPs currently suffer poorly understood photoinstability, and furthermore, the origin of the PL remains under debate.

This dissertation first describes the use of diatomaceous earth as a new precursor for the synthesis of photoluminescent Si NPs. Second, the stabilization of red PL from Si NPs in aqueous solution *via* micellar encapsulation is reported. Thirdly, red to blue PL conversion of decane-terminated Si NPs in alcohol dispersions is described and the origins (i.e., color centers) of the emission events were studied with a comprehensive characterization suite including FT-IR, UV-vis, photoluminescence excitation, and time-resolved photoluminescence spectroscopies in order to determine size or chemical changes underlying the PL color change. In this study, the red and blue PL was determined to result from intrinsic and surface states, respectively.

Lastly, we determined that the blue emission band assigned to a surface state can be introduced by base addition in originally red-emitting silicon nanoparticles, and that red PL can be restored by subsequent acid addition. This experimentally demonstrates blue PL is surface state related and can overcome the intrinsic state related excitonic

resombination pathway in red PL event. Based on all the data collected and analyzed, we present a simple energy level diagram detailing the multiple origins of Si NP PL, which are related to both size and surface chemistry.

## Dedication

To my father who passed away on June 5th, 1999.

To my mother, brothers, wife, and my children, both current and future.

**Acknowledgments**

I am heartily grateful to my advisor, Dr. Andrea M. Goforth, for her guidance, inspiration, and support in my 5-year Ph. D. program study. In the meantime, I also want to thank all of my committee, Drs. Robert Strongin, Shankar Rananaware, Erik Johansson, and Jun Jiao, for their tremendous suggestions in research.

I would like to give my gratitude to the post-doctoral associates and fellow graduate and undergraduate students in Goforth Lab and colleagues in the Chemistry Department and Center for Electron Microscopy and Nanofabrication, Dr. Jun Jiao, Dr. Zhiqiang Chen, Dr. Andy Frame, Dr. Lihong Liu, Dr. Beth Manhat, Dr. Anna Brown, William J.I. Debendetii, Victor Benavides Montes, Christine Radlinger, Colin Hiatt, Rylie Ellison, Andrew Barnum, Micah Eastman, Lester Lampert, SudhaPrasanna Kumar Padigi, for great discussions in science and assistances in research.

I also owe my deepest gratitude to my friends for their friendships and encouragements to me. I also would like to thank my family, especially my mother, brothers, and my family, for their unconditional love and consistent support through my life. Furthermore, I would like to dedicate this dissertation to my passed-away father, who always believes that I will become a doctor in the future. Last not least, I want to thank God for being with me when I need him, and help me when I have difficult time during the Ph.D. program.

*I am going to send you what my Father has promised; but stay in the city until you have been clothed with power from on high.* **– Luke 24:49 NIV**

## Table of Contents

## List of Tables

## List of Figures

## List of Schemes

## Chapter 1

# General Introduction to Fluorescent Substances and Their Application in Cellular Imaging

## 1.1 General information to early fluorescent substances, fluorescence, and its application

One of the earliest recorded observations of photoluminescence involved the detection of a unique blue light emitted from an infusion of wood in 1565, reported by the Spanish physician, Nicolás Monardes (as shown in Figure 1.1 a).[1] Later, in 1819, Edward D. Clarke, a Professor of Mineralogy at the University of Cambridge, discovered a peculiar blue color emanating from fluorite crystals in Weardale, Durham, England (as shown in Figure 1.1 b).[1]

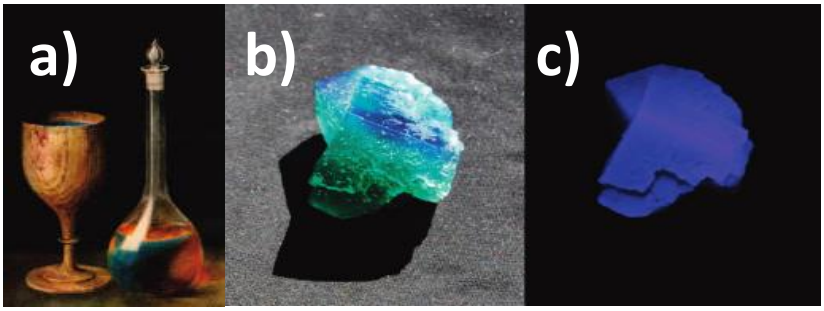


**Figure 1.1** a) Blue fluorescent color of infusions in a wood illuminated with sunlight, b) a crystal of green fluorite under sunlight, and c) blue fluorescent color observed from the crystal of fluorite under UV light.

The following year in 1820, French researchers Pierre Joseph Pelletier and Joseph Bienaimé Caventou observed that quinine, now a well-known anti-malarial medication isolated from the bark of trees, exhibited a cyan green color when irradiated with ultraviolet light.[2] After the discovery of fluorescence, researchers began to question its causes, as the reason behind this unusual phenomenon was not understood. In 1852, Sir George Stokes described the phenomenon of fluorescence, whereby "dark light" or invisible ultraviolet light was converted into longer wavelength radiation in the region of visible light. Such conversion was termed as Stokes Shift,[3] and a chemical compound having the property of fluorescence was later on defined as a "fluorophore" by Richard Meyer in 1897.[4]

The mechanism of fluorescence was first described by Alexander Jablonski, in an article published in *Nature* in 1933. The Jablonski diagram illustrates how electrons transit between electronic states in a fluorophore.[5] Radiative transition is initiated *via* UV absorption, followed by fluorescence in the form of photon (light) emission.

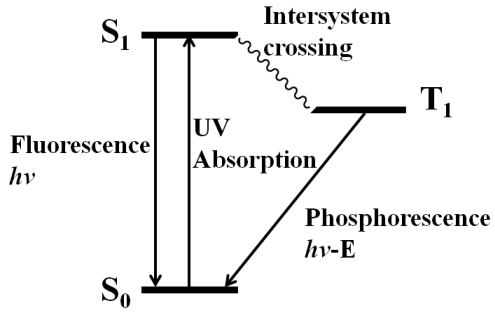


**Figure 1.2** A simplified Jablonski diagram illustrating fluorescence and phosphorescence mechanisms. $S_0$: ground state, $S_1$: singlet excited state, $T_1$: triplet excited state, *hv*: UV-excitation, *hv*-**E**: photon emission.

This process may compete with intersystem crossing and phosphorescence if the excited state electron is able to transition from a singlet excitated state ($S_1$) to a triplet excited state ($T_1$). In this situation, the electron eventually returns to the ground state ($S_0$) from the triplet state ($T_1$) and emits a photon with a much slower decay time (i.e., from a longer lived excited state) vs. fluorescence (as shown in Figure 1.2).

To see is to believe. After the mechanism of fluorescence was discovered, researchers developed equipment to observe and study fluorescent compounds, including those with potential applications in biomedical fields. Therefore, in the early 20$^{th}$ century, fluorescence microscopy was developed by Heimstaedt and Lehman,[6] which was a paramount advance in the study of fluorescence. As a result, in 1924, nucleic acids were successfully labeled with a fluorophore that emitted visible light and this study advanced our understanding and knowledge of nucleic acids. Today a wide variety of biomedical research utilizes fluorophores in applications such as cellular imaging, flow cytometry, histological staining, and as analytical probes.[6]

Because the unique actions of bioactive small molecules can be visualized and tracked in real time, those molecular fluorophores have become very important for cell biology. The first *in vitro* study of tumor cells using a fluorophore as a cellular imaging agent was reported by Musajo and co-workers in 1967.[7] Later, in 1972, a patent was filed for the first *in vivo* method of analyzing blood using a fluorophore as a cellular labeling agent.[8] In the late 20$^{th}$ century, as molecular fluorophores came to be commonly used in biomedical research, problems were encountered with their use as analytical probes, such as photobleaching issues in biological media.

## 1.2 General information to photoluminescence in semiconductor material

Unlike a molecule's energy levels, which are very discrete and energetically well separated, semiconductor energy levels are discrete but energetically closely spaced; thus, they behave as broad bands, since the energy separations between discrete levels are easily overcome (e.g., with thermal energy). The energy bands are constructed from orbitals that originate from atoms, which are periodically arranged in a crystalline solid such as a semiconductor. In a semiconductor, the conduction band is formed by vacant frontier orbitals, and frontier orbitals filled with electrons form the valance band. Some semiconductor materials can also generate visible light after UV excitation due to their unique direct bandgap nature, and this phenomenon is called photoluminescence (PL), one of the fluorescence processes.

Briefly, PL in a semiconductor material occurs where an electron is excited from the valence band to the conduction band by UV excitation (photoexcitaiton). Subsequently, the excited electron will undergo relaxation to the bottom of the conduction band, recombine with a hole at the top of the valance band, and emit a photon with energy corresponding to the band gap energy. If the band gap is in 1.5 -3.1 eV range, which is the visible spectrum range from 400 to 800 nm, then visible light emission can be generated by UV excitation.

When the crystalline domain size of a semiconductor is reduced to the nanoscale, there is a remarkable effect on the PL. For example, II-VI semiconductors (*e.g.*, CdSe) have a tunable band gap over the entire visible region (as shown in Figure 1.3), which is a

function of particle size on the nanometer length scale, a phenomenon known as quantum confinement (QC).

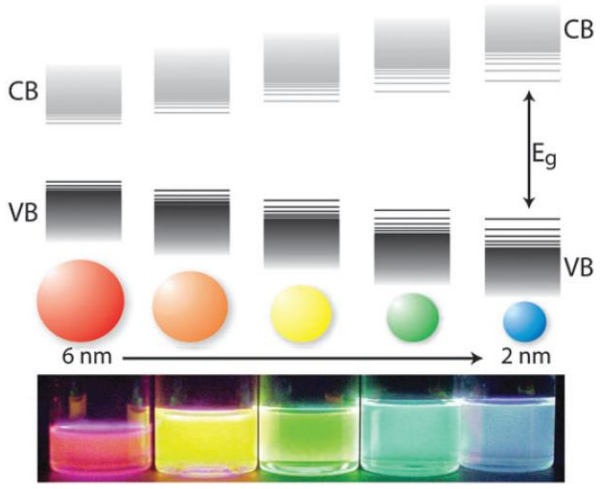


**Figure 1.3.** Simplified band gap diagram illustrating the band gap energy as a function of CdSe particle size. A digital image of CdSe QDs under UV light excitation, ranging from 2 nm to 6 nm in diameter, shows blue to red PL spanning the visible from different sized CdSe QDs. VB: valence band, CB: conduction band, $E_g$: band gap energy separation.[11]

Quantum confinement occurs on the nanometer length scale when the size of semiconductor crystallites is smaller than the bulk semiconductor's Bohr exciton radius, which refers to the distance between a hole and an electron in the excited state. As a semiconductor nanoparticle's radius become smaller than the Bohr exciton radius, the band gap (energy separation) of the semiconductor nanoparticle because a function of nanoparticle radius (QC effect), since the electron-hole pair are confined to a physical space smaller than the electron-hole mean free path. Kayanuma reported an approximate expression for the confinement energy (E), shown below:

$$E = \frac{h^2}{2}\left(\frac{1}{m_e} + \frac{1}{m_h}\right)\frac{\pi^2}{R^2} - 1.786\frac{e^2}{\varepsilon R} - 0.248E^*_{Ry} \qquad \text{Equation 1.1}$$

In the equation, h is Planck's constant, $m_e$ and $m_h$ are the bulk semiconductor's electron and hole effective masses, respectively, ε is the dielectric constant of the semiconductor, R is nanoparticle radius, and $E^*_{Ry}$ is the effective Rydberg constant.[9] As the equation illustrates, the energy of the electronic transition corresponding to the band gap energy is a function of nanoparticle radius; as size decreases, the band gap energy is increased. Semiconductor NPs that show quantum confinement effects are called quantum dots (QDs).[10, 11] For a semiconductor that has a direct band gap, such as the II-VI semiconductors, size-tunable emission across the visible spectrum from red to blue can be accomplished solely by manipulating the QDs size (as shown in Figure 1.3).[12] PL occurs as a result of the radiative recombination of excitons (electron/hole pairs) within QDs at the size-dependent band gap energies.

In 1998, Nie and co-workers published the first application of fluorescent QDs to cellular imaging, the first report that studied the use of QDs in living cells *in vitro*. In their report, cadmium selenide (CdSe) QDs proved to be 20 times brighter than a molecular dye, 100 times more resistant to photobleaching, and had a narrower emission spectrum.[13]

However, a heavy metal like cadmium is highly toxic to biological systems,[14, 15] and therefore is not well-suited to use in biological systems. In order to overcome this, core-shell structures, such as CdSe core/ZnS shell nanoparticles have been synthesized to make CdSe QDs less toxic. Although CdSe QDs appear to be non-toxic after coating with

biologically benign materials (*e.g.*, ZnS, $SiO_2$), the use of a heavy metal is also environmentally undesirable. Therefore, finding a biologically benign material for use as a cellular imaging agent in practical biomedical applications becomes a primary task.

### 1.3 Photoluminescent silicon nanoparticles as fluorescent imaging agents

Silicon, an environmentally and biologically benign element, is widely used in the electronics industry and biomedical engineering, as well as commonly studied in academic labs because of its unique electronic and optical properties. For bulk silicon with an indirect band gap energy of 1.1 eV, the PL efficiency is low and this low efficiency of radiative recombination doesn't favor silicon's use in fluorescence applications. However, Canham reported the first observation of efficient visible PL form porous silicon at room temperature in 1990;[16] this report revealed a potential alternative material to II-VI semiconductors in fluorescence applications.

Eight years later, Liu and co-workers reported a feasible biological clearance mechanism for silicon nanoparticles (Si NPs) by decomposition into silicic acid followed by excretion from the kidneys. This work indicated that Si NPs are biologically non-toxic and suitable for cellular, and perhaps *in vivo*, imaging applications.[17] Given that silicon is the second most abundant element in the earth's crust, has unique electronic and optical properties, emits light efficiently as nanocrystallites, and is nontoxic to biological systems, Si NPs are attractive candidates as next-generation fluescent imaging agents.

The synthesis of red-emitting Si NPs has been increasingly studied for their potential use in fluorescence imaging applications. Recently, a number of studies have been published on water-soluble, red-emitting Si NPs. Ruckenstein and co-workers described the use of water-soluble poly(acrylic acid) (PAA) grafted luminescent Si NPs for fluorescent biological staining applications.[18] They used $CO_2$ laser ablation to synthesize Si NPs by heating $SiH_4/H_2$/He mixtures. HF chemical etching and PAA passivation techniques were utilized to synthesize aqueous red-emitting Si NPs. An *in vitro* cellular imaging study conducted on Chinese hamster ovary (CHO) cells using the PAA Si NPs is shown in Figure 1.4, A.

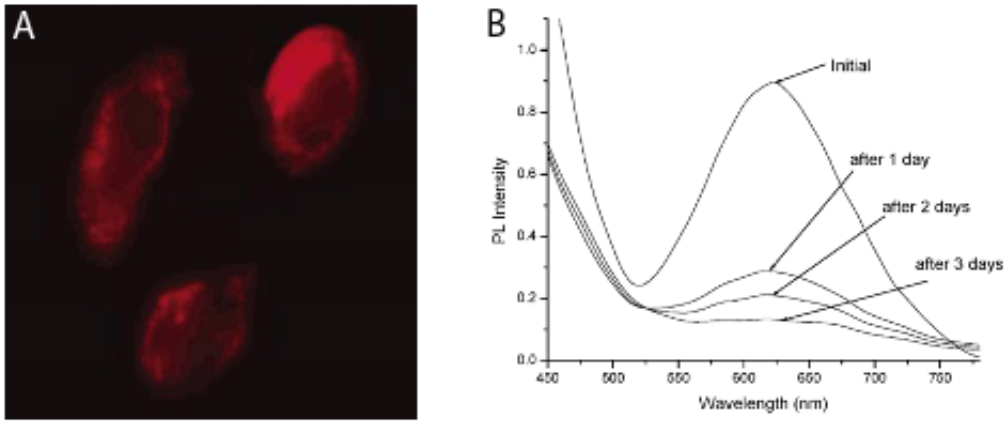


**Figure 1.4. (A)** Fluorescence microscopy study of CHO cells incubated with PAA-Si NPs, (B) The intensity of the red emission of Si NPs was a function of time after PAA-Si NPs immersed in deionized water.[18]

PL cellular imaging has been used in biomedical and chemical research because of the rapid response inherent to fluorescence. A fluorescent imaging agent can be utilized for both *in vitro* and *in vivo* studies of living organisms. Fluorescent probes can

be used to track tumor cells, understand cell behavior, and find treatments for cancer.[19-21] However, a crucial factor in obtaining effective imaging in tissues is the use of fluorophores that emit from 600 nm to 1000 nm, because autofluorescence interference is less in the near-infrared (NIR) wavelength region (700 – 900 nm) and the depth of light penetration is greater (vs. the visible), and since it is not efficiently absorbed by cellular and blood components.[20, 22]

Two of the main challenges to using photoluminescent Si NPs as fluorescence imaging agents are changes in PL intensity and spectral position ($\lambda_{max, em}$). As seen in Figure 1.4, B, the PL intensity of PAA-Si NPs is not stable in aqueous solutions; the intensity of the red emission in the PL spectrum is significantly reduced after 24 hrs. In addition to this, several other reports have shown the conversion from red to blue PL when Si NPs are oxidized in aqueous solution.[23,24,25] For fluorescent cellular imaging, it is necessary to synthesize water soluble red- to NIR-emitting Si NPs, with stable photophysical properties in biological media for practice use.

After Canham discovered visible red emission from porous silicon,[26, 27] many syntheses of photoluminescent silicon quantum dots using various methods have been reported over the past two decades. In general, red-emitting Si NPs haven't been reported to be synthesized *via* chemical solution based syntheses; however, high temperature annealing, laser ablation, and electrochemical/chemical etching methods have been routinely shown to generate free-standing silicon quantum dots that have red or near-infrared emission. For Si NPs generated by these methods, the red emission has frequently been observed to be unstable in aqueous and biological media. Surface state

formation with chemical changes to the surface have been implicated as underlying this photo-instability. Thus, our recent research has focused on identifying and controlling surface (and other) defects that may adversely impact the PL intensity and wavelength.

### 1.4 Present state of knowledge concerning photoluminescence behavior in bulk and nanocrystalline silicon: Size and surface effects

Unlike II-VI semiconductors, which have only a direct band gap, bulk silicon (a group IV semiconductor) has an indirect band gap energy of 1.1 eV and a direct band gap energy of 3.4 eV.[16] A band gap is defined as indirect when the minimum of the conduction band (CB) is not directly above the maximum of the valence band (VB) in momentum space (k), as shown in Figure 1.5.[28] Because the electronic transition from CB to VB across the band gap is a momentum-forbidden transition for an indirect band gap semiconductor, emission can only occur efficiently as a phonon-assisted process. However, when a Si NP is smaller than 4 nm (the Si Bohr exciton radius),[29] it is theorized to display efficient, variable wavelength light emission as a function of size due to increased efficiency of the momentum-forbidden transition with greater positional certainty and to QC effects.[30,31]

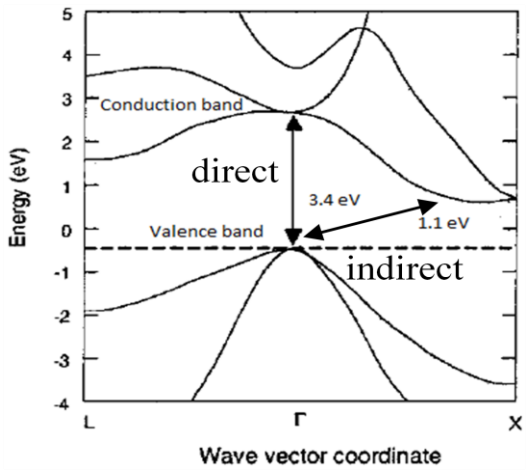


**Figure 1.5.** The band structure of bulk silicon, modified from reference 21. Γ indicates [000] direction where wave vector of electron waves k=0; L and X are wavevectors in the [111] and [100] directions, respectively, where wave vectors of electron waves $k \neq 0$.[28]

For $Si^0$ domains that are on the nanometer length scale, previous literature has shown that, it is not only the size of the Si NPs that matters. Both nanoparticle size and surface chemical composition have been found to exert a significant influence on PL emission behavior. In some reports, it has been shown that the emission energy is adjustable as a function of size, which may indicate that the QC effect dominates the PL mechanism. As one example of this, Veinot and coworkers reported hydride-terminated free-standing Si NPs (3.41 nm) with yellow luminescence after a HF wet-etch, and a blue-shift in emission was observed with an increase in etching time.[32,33,34] This is consistent with HF etching of silicon, and with the expectation that as the size of Si NPs is reduced in etching, the band gap increases and the PL blue shifts in accordance with the QC effect.[35]

At smaller Si NP sizes (< 4 nm), higher energy emission is expected for quantum confined Si NPs, according to Equation 1.1. However, although red emission is predicted and often observed for ~ 4 nm Si NPs, blue emission also has been reported for Si NPs with sizes larger than 4 nm after surface oxidation.[36-38] Surface traps and surface defects in Si NPs prepared using various synthetic methods have been reported to induce blue or red shifts in PL, indicating that the PL of Si NPs is not driven solely by QC in larger Si NPs.[39,40] Several reports have also shown that blue emission can be obtained through localized surface defect states.[41,42,43] As one example of this, Manhat et al. reported blue emission from aqueous Si NPs approximately 4 nm in size, which they attributed to Si-O surface states.[37] Furthermore, several recent reports have attributed blue emission only or blue emission alongside other red emission events to localized Si-O surface states lying outside the band gap.[38, 41, 44] This is consistent with the frequent observation of only blue emission for Si NPs in water due to the possibility of passivation of Si surface sites by $OH^-$ or $H_2O$. Furthermore, while it is expected that ultrasmall, 1–2 nm quantum-confined Si NPs should emit blue light,[45] the observation of blue emission from larger Si NPs (> 4 nm) is unexpected according to QC expectations.[29, 45, 46] Thus, the many examples of 4–5 nm, blue-emitting aqueous Si NPs that have been reported to date also support the origin of aqueous, blue emission as arising from Si-O surface states.

The causes underlying the polychromatic emissions and emission-shifts in Si NPs are quite complex, and are the problem that has attracted the most current attention from researchers in the Si NP community. Gaining a better understanding of the mechanisms of PL from Si NPs and stabilizing the photophysical properties, including emission color

and intensity are major tasks to be resolved for future applications of Si NPs in biomedical cellular imaging.

### 1.5 Outlook of this work

The core of this dissertation focuses on the PL behavior of photoluminescent Si NPs and their applications in cellular imaging. Aqueous, red-emitting Si NPs were successfully synthesized and the red emission was persistent for more than six months in aqueous solutions at pH $\leq$ 7 (Chapter 2). Then, we demonstrate conversion from red to blue emission (Chapter 3) and reversible switching between red and blue PL (Chapter 4), the latter achieved through experimental design with the knowledge gained by identifying intrinsic and extrinsic PL pathways in Chapters 2 and 3. Finally, we describe a new synthesis of Si NPs from diatomaceous earth (Chapter 5). Diatomaceous earth is an inexpensive, earth abundant, and environmentally benign substance, and was found to produce photoluminescent Si NPs under heat treatment at 1100 °C in a reducing atomsphere. UV-Vis, PL spectroscopy, and time-resolved PL spectroscopy were utilized to study dynamic electron transitions and steady-state optical properties of Si NPs. Surface passivations and chemical compositions of Si NPs were studied *via* Fourier transform infrared spectroscopy. The size crystallinity and morphology of Si NPs was studied by Raman spectroscopy, energy dispersive X-ray spectroscopy, high-resolution transmission electron microscopy, and powder/thin film X-ray diffraction.

## 1.6 References


1. Valeur, B.; Berberan-Santos, M. N., A Brief History of Fluorescence and Phosphorescence before the Emergence of Quantum Theory. *Journal of Chemical Education* **2011,** 88, (6), 731-738.

2. Flückiger, F. A., Hanbury,Daniel., *Pharmacographia: A history of the principal drugs of vegetable origin, met with in Great Britain and British India*. Macmillan: London, UK, 1879.

3. Stokes, G. *G.*, On the change of refrangibility of light. *Philosophical Transcations of the Royal Society of London* **1852,** 142, 463-562.

4. Meyerm, R., *Zeitschrift fur Physikalische Chemie, Stochiometrie und Verwandtschaftslehre*. Leipzig, Verlag von Wilhelm Engelmann: 1887.

5. Jablonski, A., Efficiency of anti-stokes fluorescence in dyes. *Nature* **1933,** 131, 839-840.

6. Kricka, L. J.; Fortina, P., Analytical Ancestry: "Firsts" in Fluorescent Labeling of Nucleosides, Nucleotides, and Nucleic Acids. *Clinical Chemistry* **2009,** 55, (4), 670-683.

7. Musajo, L., Visentini, P., Bacchinetti, F., Razzi, M. A., Photoinactivation of Ehrlich ascites tumor cells in vitro obtained with skin-photosensitizing furocoumarins. *Experientia* **1967,** 23, (5).

8. Adams, L. R., Kamentsky, Louis A. Method for analysis of blood by optical analysis of living cells. 1972.

9. Einevoll, G. T., CONFINEMENT OF EXCITONS IN QUANTUM DOTS. *Physical Review B* **1992,** 45, (7), 3410-3417.

10. Alivisatos, A. P., Perspectives on the physical chemistry of semiconductor nanocrystals. *Journal of Physical Chemistry* **1996,** 100, (31), 13226-13239.

11. Bukowski, T. J.; Simmons, J. H., Quantum dot research: Current state and future prospects. *Critical Reviews in Solid State and Materials Sciences* **2002,** 27, (3-4), 119-142.

12. Donega, C. D., Synthesis and properties of colloidal heteronanocrystals. *Chemical Society Reviews* **2011,** 40, (3), 1512-1546.

13. Chan, W. C. W.; Nie, S. M., Quantum dot bioconjugates for ultrasensitive nonisotopic detection. *Science* **1998,** 281, (5385), 2016-2018.

14. Chen, N.; He, Y.; Su, Y. Y.; Li, X. M.; Huang, Q.; Wang, H. F.; Zhang, X. Z.; Tai, R. Z.; Fan, C. H., The cytotoxicity of cadmium-based quantum dots. *Biomaterials* **2012,** 33, (5), 1238-1244.

15. Derfus, A. M.; Chan, W. C. W.; Bhatia, S. N., Probing the cytotoxicity of semiconductor quantum dots. *Nano Letters* **2004,** 4, (1), 11-18.

16. Canham, L. T., Silicon quantum wire array fabrication by electrochemical and chemical dissolution of wafers. *Applied Physics Letters* **1990,** 57, (10), 1046.

17. Popplewell, J. F.; King, S. J.; Day, J. P.; Ackrill, P.; Fifield, L. K.; Cresswell, R. G.; Di Tada, M. L.; Liu, K., Kinetics of uptake and elimination of silicic acid by a human subject: A novel application of Si-32 and accelerator mass spectrometry. *Journal of Inorganic Biochemistry* **1998,** 69, (3), 177-180.

18. Li, Z. F.; Ruckenstein, E., Water-soluble poly(acrylic acid) grafted luminescent silicon nanoparticles and their use as fluorescent biological staining labels. *Nano Letters* **2004,** 4, (8), 1463-1467.

19. Aswathy, R. G.; Yoshida, Y.; Maekawa, T.; Kumar, D. S., Near-infrared quantum dots for deep tissue imaging. *Analytical and Bioanalytical Chemistry* **2010,** 397, (4), 1417-1435.

20. Hahn, M. A.; Singh, A. K.; Sharma, P.; Brown, S. C.; Moudgil, B. M., Nanoparticles as contrast agents for in-vivo bioimaging: current status and future perspectives. *Analytical and Bioanalytical Chemistry* **2011,** 399, (1), 3-27.

21. Michalet, X.; Pinaud, F. F.; Bentolila, L. A.; Tsay, J. M.; Doose, S.; Li, J. J.; Sundaresan, G.; Wu, A. M.; Gambhir, S. S.; Weiss, S., Quantum dots for live cells, in vivo imaging, and diagnostics. *Science* **2005,** 307, (5709), 538-544.

22. Hilderbrand, S. A.; Weissleder, R., Near-infrared fluorescence: application to in vivo molecular imaging. *Current Opinion in Chemical Biology* **2010,** 14, (1), 71-79.

23. Dasog, M.; Yang, Z. Y.; Regli, S.; Atkins, T. M.; Faramus, A.; Singh, M. P.; Muthuswamy, E.; Kauzlarich, S. M.; Tilley, R. D.; Veinot, J. G. C., Chemical Insight into the Origin of Red and Blue Photoluminescence Arising from Freestanding Silicon Nanocrystals. *Acs Nano* **2013,** 7, (3), 2676-2685.

24. Vincent, J.; Maurice, V.; Paquez, X.; Sublemontier, O.; Leconte, Y.; Guillois, O.; Reynaud, C.; Herlin-Boime, N.; Raccurt, O.; Tardif, F., Effect of water and UV passivation on the luminescence of suspensions of silicon quantum dots. *Journal of Nanoparticle Research* **2009,** 12, (1), 39-46.

25. Shiohara, A.; Hanada, S.; Prabakar, S.; Fujioka, K.; Lim, T. H.; Yamamoto, K.; Northcote, P. T.; Tilley, R. D., Chemical Reactions on Surface Molecules Attached to Silicon Quantum Dots. *Journal of the American Chemical Society* **2010,** 132, (1), 248-253.

26. Cullis, A. G.; Canham, L. T.; Calcott, P. D. J., The structural and luminescence properties of porous silicon. *Journal of Applied Physics* **1997,** 82, (3), 909.

27. Cullis, A. G.; Canham, L. T., VISIBLE-LIGHT EMISSION DUE TO QUANTUM SIZE EFFECTS IN HIGHLY POROUS CRYSTALLINE SILICON. *Nature* **1991,** 353, (6342), 335-338.

28. Holmes, J. D.; Ziegler, K. J.; Doty, R. C.; Pell, L. E.; Johnston, K. P.; Korgel, B. A., Highly luminescent silicon nanocrystals with discrete optical transitions. *Journal of the American Chemical Society* **2001,** 123, (16), 3743-3748.

29. Kang, Z. H.; Liu, Y.; Tsang, C. H. A.; Ma, D. D. D.; Fan, X.; Wong, N. B.; Lee, S. T., Water-Soluble Silicon Quantum Dots with Wavelength-Tunable Photoluminescence. *Advanced Materials* **2009,** 21, (6), 661-+.

30. Kim, T.-W.; Cho, C.-H.; Kim, B.-H.; Park, S.-J., Quantum confinement effect in crystalline silicon quantum dots in silicon nitride grown using SiH[sub 4] and NH[sub 3]. *Applied Physics Letters* **2006,** 88, (12), 123102.

31. Ledoux, G.; Gong, J.; Huisken, F.; Guillois, O.; Reynaud, C., Photoluminescence of size-separated silicon nanocrystals: Confirmation of quantum confinement. *Applied Physics Letters* **2002,** 80, (25), 4834-4836.

32. Hessel, C. M.; Henderson, E. J.; Veinot, J. G. C., Hydrogen silsesquioxane: A molecular precursor for nanocrystalline Si-SiO2 composites and freestanding hydride-surface-terminated silicon nanoparticles. *Chemistry of Materials* **2006,** 18, (26), 6139-6146.

33. Ray, M.; Hossain, S. M.; Klie, R. F.; Banerjee, K.; Ghosh, S., Free standing luminescent silicon quantum dots: evidence of quantum confinement and defect related transitions. *Nanotechnology* **2010,** 21, (50), 505602.

34. Hapala, P.; Kůsová, K.; Pelant, I.; Jelínek, P., Theoretical analysis of electronic band structure of 2- to 3-nm Si nanocrystals. *Physical Review B* **2013,** 87, (19).

35. Trucks, G.; Raghavachari, K.; Higashi, G.; Chabal, Y., Mechanism of HF etching of silicon surfaces: A theoretical understanding of hydrogen passivation. *Physical Review Letters* **1990,** 65, (4), 504-507.

36. Wolkin, M. V.; Jorne, J.; Fauchet, P. M.; Allan, G.; Delerue, C., Electronic states and luminescence in porous silicon quantum dots: The role of oxygen. *Physical Review Letters* **1999,** 82, (1), 197-200.

37. Manhat, B. A.; Brown, A. L.; Black, L. A.; Ross, J. B.; Fichter, K.; Vu, T.; Richman, E.; Goforth, A. M., One-step Melt Synthesis of Water Soluble, Photoluminescent, Surface-Oxidized Silicon Nanoparticles for Cellular Imaging Applications. *Chem Mater* **2011,** 23, (9), 2407-2418.

38. Yang, S. K.; Li, W. Z.; Cao, B. Q.; Zeng, H. B.; Cai, W. P., Origin of Blue Emission from Silicon Nanoparticles: Direct Transition and Interface Recombination. *Journal of Physical Chemistry C* **2011,** 115, (43), 21056-21062.

39. Chiu, S. K.; Manhat, B. A.; DeBenedetti, W. J. I.; Brown, A. L.; Fichter, K.; Vu, T.; Eastman, M.; Jiao, J.; Goforth, A. M., Aqueous red-emitting silicon nanoparticles for cellular imaging: Consequences of protecting against surface passivation by hydroxide and water for stable red emission. *Journal of Materials Research* **2013,** 28, (2), 216-230.

40. Kůsová, K. i.; Ondič, L. s.; Klimešová, E.; Herynková, K. i.; Pelant, I.; Daniš, S.; Valenta, J.; Gallart, M.; Ziegler, M.; Hönerlage, B.; Gilliot, P., Luminescence of free-standing versus matrix-embedded oxide-passivated silicon nanocrystals: The role of matrix-induced strain. *Applied Physics Letters* **2012,** 101, (14), 143101.

41. de Boer, W. D. A. M.; Timmerman, D.; Dohnalova, K.; Yassievich, I. N.; Zhang, H.; Buma, W. J.; Gregorkiewicz, T., Red spectral shift and enhanced quantum efficiency in phonon-free photoluminescence from silicon nanocrystals. *Nature Nanotechnology* **2010,** 5, (12), 878-884.

42. Godefroo, S.; Hayne, M.; Jivanescu, M.; Stesmans, A.; Zacharias, M.; Lebedev, O. I.; Van Tendeloo, G.; Moshchalkov, V. V., Classification and control of the origin of photoluminescence from Si nanocrystals. *Nat Nanotechnol* **2008,** 3, (3), 174-8.

43. Hua, F. J.; Swihart, M. T.; Ruckenstein, E., Efficient surface grafting of luminescent silicon quantum dots by photoinitiated hydrosilylation. *Langmuir* **2005,** 21, (13), 6054-6062.

44. Brewer, A.; von Haeften, K., In situ passivation and blue luminescence of silicon clusters using a cluster beam/H[sub 2]O codeposition production method. *Applied Physics Letters* **2009,** 94, (26), 261102.

45. Tilley, R. D.; Warner, J. H.; Yamamoto, K.; Matsui, I.; Fujimori, H., Micro-emulsion synthesis of monodisperse surface stabilized silicon nanocrystals. *Chemical Communications* **2005**, (14), 1833-1835.

46. Wilcoxon, J. P.; Samara, G. A.; Provencio, P. N., Optical and electronic properties of Si nanoclusters synthesized in inverse micelles. *Physical Review B* **1999,** 60, (4), 2704-2714.

## Chapter 2

## Aqueous, red-emitting silicon nanoparticles for cellular imaging: Consequences of protecting against surface passivation by hydroxide and water for stable, red emission

Published as: Chiu, S. K.; Manhat, B. A.; DeBenedetti, W. J. I.; Brown, A. L.; Fichter, K.; Vu, T.; Eastman, M.; Jiao, J.; Goforth, A. M., *Journal of Materials Research* **2013,** *28* (2), 216-230.[1] Repriented with permission.

### 2.1 Abstract

Stable, aqueous, red-to-NIR emission is critical for the use of silicon nanoparticles (Si NPs) in biological fluorescence assays, but such Si NPs have been difficult to attain. We report a synthesis and surface modification strategy that protects Si NPs and preserves red photoluminescence (PL) in water for more than six months. The Si NPs were synthesized *via* high-temperature reaction, liberated from oxide matrix, and functionalized *via* hydrosilylation to yield hydrophobic particles. The hydrophobic Si NPs were phase transferred to water using the surfactant cetyl-trimethylammonium bromide (CTAB) with retention of red PL. CTAB apparently serves a double role in providing stable, aqueous, red-emitting Si NPs in 1) forming a hydrophobic barrier between the Si NPs and water and, 2) in providing aqueous colloidal stability *via* the polar head group. We demonstrate preservation of the aqueous, red emission of these Si NPs in biological media and examine the effect of pH on emission color.

## 2.2 Introduction

Semiconductor nanoparticles (NPs) have received widespread attention in recent years for their size-tunable UV-to-NIR light emission governed by the quantum confinement effect. These photoluminescent particles with size-tunable, narrow emission and broad absorption spectra have been exploited in numerous applications, including in light emitting/harvesting devices[2,3] and as handles for biomedical tracking and imaging.[4,5] Although predominantly direct band gap semiconductor nanoparticles, *i.e.*, quantum dots (QDs), have thrived in semiconductor NP synthesis and application studies, attention has more recently turned toward the development of potentially less toxic (relative to II-VI Cd- and Pb-based QD) Si NP fluorophores after the observation of efficient visible photoluminescence from porous silicon containing nm-sized Si domains in the 1990s.[6] Observation of efficient, visible photoluminescence from nm-sized, indirect band gap Si has been attributed to relaxation of the momentum-forbidden radiative exciton recombination across the indirect band gap with increased certainty in carrier position on the nanoscale.[7,8]

Despite potential toxitcity and compatibility advantages in using fluorescent Si NPs over CdQ and PbQ (Q = S, Se, Te) quantum dots in both devices (*e.g.*, solely Si-based opto-electronics)[9,10,11] and biomedical applications,[5,12,13] synthetic control over Si NP emission color and quantum yield is poor relative to II-VI QDs and emission wavelength is not always correlated with particle size according to expectations of quantum confinement.[8,14,15,16,17] Not only is it expected that biological organisms would exhibit a greater tolerance to Si NPs over CdQ and PbQ QDs, but other advantages of Si NPs over CdQ and PbQ QDs include: the ability to form robust covalent surface bonds

to Si for surface modification, *versus* weaker dative bonds for II-VI QDs,[18,19] and a viable mechanism of biological clearance for Si NPs (decomposition and renal clearance of hydrolyzed Si NPs as silicic acid)[5,20,21] *versus* bioaccumulation and/or cytotoxicity for CdQ and PbQ QDs.[12,13,22] Nonetheless, because of the possibility of radiative events occurring from both delocalized core states (*i.e.*, quantum-confinement related emission) and from localized surface-defect or other trap states (*e.g.*, at the Si NP/ligand or Si NP-surface oxide interface),[15, 23-29] Si NP emission dominated by core states alone is difficult to achieve, emission quantum yields are generally low, and polychromatic emission (*e.g.*, having two or more distinct emission events)[24-32] is frequently observed. Both theoretical[33, 34] and experimental[23,27,29,35] reports support the hypothesis that surface and/or defect states, in addition to quantum-confined states, significantly influence the observed emission properties of Si NPs, whether they are free-standing in solution or embedded in solid hosts (*e.g.*, in porous silicon).

To overcome the challenges in emission wavelength and efficiency control in Si NPs, it is desirable to identify and mitigate pathways leading to defect-related emission, which should provide synthetic strategies for emission property tuning to allow the size-dependent core state emission pathway to dominate the observed optical properties. This is particularly important for biomedical applications of Si NPs, since narrow, resolvable emission in the red-to-NIR spectral region is necessary for avoiding cellular autofluorescence interferance of the Si NP signal, as well as tissue penetration limitations, and since unstable emission characteristics (including, color and quantum yield) would result in loss of information. To date, Si NPs have been synthesized with relatively high emission quantum yields (10-70% absolute quantum yields)[36,37,38,39] and

quantum-confinement related emission spanning the entire visible spectrum has also been observed in a few reports.[40,41,42,43,44,45] Numerous publications have reported red-to-NIR (600-800 nm) emitting hydrophobic Si NPs 3-10 nm in diameter with suitable optical but unsuitable miscibility properties for biomedical fluorescence assays. However, when Si NPs are surface functionalized or surface oxidized to allow dispersion in water, strong blue (400-500 nm) emission is most frequently observed,[14,16,17,46-47] even for aqueous samples having the same or similar sizes and size distributions as the red-emitting, hydrophobic particles.[14, 16, 46, 48]

Several recent reports have attributed blue emission only or blue emission alongside other redder emission events to localized Si-O surface states lying outside the band gap,[28, 29, 49] which is consistent with the frequent observation of blue emission only for Si NPs in water due to the possibility of passivation of unreacted Si surface sites by $OH^-$ or $H_2O$. Furthermore, while it is expected that ultrasmall, 1-2 nm quantum confined Si NPs should emit blue,[50] the observation of blue emission from larger Si particles close to the bulk Si Bohr exciton radius (~4 nm)[40, 50, 51] is unexpected according to quantum confinement expectations. Thus, the many examples of 4-5 nm, blue-emitting aqueous Si NPs that have been reported to date[14, 16, 46, 48] also support the origin of aqueous, blue emission as arising from Si-O surface states outside the band gap. Researchers have previously attributed localized Si-O states to self-trapped luminescent centers (also called self-trapped excitons) with direct excitation and emission ability[35, 52] or to sites where photogenerated core excitons can decay, radiatively or non-radiatively.[28, 53, 54] Regardless of what role the localized surface state plays, emission from localized states is generally accepted to be much faster than radiative exciton recombination, and thus would

dominate due to the relatively faster time scale of the surface state decay (ns-ps) *versus* the core state decay (μs-ns) process.[29]

Several observations of stable, red-to-NIR emitting, aqueous Si NPs have been reported,[5,12,21,30,40,55-59] and most of these describe steps to modify the surface of the Si NP core to protect it from further undesirable passivation or oxidation. One method of surface modification is the conversion of Si NPs to Si NP/$SiO_xH_y$ core/shell structures.[5,30,40] These methods result in a size-tunable (and consequently, an emission wavelength-tunable) Si NP core with a uniformly grown oxide shell that is shown to provide stable surface and photoluminescence characteristics. The oxide shell also confers water solubility on the Si NPs and apparently preserves red-to-NIR photoluminescence with maximum emission wavelengths as high as 750-850 nm in water.[5] Unfortunately, the red-to-NIR emission properties are not always stable with respect to time, and certain Si NP/$SiO_xH_y$ core/shell structures exhibit a blue-shifted emission ($\lambda_{max,em}$ = 430 nm) with a slow onset.[30]

Others seeking to preserve red emission in water have used various surface stabilizing agents to better protect the Si NP surfaces from further undesired surface passivation. Kravitz *et al*. have prepared Si NPs *via* a solid state synthesis from commercial, amorphous nanosilica in the presence of magnesium powder, and these particles were subsequently dispersed in water, using poly(vinyl alcohol) (13,000-23,000 MW) to confer water solubility and to stabilize the particle surfaces.[56] The red emission at $\lambda_{max}$ = 710 nm observed from the neat, PVA-coated Si powders was apparently maintained in poly(vinyl alcohol)/water dispersions for some time. However, the study does not comment on the temporal behavior of the photoluminescence. Li *et al*. reported

that Si NPs prepared *via* $CO_2$ laser-induced pyrolysis of silane, followed by an $HF/HNO_3$ etch, can be coated using poly(acrylic acid) (PAA) through a graft polymerization of 10 wt% acrylic acid under intense UV irradiation.[55] The PAA coating around the Si NPs helped preserve 80% of the emission intensity at $\lambda_{max}$ = 605 nm for 1 week in water. The authors concluded that PAA provided an insulating barrier between the Si NP surface and the water molecules, temporarily preventing water passivation of the Si NP surface. He *et al.* have also used PAA to modify the surface of H-Si NPs prepared electrochemically.[22] However, rather than coating the Si NPs with PAA directly, the as-prepared, hydride-terminated Si NPs first underwent hyrdosilylation with monomers of acrylic acid, and then were coated with PAA. This method takes advantage of the ability of Si NPs to form stable covalent bonds with unsaturated hydrocarbons, such as biocompatible acrylic acid, and further cross-linking with PAA, to better protect the Si NPs from further undesirable surface passivation while apparently preserving red emission ($\lambda_{max}$ = 595 nm) in water for up to six months.

Herein, we report a new synthetic method to produce stable, red-emitting aqueous Si NPs that retain their red emission ($\lambda_{max}$ = 580 nm, or $\lambda_{max}$ = 740 nm when correcting for wavelength sensitivity of our photomultiplier tube detector) for longer than 6 months in aqueous solutions of pH $\leq$ 7. The method involves solid state synthesis of Si NPs, followed by a wet chemical etch and hydrophobic workup, and subsequently phase transfer of decane-terminated Si NPs into aqueous media through alkyl chain self-assembly using the surfactant cetyl-trimethylammonium bromide (CTAB). The hydrophobic tail of CTAB is capable of intercalating within the long hydrocarbon chains on the surfaces of the Si NPs, thus forming a micellar structure around the Si NPs that

allows stable dispersion in water *via* the quaternary ammonium head groups and retention of the red photoluminescence *via* hydrophobic protection against further, undesirable surface passivation. Additionally, these CTAB-coated, decane-terminated Si NPs can be further wrapped with poly(acrylic)acid (PAA) polymer, which imparts a more ideal, negative surface charge (for biological applications, over a wide pH range) and provides reactive carboxylic acid groups for bioconjugation. The consequence of protecting the Si NP surfaces against further, undesirable Si-OH passivation in preserving the aqueous red emission of Si NPs is demonstrated by the destruction of the micelles in high pH solution ($pH \geq 8$), which is commensurate with the observation of strong, blue PL, loss of red PL, and increased Si-OH and $Si-OH_2$ bonding features. We also demonstrate the facile uptake of these red emitting Si NPs into live neuroblastoma cells with the preservation of the photophysical properties and observe an even distribution of the red emission from the Si NPs throughout the cytoplasm.

### 2.3 Experimental

**Materials.** Some chemicals or synthetic procedures were handled under inert (argon or nitrogen) atmosphere on a Schlenk line, using standard air-free techniques, where specified. Other steps, including: etching, phase transfer and aqueous workups were done in air. Electrophoretically pure water (nanopure water, 18 MΩ•cm resistivity) was used for preparing all aqueous solutions. Trichlorosilane ($HSiCl_3$, Alfa Aesar, ≥ 98%), 1-decene ($CH_3(CH_2)_7CH=CH_2$, Aldrich, ≥ 97%), cetyl-trimethylammonium bromide (**(**$CH_3(CH_2)_{15}N(CH_3)_3Br$, Fisher, ≥ 99%), poly(acrylic acid) sodium salt ($(C_3H_3NaO_2)_n$, MW: 6000 De, moisture: < 10%), and aqueous hydrofluoric acid ($HF_{(aq)}$, 48.0-51.0%)

were purchased from Fisher Scientific and used as received with the exception of the polymer salt. Prior to use, 2 g of the poly(acrylic acid) sodium salt was dissolved in 150 mL of 12 N NaOH; the aqueous polymer solution was then dialyzed against nanopure water using 1000 Da MWCO dialysis tubing (regenerated cellulose, Fisher Brand). Following dialysis, the retentate solution underwent rotary evaporation to obtain dried, purified poly(acrylic acid). For cellular studies, D-MEM, Opti-MEM, and fetal bovine serum (FBS) solutions were purchased from Invitrogen/Life Technologies, Grand Island, NY.

**Synthesis of water-soluble, red-emitting silicon nanoparticles (Si NPs).** A sol-gel polymer of putative stoichiometry $(HSiO_{1.5})_n$ was prepared by hydrolysis and polycondensation of tricholosilane (5 mL) as previously reported.[57] This solid precursor (0.9 g) was subsequently annealed at 1100°C under flowing $N_2$ in a horizontal tube furnace (Lindberg Blue, Model TF55035A) for 10 hrs to generate nanocrystalline silicon (Si NC) encapsulated in $SiO_2$ matrix. The Si NC/$SiO_2$ powder was then ball milled under ambient atmosphere for 10 sec using a tungsten carbide-lined milling vial with two 1-cm tungsten carbide balls and a Spex 8000M mill mixer. Hydrogen terminated Si NPs (H-Si NPs) were liberated from the mechanically milled matrix (~0.5 g) by a 60 min chemical etch using a 15 mL solution of 1:1:1 (by volume) ethanol/water/HF(aq), according to a literature method.[41] Following extraction of red-emitting, H-Si NPs into pentane (~40 mL), decane-capped Si NPs (Dec-Si NPs) were prepared by thermal hydrosilylation by refluxing the H-Si NPs in 3 mL of neat 1-decene under Ar gas for 18 hrs. Hexane was used to disperse the Dec-Si NPs several times and rotary evaporation was used to remove

excess capping agent and hexane. Water soluble, red-emitting Si NPs were prepared from the red-emitting, decane-terminated Si NPs by coating with cetyl-trimethylammonium bromide (CTAB) and/or coating with CTAB followed by wrapping with poly(acrylic acid) (PAA), as described below. The synthesis of CTAB-coated/decane-terminated Si NPs from hydrolyzed trichlorosilane (*i.e.*, $(HSiO_{1.5})_n$ polymer) is outlined in Scheme 2.1.

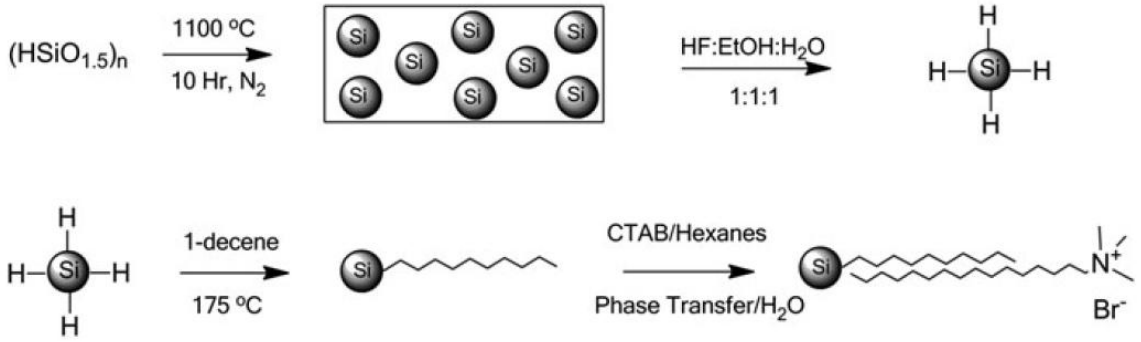


**Scheme 2.1** Synthetic procedure for the preparation of stable, aqueous, red-emitting, CTAB-coated/decane-terminated silicon nanoparticles.

CTAB-coated, decane-terminated Si NPs (CTAB/Dec-Si NPs or CTAB/Dec-Si NP micelles) were prepared by loading 0.073 g (0.2 mmol) of CTAB into an air-free two-neck, round-bottomed flask to which 3 mL of decane-terminated Si NPs in hexanes was transferred. The reaction vessel was sonicated for 30 minutes, and the contents were subsequently dried under dynamic vacuum for 8 hrs. After transferring 3.5 mL of water into the flask, the sample was sonicated for 90 min in a 50°C water bath to obtain aqueous, red-emitting CTAB/Dec-Si NPs. The aqueous layer containing the CTAB/Dec-Si NPs was dialyzed against nanopure water using 1000 Da MWCO dialysis tubing to

remove excess CTAB; the measured pH values of aqueous CTAB/Dec-Si NP samples following dialysis were 6.5±0.5. We have observed that the amount of CTAB required for aqueous nanocrystal stabilization (*i.e.*, colloidal stabilization) is variable, depending on whether larger or smaller micelles are desired. We have been able to produce aqueous, single Si NPs using variations of the method presented in this work, using a smaller excess of CTAB.

PAA-wrapped/CTAB-coated/decane-terminated Si NPs (PAA/CTAB/Dec-Si NPs) were prepared by dissolving 0.05 g of dried, purified PAA in 10 mL of water to form a poly(acrylic acid) solution. An aqueous CTAB/Dec-Si NP solution (0.2 mL) was transferred into an ambient atmosphere two-neck, round-bottomed flask and 2 mL of the PAA solution was added. The resulting solution was stirred for 10 min to generate the PAA/CTAB/Dec-Si NPs. To remove excess PAA, the aqueous Si NP solution was dialyzed against nanopure water using 1000 Da MWCO dialysis tubing for 24 hrs. These synthetic methods are outlined in Scheme 1.

**Characterization of water-soluble, red emitting Si NPs and Si NP synthetic intermediates.**

*In situ Powder X-ray Diffraction Studies (PXRD) of Solid-State Precursor.* The sol-gel hydrosilicate $(HSiO_{1.5})_n$ (0.10 g) was loaded onto a Pt sample holder and pressed flat before loading into the instrument's furnace for annealing (under vacuum atmosphere). Data was collected at 30$^{o}$C and the sample was then heated to 200$^{o}$C at 20$^{o}$C/min. The temperature of the stage was increased in 200$^{o}$C intervals at a heating rate of 20$^{o}$C/min and held at a given temperature (200, 400, 600, 800, or 1000$^{o}$C) for 1 hr prior to the

PXRD scan (30 mins). The temperature of the stage was then further increased in 100°C intervals at a heating rate of 20°C/min and held at a given temperature (1100, 1200, 1300, or 1400°C) for 1 hr prior to the PXRD scan (30 minutes). Data was collected from 10-60° 2 θ on a Rigaku Ultima IV X-ray diffraction system in parallel beam geometry.

*Characterization by Transmission Electron Microscopy (TEM) Equipped with Energy Dispersive X-ray Spectroscopy (EDX), Raman Spectroscopy, and Dynamic Light Scattering (DLS).*

Size, composition, and morphology analyses of Si NP colloids were done by TEM, EDX spectroscopy, Raman spectroscopy and DLS. TEM and EDX were performed on an FEI Tecnai F-20 TEM operating at 200 kV. Aqueous samples were prepared by drop-casting concentrated solutions of purified (as described in the synthesis section) Si NPs in phosphate buffered saline (PBS, pH = 7.4) onto 400 mesh holey carbon coated, Cu grids (Ted Pella), which were dried in air at 100°C overnight prior to imaging. Point EDX spectra (collection time = 30-180 s) were collected on several spots within the same CTAB/Dec-Si NP micelle, as well as on several other micelles on the same TEM grid. HR-TEM was performed on the same instrument and the d-spacing reported herein is calculated from the intensity profile of a single Si NP (5 spacings were averaged) within a micelle. Raman spectroscopy was performed on a J-Y Lab RAM HR800 UV micro-Raman spectrometer using laser excitation at 532 nm. Aqueous samples were prepared by drop-casting concentrated solutions of purified Si NPs onto carbon tape adhered to glass slides. Sample films were deposited in air. DLS measurements were done on the

aqueous Si NP colloids using a Horiba LB-550 DLS instrument. Purified samples were diluted in syringe filtered nanopure water for measurement, and measurements were taken on serially diluted samples to ensure that size measurements were independent of multiple scattering effects.

*Characterization by Fourier Transform Infrared Spectroscopy (FT-IR) and Gel Electrophoresis.* To examine Si NP surfaces, FT-IR spectroscopy was performed on a ThermoFisher Nicolet iS10 infrared spectrometer in reflection geometry using a single bounce diamond attenuated total reflectance (ATR) accessory. Purified, concentrated colloids of the Si NPs were drop-cast and evaporated onto the ATR crystal to deposit a sample film for analysis. Gel electrophoresis was used to qualitatively determine the Si NP surface charge after CTAB coating or CTAB coating/PAA wrapping steps. An agarose gel (0.2% by weight) was made using TBE buffer (90 mM Tris, 90 mM borate, 4 mM EDTA) at pH 8.17 with 200 mM NaCl to enhance ionic strength. CTAB/Dec-Si NP and PAA/CTAB/Dec-Si NP solutions of different volumes (1-10 μL) were mixed with 5 μL of 50% glycerol, and the samples of varying concentration and surface charge were loaded into the wells in the center of the gel. Gels were run at 65 V for 1 hr and were photographed under a 302 nm light source.

*Steady State Photoluminescence Spectroscopy (PL) and Quantum Yield (QY) Measurements.* The emission properties of all Si NP colloids (H-Si NPs in hexanes, Dec-Si NPs in hexanes, CTAB/Dec-Si NPs in water, and PAA/CTAB/Dec-Si NPs in water) were examined using a Shimadzu-RF5310 PC spectrophotometer. Steady state emission

spectra were collected in the 350-750 nm range on suitably diluted, purified samples using excitation wavelengths varying from 250-400 nm. The instrument has a standard photomultiplier tube (PMT) detector (range 220-750 nm, wavelength accuracy ±1.5 nm), with diminished sensitivity over the red-to-NIR spectral region.

Quantum yield measurements were done on a Horiba Jobin Yvon FL3-21 spectrofluorometer for the CTAB/Dec-Si NPs in water and the PAA/CTAB/Dec-Si NPs in water. Emission spectra were collected in the 385-850 and 470-850 nm ranges at excitation wavelengths of 365 and 450 nm, respectively, using purified samples of suitable dilution and water as a reference. Also, excitation scans were performed over a ± 20 nm range about each excitation wavelength to determine sample and blank absorptivity. Both excitation and emission scans were obtained with the sample (in a quartz cuvette) placed inside the integrating sphere, both in and out of direct light excitation, and with a solvent (water) sample in direct light excitation. The resulting 6 data sets (sample excitation scan, in beam and out of beam; sample emission scan, in beam and out of beam; and water blank excitation and emission scans, in beam only) for each excitation wavelength were analyzed *via* two slightly different procedures previously reported[58,59] to give both absorbance and quantum yield values. The raw data sets were corrected for detector sensitivity (according to a system-specific calibration algorithm supplied by the instrument's manufacturer) and integrating sphere reflectance, as well as for the measured transmittances of various filters used in the beam paths and variations in the excitation beam intensities.

*Live Cell Microscopy of Si NP Internalization*. Murine neuroblastoma (N2a) cells were plated on 25 mm PDL-coated glass coverslips and cultured in medium containing 47.5% D-MEM, 47.5% Opti-MEM, and 5% FBS for 48 hrs at 37°C under a 5% $CO_2$ atmosphere. The cellular medium was aspirated and cells were incubated with a solution of CTAB/Dec-Si NPs in Opti-MEM solution, and then returned to the incubator for 1 hr. Afterwards, this solution was aspirated, and the cells were washed once with PBS, then transferred to an imaging chamber with Opti-MEM media for live cell imaging. Cells were imaged with a Zeiss Axiovert 200m epifluorescence microscope, fitted with an Andor iXON CCD camera, a stage and objective heater, an appropriate filter set (excitation: 350 nm +/- 25 nm, dichroic: 400 nm long pass, emission: 420 nm long pass), and an Apochromat 100x 1.4 NA oil immersion objective. Control cells were treated the same way except were not exposed to Si NPs. Images were minimally processed for background subtraction and brightness/contrast adjustment using the NIH freely-distributed software ImageJ.[60]

## 2.4 Results

### 2.4.1 Synthesis of Red-emitting, Water Soluble Si NPs.

The synthesis of hydride-terminated Si NPs *via* disproportionation of solid-state silicon rich oxides (O:Si ratio, less than 2:1), polymeric alkyl or hydrido-silicates, or molecular alkyl or hydrogen silsesquioxanes (O:Si ratio, 1.5:1) has been previously reported.[8,23,41,57,61,62] Briefly, silicon rich oxide precursors, particularly those of stoichiometry O:Si 1.5:1, [23,41,57,61,62] are known to undergo thermodynamic disproportionation at elevated temperatures (*e.g.*, 900 to 1500°C), producing nanoscale Si

domains encapsulated in an amorphous silica matrix. Such a reaction is usually done by heating a Si-rich oxide precursor under flowing forming gas (*e.g.*, 10% $H_2$ in $N_2$), although qualitatively the same product is obtained using inert ($N_2$ or Ar) or vacuum atmosphere, according to our comparative results (using hydrolysis trichlorosilane polymer as a precursor in these atmospheres, results not shown).

For all Si NP syntheses reported herein, trichlorosilane was used as the silicon source. The trichlorosilane was first hydrolyzed and polycondensed to produce a polymeric sol-gel hydrosilicate precursor of putative stoichiometry O:Si = 1.5:1,[57] which was subsequently subjected to various heating schemes under flowing $N_2$. Though the subtle differences in reaction product as a function of heating scheme are beyond the scope of this paper (and have been covered elsewhere),[62] in general we have observed that longer heating times and higher reaction temperatures facilitate the disproportionation reaction. For example, as shown in Figure 2.1, heating the $(HSiO_{1.5})_n$ polymer at 1100°C (here under vacuum, *in situ* measurement) for 1 hr does not produce crystalline Si domains, while crystalline domains are observed at the end of 1 hr using a reaction temperature of 1400°C. However, using longer reaction times, usually 10 hrs or longer, the crystalline Si domains can be generated at 1100°C (see characterization of product synthesized at 1100°C below), a temperature achievable in standard laboratory tube furnaces. It should be noted that the as-synthesized, solid state product containing the nanoscale Si domains is red-emissive under 365 nm excitation, regardless of heating parameters and prior to liberation from the oxide matrix.

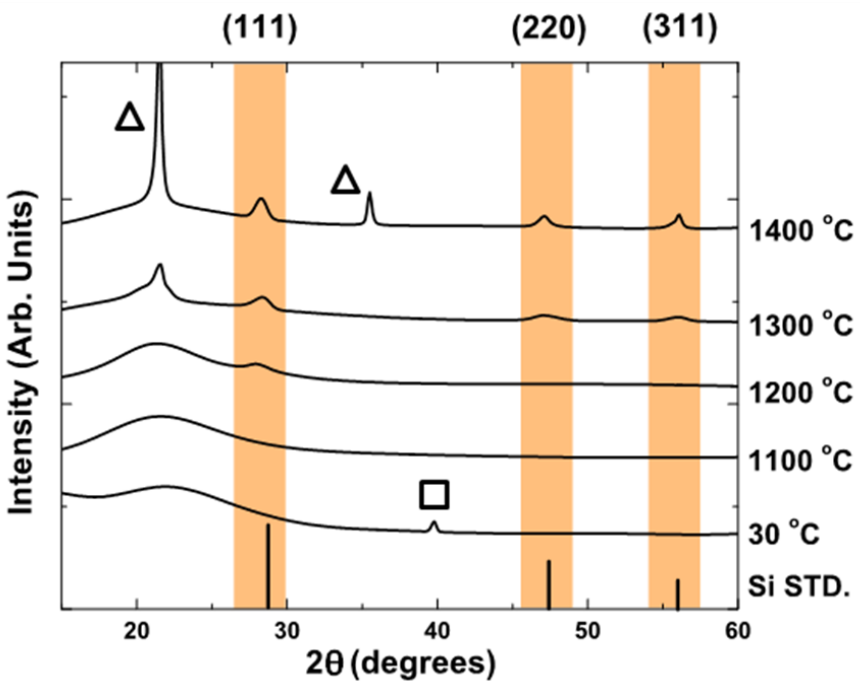


**Figure 2.1** *In situ* variable temperature PXRD study of the disproportionation of $(HSiO_{1.5})_n$ precursor to produce nanocrystalline Si domains. Vertical reflection markers are the calculated reflections for bulk silicon and highlighted regions are added to guide the eye. □ and Δ are sample holder (Pt) background and $SiO_2$, reprectively.

The crystalline, nanometer-sized Si domains generated in the disproportionation of the $(HSiO_{1.5})_n$ polymeric precursor at 1100°C were liberated from the oxide host *via* a wet chemical etch (*i.e.*, with HF/EtOH/$H_2O$) to result in red-emitting, hydride-terminated Si NPs ($\lambda_{max,em}$ = 580 nm, Figure 2.2 (a); full spectrum, Figure 2.3(a)) that can subsequently be surface functionalized by thermal, photochemical, or chemically initiated hydrosilylation with a variety of terminal olefins. The neat Si NPs, as extracted from the aqueous ethanol/HF etching solution, were shown to have hydride-surface termination by FT-IR spectroscopy. The Si-H stretching, deformation, and bending modes[63,64] are

observed at 2093, 958, and 617 $cm^{-1}$, respectively (Figure 3a), and little indication of surface oxide formation (as indicated by the Si-O-Si region, 1000-1100$cm^{-1}$)[65] during the etching step is observed.

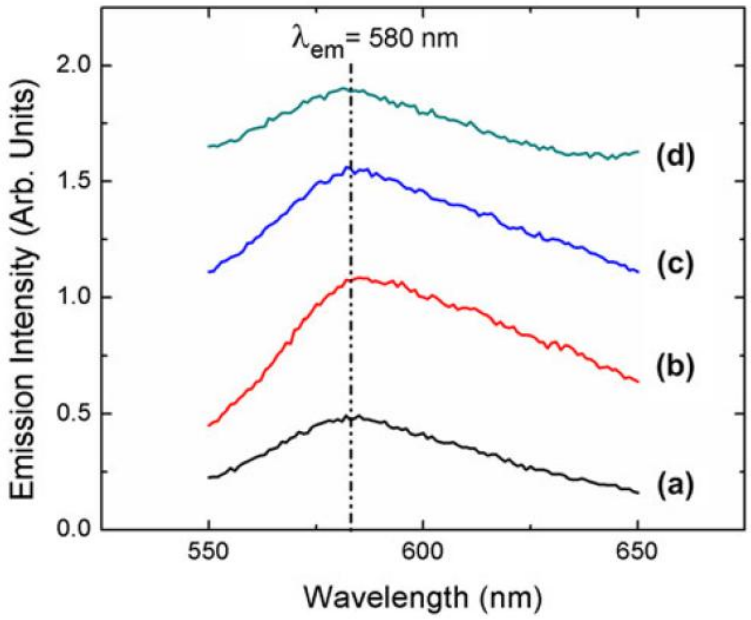


**Figure 2.2** Emission spectra of (a) H-Si NPs (in hexanes), (b) Dec-Si NPs (in hexanes), (c) CTAB-coated/Dec-Si NP micelles (in water), and (d) PAA-wrapped/CTAB-coated/Dec-Si NP micelles (in water). Excitation is at 340 nm. Only the red spectral region is shown.

However, we have observed unpredictable changes in the photoluminescene of the Si NPs (usually dramatic blue shifts, data not shown) when terminal alkenecarboxylic acids, alkeneamines, and alkenethiols are used in hydrosilylation reactions, but preservation of the initial red photoluminescence when terminal alkenes and alkynes are used as capping agents. Because water-solubility with preservation of red emission could not be directly

achieved *via* hydrosilylation with bifunctional terminal alkenes (*i.e.*, having a second, reactive functional group to impart hydrophilicity), 1-decene was used to cap the Si NP surfaces, followed by a surface coating step with surfactant, to achieve water-solubility with preservation of red-emission ($\lambda_{max,em}$ = 580 nm, Figure 2.2 (b), (c) and Figure 2.3(b), (c)).

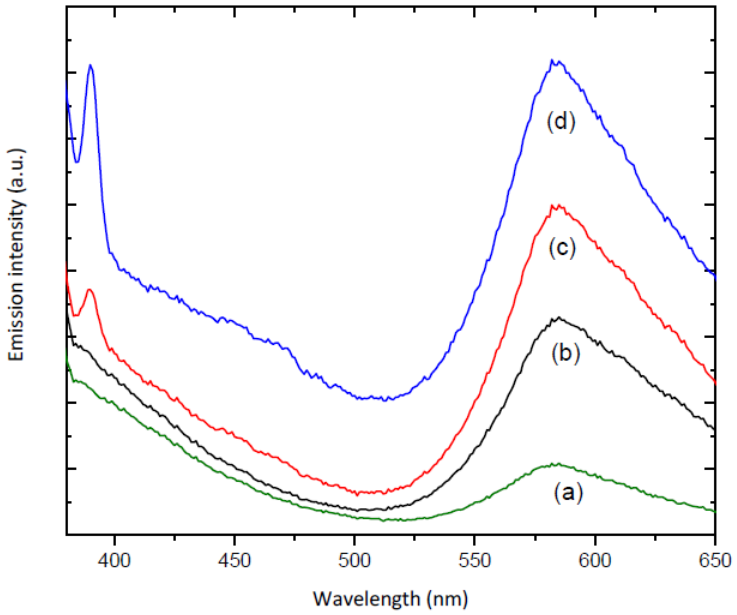


**Figure 2.3** Photoluminescence spectra of (a) H-Si NPs, (b) Dec-Si NPs, (c) CTAB/Dec-Si NPs, (d) PAA/CTAB/Dec-Si NPs at excitation wavelength 340 nm. The data collected over the entire rouge 375-650nm is shown, where emission intensity at shorter wavelength can also be scan ($< \lambda_{max}$ = 580nm)

FT-IR was used to examine the Si NP surface changes after hydrosilylation (Figure 2.4(a), before;(b), after): loss of the Si-H stretch at 2093 $cm^{-1}$ is clearly observed; the Si-H deformation and bend features (958 and 617 $cm^{-1}$) are also lost with new peaks

in these regions characteristic of decene (perhaps due to excess capping agent) at ~625, ~725 and ~900 $cm^{-1}$. The success of the hydrosilylation reaction to result in partially Si-C terminated surfaces is indicated by the appearance of an Si-C stretch at 1256 $cm^{-1}$, other weak features characteristic of decane/decane in the 1300-1600$cm^{-1}$ region, and the strong $CH_x$ features between 2800-3000 $cm^{-1}$. It is worth noting that the surface is not significantly oxidized during the hydrosilylation reaction; only weak intensity in the 1000-1100 $cm^{-1}$ region is observed. Furthermore, after hydrosilylation, the Si NP surfaces appear to be partially hydroxylated as indicated by the Si-OH stretch at 800 $cm^{-1}$.[64,66]

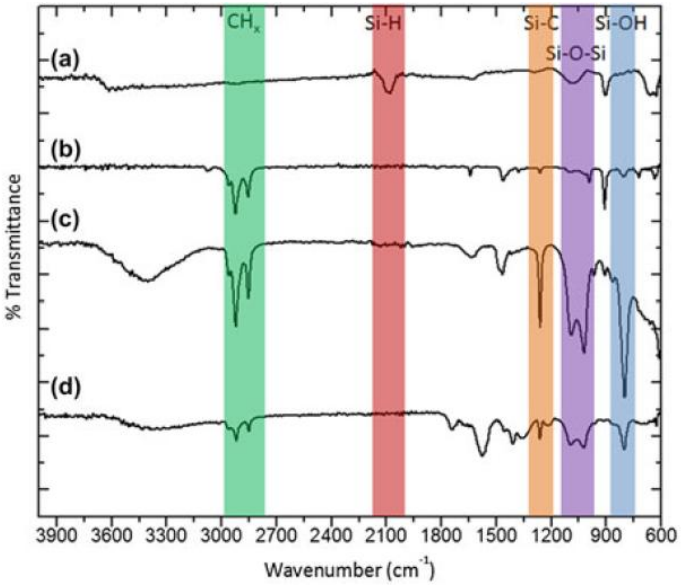


**Figure 2.4** FT-IR spectra of freshly prepared (a) H-Si NPs, (b) Dec-Si NPs, (c) CTAB/Dec-Si NPs, and (d) PAA/CTAB/Dec-Si NPs. $CH_x$ (green), Si–H (red), Si–C (orange), Si–O–Si (purple), and Si–OH (blue) regions are highlighted and labeled.

As described by Mazumder *et al*., a surfactant that intercalates hydrophobic chains on NP surfaces and is weakly bound to the NP by hydrophobic interactions can be used for phase transfer.[67] Thus, the hydrophobic, red-emitting, decane-terminated Si NPs (Dec-Si NPs) were made water-soluble through a surfactant mediator and phase transfer reagent *via* alkyl chain self-assembly (see Scheme 2.1). Cetyl-trimethylammonium bromide (CTAB) has a hydrophobic tail and a hydrophilic quaternary ammonium head group with a net-positive charge, making it an ideal surfactant to phase transfer hydrophobic, alkyl chain-terminated NPs into aqueous media. An intermolecular, hydrophobic interaction between CTAB and the decane-terminated Si NPs (previously dispersed in hexanes) occurs to generate water-soluble Si NPs (Figure 2.5), with the CTAB hydrophobic tail apparently intercalating the decyl chains on the Si NP surfaces leaving the quaternary ammonium head groups exposed to water, thus resulting in colloidally stable, water-soluble Si NP micelle assemblies [Figure 2.6 (a), (b)] with emission $\lambda_{max}$ preserved at 580 nm [Figure 2.2 (c) and Figure 2.3(c)]. It should be noted that the measured pH values of as-prepared (after purification), aqueous CTAB/Dec-Si NP solutions are consistently 6.5±0.5, and that, in general, the particles can be taken to dryness and re-dispersed in other aqueous solutions (*e.g.*, phosphate buffered saline (PBS) buffer).

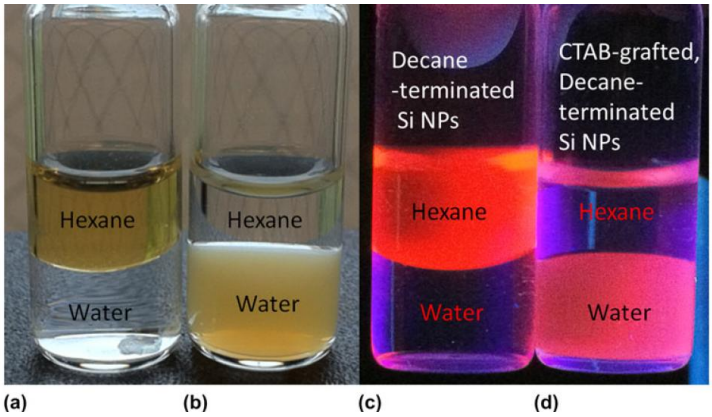


**Figure 2.5** Digital photographs of vials under ambient light [(a) and (b)] and 365-nm light [(c) and (d)] showing phase transfer of the Dec-Si NPs from hexanes to water after micelle encapsulation by CTAB. (a) and (c) are Dec-Si NPs before phase transfer, (b) and (d) are CTAB/Dec-Si NP micelles after phase transfer.

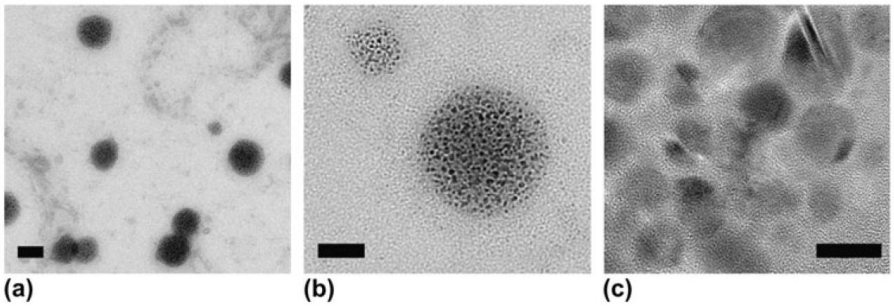


**Figure 2.6** TEM images of CTAB/Dec-Si NP micelles. Scale bars: (a) 100 nm, (b) 50 nm, and (c) 5 nm.

The Dec-Si NPs, with an average size of 5.14 $\pm$ 1.46 nm (based on the TEM analysis of over 1000 individual Si NPs in the CTAB/Dec-Si NP micelles, data not shown), are observed to be clustered within the micelles. The CTAB/Dec-Si NP micelles were found to have a very polydisperse size distribution, based on dynamic light

scattering (DLS) measurements. The effective diameter of the micelle assemblies by DLS was found to be 123.7 $\pm$ 96.1 nm (Figure 2.7). The morphology of freshly prepared CTAB/Dec-Si NPs, as seen by TEM, is shown in Figure 2.6 (a). and (b). Such assembles have been observed by Erogbogbo *et al*., who have also reported a hydrophobic chain interaction to generate micellar Si QDs.[13,68] HR-TEM [Figure 2.6 (c)] shows the high crystallinity of the Si NP cores within the micelles; inspection of the intensity profile for a single, individual Si NP revealed a lattice spacing of 0.31 ± 0.2 nm, consistent with the (111) plane spacingof diamond lattice, cubic Si (JCPDS card no.: 27-1402). Energy Dispersive X-ray spectroscopy (EDX) on a large CTAB/Dec-Si NP micelle (shown in Figure 2.8) reveals the presence of C, O, Cu (grid), Br, Si, P (from PBS), Cl (from PBS), and K (from PBS). Despite high elemental counts for the buffer components P, K, and Cl that were expected to be part of the diffuse micelles, Si and Br belonging to the particle and CTAB surfactant, respectively, are observed. This is consistent with CTAB-coated, decane-terminated Si NPs, where $Br^-$ is likely electrostatically associated with the positively charged micelles. The high counts from C may be attributed to a combination of the carbon grid coating, the decane surface terminating groups of the Si NPs, and likely, from CTAB coated on the Si NPs. High counts from O may be attributed to trace atmospheric oxygen and water molecules associated with the micelle. Some O counts may be due to partial oxidation or –OH passivation of the Si NP surface, which is better discerned using infrared spectroscopy (see below). Finally, while it is expected that the micelles would contain N from the polar CTAB head group, the counts from the Si NP micelles relative to the grid materials are low, thus the small expected amounts from N

may be undetectable against this background. Furthermore, the high O and C counts may hide the weak N signal, since the N signal should be observed between these two.

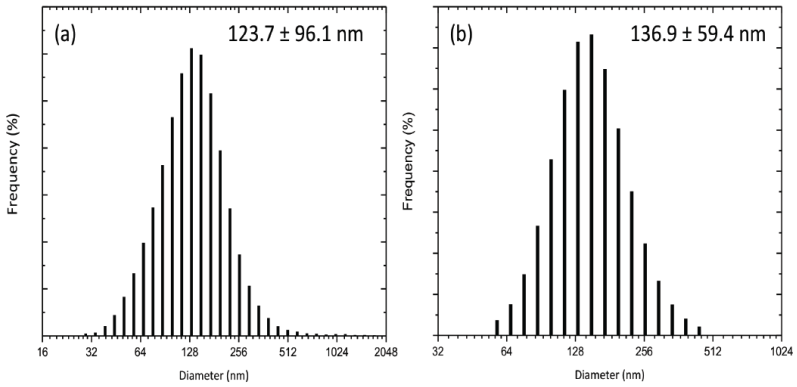


**Figure 2.7** DLS analysis of (a) CTAB/Dec-Si NP and (b) PAA/CTAB/Dec-Si NP micelle size distributions.

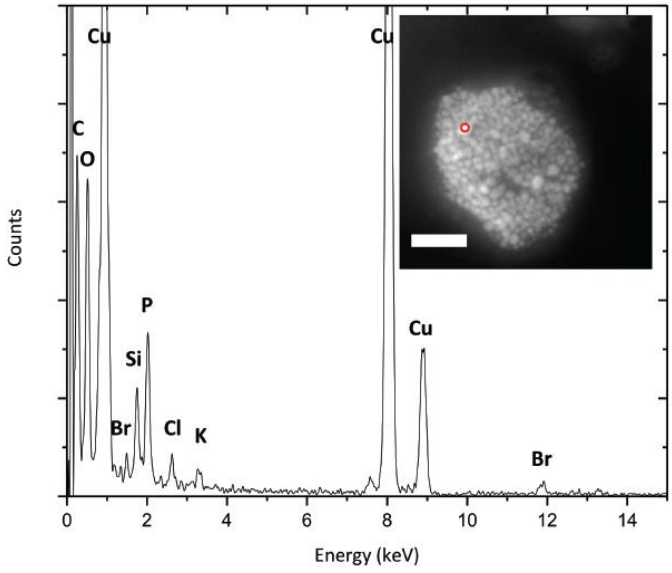


**Figure 2.8** Point EDX spectrum of CTAB/Dec-Si NPs micelles. Inset: Dark field STEM image of a CTAB/Dec-Si NP micelle, scale bar 100 nm.

Once coated with CTAB, a broader feature (relative to that in the Dec-Si NP spectrum that is assigned to the decyl chain) is observed in the FT-IR spectrum [Figure 2.4 (c)] at ~1500 $cm^{-1}$, which is likely due to CTAB C-C features superimposed on the decyl chain C-C features. Other weak intensity vibrations characteristic of CTAB are observed in the 875-1000 $cm^{-1}$ region. Comparing the relative intensities of the Si-C (1256 $cm^{-1}$), Si-O-Si (1000-1100 $cm^{-1}$), and Si-OH (800 $cm^{-1}$) features for the Dec-Si NPs *versus* the CTAB/Dec-Si NP micelles, the number and type of ligands on the Si NP surfaces appear not to have substantively changed during the CTAB coating step. There is, at best, a modest increase in the degree of Si-OH surface termination. A new broad feature between 3000-3600 $cm^{-1}$ can be assigned as a combination of water molecules part of the micelles, N-H stretches from CTAB, and SiO-H bond stretches.[64, 66] Raman spectroscopy was also performed on a macroscopic sample of the CTAB/Dec-Si NPs (Figure 2.9). The maximum vibration band was found at 515 $cm^{-1}$, which can be assigned as the Si-Si vibration of elemental Si, consistent with the results of TEM. The slight Raman blue-shift from the bulk Si-Si vibration of 516 $cm^{-1}$ has been observed for other Si NPs,[69] and has been attributed to the small domain size of nanocrystalline Si. The Raman spectrum, of the CTAB/Dec-Si NPs also shows a weaker intensity Si-O vibration centered at 493 $cm^{-1}$, which is in agreement with the FT-IR and EDX results in that the Si NPs do show some degree of surface oxidation/hydroxide passivation following the alkyl chain self-assembly and phase transfer into water.

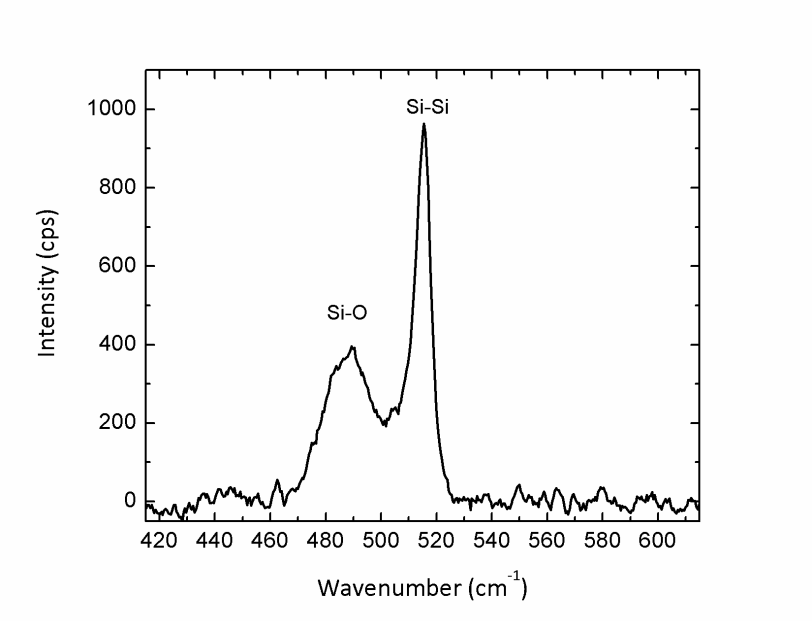


**Figure 2.9** Raman spectrum of freshly prepared CTAB/Dec-Si NP micelles.

It should be noted that in adding CTAB to accomplish phase transfer, we have experimentally observed that the amount of CTAB required for aqueous nanocrystal stabilization (*i.e.*, colloidal stabilization) is variable, depending on whether larger or smaller micelles are desired. We have been able to produce aqueous, single Si NPs using variations of the method presented in this work, using a smaller excess of CTAB. However, these particles, while equally colloidally stable, are less photophysically stable with respect to the red emission (*i.e.*, a blue shift of the emission $\lambda_{max}$, originally at 580 nm, is observed within several hrs after phase transfer to water, data not shown). No attempts were made to optimize the micelle size by optimizing the excess of CTAB used. The ratio used herein consistently yielded CTAB/Dec-Si NP micelles with persistent red emission (> 6 months) in water.

Taking advantage of the net-positive charge on the CTAB/Dec-Si NP micelles, polymer wrapping with sodium polyacrylate was also done to modify the surface charge from net positive to net negative and to provide reactive carboxylate groups for future addition of biological recognition groups. With negatively charged carboxylate groups that can interact with the positively charged CTAB/Dec-Si NP micelles, an electrostatic interaction causes PAA to wrap around the CTAB/Dec-Si NPs without precipitation. The PAA-wrapped-CTAB-coated, decane-terminated Si NPs (PAA/CTAB/Dec-Si NPs), as analyzed by DLS [Figure 2.7 (b)], were ~ 13 nm larger in diameter than the CTAB/Dec-Si NPs, supportive of PAA polymer shell encapsulation of the CTAB/Dec-Si NP micelles. As expected with a change in micelle diameter but not in Si NP core diameter or Si NP surface ligand identity (see FT-IR results below), the PAA/CTAB/Dec-Si NPs were also shown to have a persistent red emission in water [emission $\lambda_{max}$ = 580 nm, Figure 2.2 (d) and Figure 2.3(d)] for several months. When wrapped in PAA, changes are observed in the FT-IR spectrum [Figure 2.4 (d)], when compared to the FT-IR spectrum of the unwrapped micelles [Figure 2.4 (c)]. New features characteristic of polyacrylic acid/polyacrylate are observed between 1300-1450 $cm^{-1}$, at ~1550 $cm^{-1}$ ($COO^-$), and at ~1725 $cm^{-1}$ (COOH); otherwise the spectrum is unchanged in its gross features.

To illustrate the difference in surface charge between the CTAB/Dec- and PAA/CTAB/Dec-Si NPs, gel electrophoresis was used, and the particle migration under an applied voltage was followed using a handheld UV lamp ($\lambda_{ex}$ = 302 nm, Figure 2.10). As colloidal dispersions in buffer at pH ~ 8, CTAB/Dec- and PAA/CTAB/Dec-Si NPs of varying concentrations were loaded into different wells of an agarose gel. When a current

was applied, migrations to oppositely charged electrodes were observed *via* the red Si NP fluorescence signal: the CTAB/Dec-Si NPs migrated toward the negative electrode, consistent with a net positive surface charge, while the PAA/CTAB/Dec-Si NPs migrated toward the positive electrode, consistent with a net negative surface charge. These results confirm the success of each surface modification step and are consistent with the predicted positive and negative surface charges owing to the CTAB and PAA functional groups, respectively, at pH = ~8.

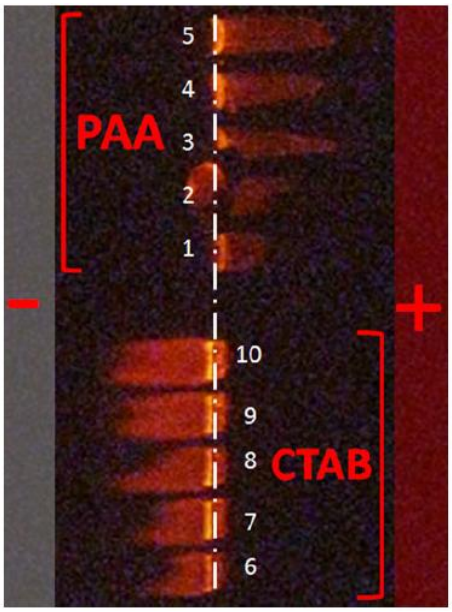


**Figure 2.10** Gel electrophoresis of PAA/CTAB/Dec-Si NPs (from lane 1 to 5, increasing concentration) and CTAB/Dec-Si NPs (from lane 6 to 10, increasing concentration). The positions of the positive (+) and negative (⁻) electrodes are indicated.

### 2.4.2 Stable red emission of Si NPs in live cells under physiological conditions.

Bright, fluorescent Si NPs have been employed as *in vivo* imaging agents and advanced tools for molecular tracking over the past 10 years.[5,13] The biocompatible

nature of fluorescent Si NPs[13] makes them ideal probes for live cellular and small animal studies involving molecular tracking, particularly for temporal studies if their emission properties are stable. For example, Rosso-Vasic *et al*. have reported that positively-charged, blue emitting, amine-terminated Si NPs are internalized by the murine cell line BV2.[15] However, red-to-NIR emitting particles are more relevant for *in vivo* applications, since these long emission wavelengths are capable of penetrating tissues, thus facilitating imaging of dense biological samples. Additionally, autofluorescence due to cellular components and common components of cellular media (*e.g.* flavins) is greatly diminished when observing fluorescence in the red-to-NIR region, resulting in a high signal-to-noise ratio.

In Figure 2.11(a)-(c) control images show murine neurobalstoma (N2a) cells that were not exposed to Si NPs. These control images demonstrate the advantage of using a filter set appropriate for red or NIR fluorophores in that practically no fluorescent signal from the cells/media is observed. Figure 2.11(d)-(f) shows images of cells that were exposed to CTAB/Dec-Si NPs. These images demonstrate the ability of these cells to internalize the positively charged CTAB/Dec-Si NP. The bright fluorescence signal, originating from red-emitting CTAB/Dec-Si NPs, is densely distributed throughout the cell, only being excluded from the nucleus. Exclusion from the nucleus is expected due to the capacity of the cell to tightly regulate transport into and out of this important organelle. These internalized Si NPs retain bright red photoluminescence, even from

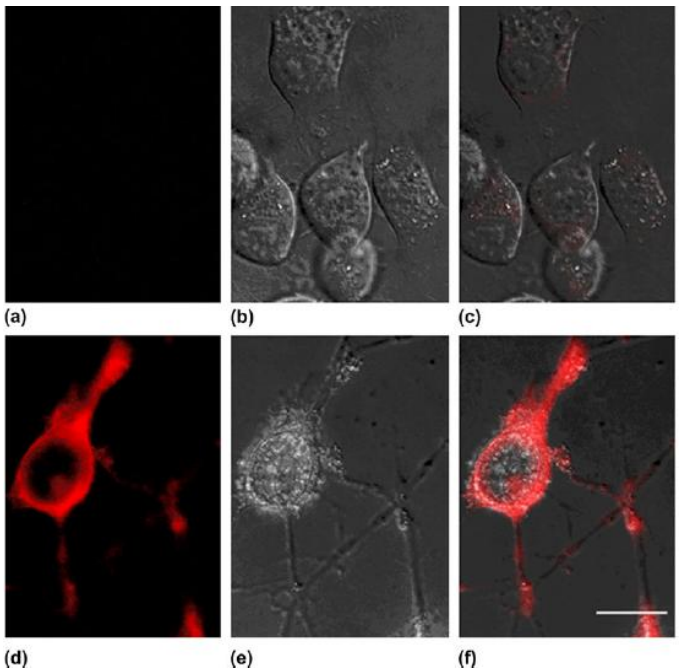


**Figure 2.11** Fluorescence microscopy study of control N2a cells [(a), (b), and (c)] and. N2a cells incubated with CTAB/Dec-Si NPs [(d), (e), and (f)].(a) and (d) are fluorescence microscopy images, (b) and (e) are differential interference contrast (DIC) images, and (c) and (f) are overlaid fluorescence and DIC images. Scale bar for all images (a-f) = 10 μm.

within the cellular interior, demonstrating that the micellar, hydrophobically protected Si NPs in a physiological environment have appropriate spectral characteristics for biological imaging (see Discussion of conditions which destroy the micelles and result in loss of red PL below). Though the ~100 nm micellar CTAB constructs and the PAA-coated micellar CTAB constructs we report herein are relatively large for use as practical biological fluorophores, optimized syntheses may produce smaller and less polydisperse micelles with similar, stable aqueous red emission properties. Ultimately however, inorganic shell passivation may provide better protection of Si NPs against water, as well as the ability to functionalize for water solubility and bioconjugation, while making the

size more appropriate (*e.g.*, a 4-5 nm Si NP, with a 2 nm ZnS shell is approximately 12-15 nm in diameter) for biological fluorescence assays. Furthermore, it should be noted that CTAB is widely known to be cytotoxic, and that in our ongoing work we have found that more biocompatible lipids can be used for phase transfer to achieve micelles with similar photophysical properties to the particles reported herein.

### 2.4.3 Effect of pH on aqueous Si NP photoluminescence.

The photoluminescence (PL) properties of the CTAB/Dec-Si NPs were also assessed in varying pH environments. TEM images, FT-IR spectra, and PL spectra for aqueous CTAB/Dec-Si NPs adjusted to pH = 3.3 or 12.3 (Figures 2.13 and 2.14) were compared against the corresponding data [Figures 2.2(c), 2.3(c), 2.4 (c), 2.6 (a)-(c), 2.12) for the as-prepared, aqueous solutions (following dialysis), which were at pH ~7, to correlate morphology and/or surface changes to PL changes as a function of pH and time. In neutral solutions the red at first and then up to 90 days at which point repeat measurements were ceased. In strongly acidic conditions (pH = 3.3), the CTAB/Dec-Si NPs maintain a persistent red emission for over 180 days, both visually [Figure 2.13 (a), (b)] and spectroscopically [Figure 2.14 (a)], with $\lambda_{max,em}$ = 580 nm when excited at 370 nm, similar to the photoluminescence behavior of CTAB/Dec-Si NPs at pH ~ 7[Figures 2.2 (c), 2.3 (c), 2.12; Note: PL data in Figure 2.2 and Figure 2.3 correspond to excitation at 340 nm, rather than 370 nm, but the red $\lambda_{max,em}$ is at 580 nm using either excitation wavelength]. By contrast, in strongly basic conditions (pH = 12.3), the emission of the CTAB/Dec-Si NPs changes drastically and rapidly. Within three days, the observed emission color has changed from red to blue [visually, Figure 2.13 (c), (d)] with a new

$\lambda_{max,em}$ at 488 nm when excited at 370 nm [Figure 2.14 (a)]. The blue emission also remains qualitatively unchanged over the course of 180 days. Unlike the red emission, which changes in intensity but not lambda max with changing excitation wavelength (data not shown), the blue emission changes substantively in both intensity and peak position with changing excitation wavelength (Figure 2.15 (b)).

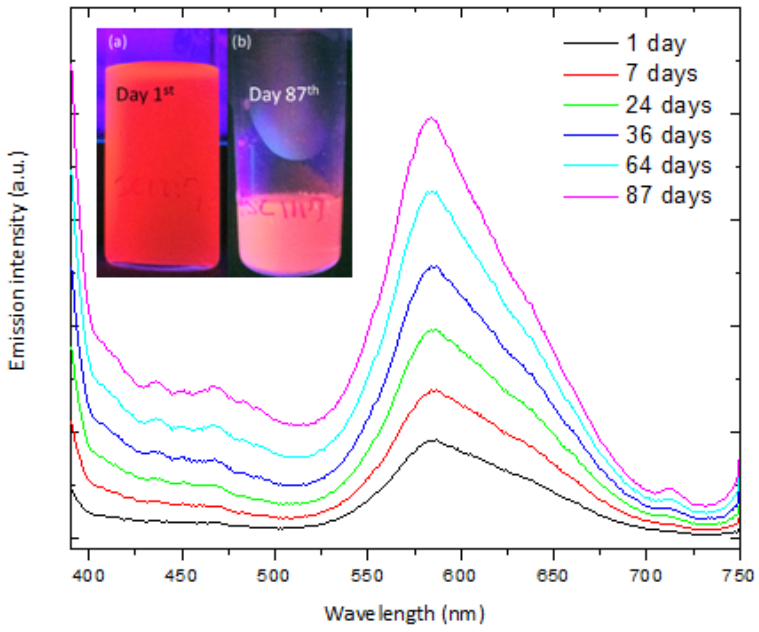


**Figure 2.12** PL spectra of CTAB/Dec-Si NPs collected a1, 7, 23, 36, 64, 87 days following synthesis using an excitation of 370 nm. Inset: UV-illuminated inspection of aqueous CTAB/Dec-Si NPs (a) on day 1 after synthesis, and (b) on day 87.

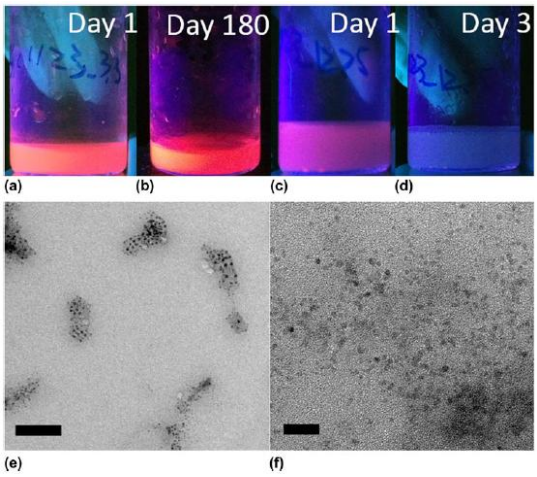


**Figure 2.13** (a) As-prepared (day 1) CTAB/Dec-Si NPs at pH = 3.3, (b) CTAB/Dec-Si NPs at pH = 3.3 after 180 days, (c) as-prepared (day 1) CTAB/Dec-Si NPs at pH = 12.3, (d) CTAB/Dec-Si NPs at pH = 12.3 after 3 days, and (e) TEM image of CTAB/Dec-Si NPs from a pH = 3.3 solution, and (f) TEM image of CTAB/Dec-Si NPs from a pH = 12.3 solution. Scale bars: (e) 50 nm, (f) 20 nm.

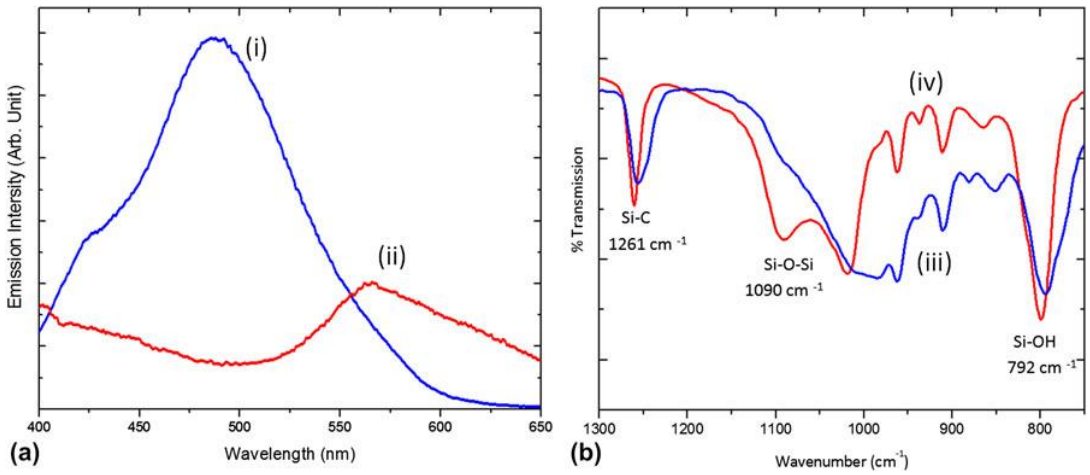


**Figure 2.14** (a) Emission profile (370-nm excitation) of CTAB/Dec-Si NPs at pH = 12.3 (blue trace, i) and pH = 3.3 (red trace, ii), and (b) corresponding FT-IR spectra of CTAB/Dec-Si NPs at pH = 12.3 (blue trace, iii) and pH = 3.3 (red trace, iv).

Since CTAB is simply coated on or intercalated with the decane-surface groups of the Si NPs, it is possible that electrostatic interactions between the positively-charged CTAB and negatively-charged hydroxide ions may have occurred in the very basic solution. Such an effect has been previously observed for nanovalves synthesized in the presence of CTAB.[70] Liu *et al*. report that as the pH and deprotonation of the solvent increases, the electrostatic interaction between CTAB and $OH^-$ ions is significant enough to remove CTAB from the surface, causing the nanovalve to open. For the as-synthesized CTAB/Dec-Si NPs presented herein, a similar result may be expected: if the CTAB becomes de-intercalated from within the decane chains under basic conditions, this would result in gaps along the protective layer, thus exposing the Si NP surface to water and/or hydroxide that can passivate unsaturated surface sites, remove alkyl surface passivation, partially or wholely dissolve the Si NPs, or otherwise corrode the Si NP surfaces.

TEM was used to analyze the morphology of the CTAB/Dec-Si NP micelles after exposure to acidic or basic conditions, and as shown in Figure 2.13 (e), (f), particles exposed to basic conditions no longer maintain the micellar structure [Figure 2.13 (f)], whereas the micelles are preserved (from near neutral pH solutions, see Figure 2.6 for comparison) at acidic pH [Figure 2.13 (e)]. The breakdown of the micellar structure can cause the Si NP surfaces to be more susceptible to oxidation, other passivation, surface re-construction, or dissolution (partial or whole), although, with respect to the latter, the Si NPs after breakdown of the micelles in base are still abundant in number, not significantly different in size, and still contain crystalline cores (see HR-TEM image, Figure 2.15 (a)). Furthermore, evidence for retention of $Si^0$ cores at high pH also comes

from the photoluminescence spectra, which show an excitation wavelength dependence of $\lambda_{max,em}$ (Figure 2.15) that others have reported as characteristic of aqueous, blue-emitting particles that have been confirmed to contain nanoscale $Si^0$ domains.

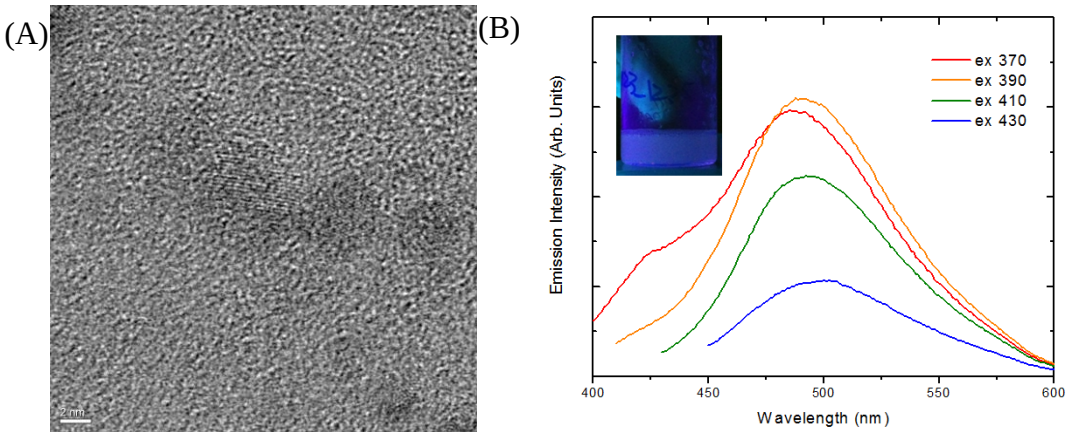


**Figure 2.15** (A): HR-TEM image of Si NPs at pH = 12.3 showing crystallinity (lattice fringes); (B): PL spectra of CTAB/Dec-Si NPs at pH = 12.3. Inset: UV-illuminated inspection of CTAB/Dec-Si NPs.

While there are not significant differences in the sizes of individual Si NPs regardless of pH, the FT-IR spectra of these pH adjusted samples [Figure 2.14 (b)] indicates a large difference in the degree of surface oxidation/hydroxide passivation in acidic *versus* basic media. While both the Si-O-Si and Si-OH features are observed for the CTAB/Dec-Si NP micelles regardless of pH [Figures 2.4 (c), (pH ~ 7), and 2.14 (b), (red, pH = 3.3; blue, pH =12.3)], the breath of both features is greater in highly basic *versus* highly acidic or near neutral media, suggesting a greater number and variety in the various Si-O surface bonding environments with greater accessible Si NP surface area in aqueous base. FT-IR spectroscopy is thus supportive of the hypothesis that electrostatic

interaction between CTAB and hydroxide essentially deprotects the Si NP surfaces, making them more susceptible to formation of Si-O bonds. Conversely, the FT-IR spectrum of the CTAB/Dec-Si NPs at pH = 3.3 [Figure 2.14 (b)] does not show a significant difference in the Si-O-Si and Si-OH regions as compared to the FT-IR spectrum of the CTAB/Dec-Si NPs in neutral water [Figure 2.4 (c)]. The qualitative behavior of the PAA/CTAB/Dec-Si NPs as a function of pH is the same as that of the unwrapped CTAB/Dec-Si NPs (not shown).

## 2.5 Discussion

### 2.5.1 Photoluminescence Properties of Water Soluble Si NPs: Consequences of Protecting Against Surface Passivation by $OH^-$ and $H_2O$ in Preservation of Aqueous, Red Photoluminescence

We have shown persistent, red emission (> 6 months) from aqueous Si NPs encapsulated in sufficiently large micelles, on the order of 100 nm in size. We have also observed a rapid onset of blue emission (< 3 days) intensity with commensurate loss of red emission intensity for single Dec-Si NPs rendered hydrophobic by CTAB coating (data not shown) and we have shown herein a similar, rapid (< 3 days) red to blue photoluminescence change when the large CTAB/Dec-Si NP micelles are destroyed by base. These results demonstrate the importance of protecting Si NPs against water and hydroxide in achieving persistent red emission in aqueous media. It should be noted that for the ~100 nm, micellar CTAB/Dec-Si NPs reported herein there is a gradual intensity increase in the blue region (400-500 nm) in neutral to acidic pH solutions (see Figure 2.14, which is at pH ~7), indicating that even with the micellar constructs intact, the presumably diffuse

hydrophobic organic shell around the Si NPs is somewhat permeable to $H_2O$ and $OH^-$, which is consistent with other reports of somewhat long-term stable red emission from micellar Si NPs. [13,22,68] Despite the gradual increase in blue emission intensity over time, we observe that the red emission event remains dominant over the blue emission event for prolonged periods, likely because the majority of particles are well-protected from $H_2O$ and $OH^-$ within the interior of the large, intact micelles. However, although the diffuse organic shell provides reasonable protection against further $H_2O$ and $OH^-$ reaction with Si NP surfaces, an epitaxially grown inorganic shell should ultimately provide better long-term surface protection, and thus more stable emission properties, and we are examining this in our ongoing work.

While our data show the consequences of protecting Si NPs against water and hydroxide in achieving persistently red, aqueous emission, they do not fully explain the origin of the red emission, the origin of the blue emission, or the reason for the observed red-to-blue photoluminescence change. However, recent literature reports have suggested that either slow, unintended surface oxidation of Si NPs or passivation of Si NP surfaces by coordinating solvents or ligands (*e.g.*, water or hydroxide), result in a blue emission due to formation of emissive Si-O surface states.[28, 29, 49] Our FT-IR and accompanying PL data indicate that the blue emission is likely not originating due to the formation of states associated with pure surface oxide, consistent with prior reports of stable red emission from purposefully oxidized Si NPs,[5, 40 30] since red emission is observed here alongside significant indications of surface oxidation. Our data are not contra-indicated with previous suggestions that strong blue PL from Si NPs results from

localized Si-OR states lying outside the Si NP band gap, since we have observed that at low to neutral pH, samples exhibiting a lesser degree (relative to their basic counterpart) of Si-OH bonding features characteristic of water or hydroxide surface passivation remain red-emitting, while at high pH a large increase in the degree of Si-OH bonding is observed and is accompanied by a rapid emission color change from red to blue. However, it is also possible that Si-OH surface bonding deactivates or destroys a red emission pathway, *versus* activating or creating a blue emission pathway, or that invasive corrosion, dissolution, or surface reconstruction of the Si NPs by $H_2O$ or $OH^-$, *versus* simple surface passivation by these species, results in the formation of a competitive, blue emissive state. We are examining these and other reasonable origins of the red and blue photoluminescence events in our ongoing work.

### 2.5.2 Photoluminescence Properties of Water Soluble Si NPs. Quantum Yield and Detector Sensitivity

In addition to photoluminescence emission scans done on a standard laboratory fluorimeter (light collection from the sample only at 90° to the incident angle), we also measured emission quantum yields for the aqueous Si NPs using an instrument having an integrating sphere (light collection from the sample over a sphere, with the sample both in and out of direct light excitation). Both instruments have photomultiplier tube detectors; the latter has an instrument specific algorithm to correct for the variable wavelength sensitivity of the detector, while the former currently does not. The two instruments, consequently, give qualitatively the same raw emission spectra, but slightly different processed emission spectra, as we discuss below.

The peak of the emission spectrum for the CTAB/Dec-Si NPs using a 365 nm excitation and after correcting for both background and detector sensitivity is at 740 nm [Figure 2.16 (a)], *versus* at 655 (not shown) in the uncorrected data, which is greatly red shifted as compared to the observed emission $\lambda_{max}$ at 580 using the 340 nm and 370 nm excitation lights of the traditional laboratory instrument without detector sensitivity correction. For the most part, sensitivity of a photomultiplier tube detector steeply decreases over the emission wavelength range of 555-850 nm, which is consistent with the large, observed red-shift of $\lambda_{max,em}$ in the raw *versus* processed data when a detector sensitivity correction is applied. It should be noted that the two instrument detectors also vary in their sensitivity and operable wavelength range, enough to produce differences in the raw emission data. However, this result shows that the CTAB/Dec-Si NPs also have considerable NIR fluorescence intensity, which spans a wavelength range of over 200 nm [FWHM = 185 nm, Figure 2.16 (a)]. The absolute quantum yield of the CTAB/Dec-Si NPs was determined to be 4.8 ± 0.1% when excited at 365 nm and 3.9 ± 0.2% when excited at 450 nm. The $\lambda_{max,em}$ at 740 nm does not substantively change as a function of excitation wavelength, which we also observe using the standard laboratory instrument. The PAA/CTAB/Dec-Si NPs also have an emission $\lambda_{max}$ at 740 nm [Figure 2.16 (b)] when excited at 365 nm. The absolute quantum yield of the PAA/CTAB/Dec-Si NPs was determined to be 4.6 ± 0.2% when excited at 365 nm and 3.8 ± 0.3% when excited at 450 nm. The samples used in this measurement were of unknown concentration, but the solution absorptance values were 91.1 ± 0.6% (excitation at 365 nm) or 66 ± 3% (excitation at 450 nm) for CTAB/Dec-Si NP and 47.3 ± 2% (excitation at 365 nm) or 11.3 ± 1% for PAA/CTAB/Dec-Si NP [Figure 2.16 (a), (b)].

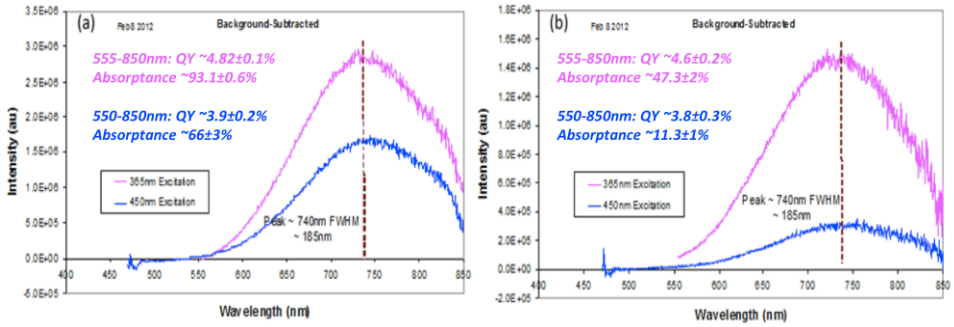


**Figure 2.16** Quantum yield analysis of (a) CTAB/Dec-Si NPs and (b) PAA/CTAB/Dec-Si NPs.

## 2.6 Conclusions

We have developed a new synthetic strategy that produces aqueous, red-emitting micellar silicon nanoparticles, where red photoluminescence is stable in water and certain other aqueous solutions for longer than 6 months. Micellar protection by CTAB encapsulation provides water solubility and protection against surface interaction with water and hydroxide, which we have shown is crucial for preserving red photoluminescence and avoiding blue photoluminescence in aqueous solutions. We have also shown, as others have reported in the past, that gradual or purposeful oxidation of Si surfaces occurs with preservation of red emission. The photophysical properties of the ~100 nm CTAB/Dec-Si NP and PAA/CTAB/Dec-Si NP micelles are stable in water and aqueous buffers with pH less than or equal to 7, as well as in cellular media at physiological pH (7.4), but unstable in sufficiently basic environments (greater that or equal to 8) where substantive interaction with $H_2O$ and $OH^-$ occurs.

## 2.7 Acknowledgements

Financial support for this project was provided by the Burroughs Wellcome Fund (Award No. 1007294.01; A.M.G. holds a Career Award at the Scientific Interface from the Burroughs Wellcome Fund), the Oregon Nanoscience and Microtechnologies Institute and the Office of Navel Research (Task Order No 3. of the Master Grant Agreement, A.M.G. is a Signature Research Fellow; and Award No. GBMEN0105A, T.V.Q. and A.M.G.), Portland State University, and Sharp Laboratories of America. We also acknowledge the National Science Foundation for x-ray diffraction instrumentation (NSF-MRI, Award No. DMR-0923572) and other related support (Award No. 1057565). Microstructural and compositional analysis was performed at the Center for Electron Microscopy and Nanofabrication, Portland State University. Finally, the authors thank Dr. Douglas Tweet and Sharp Laboratories of America (Camas, WA) for assistance with QY measurements.

## 2.8 Contributions by author

Sheng-Kuei Chiu

Experimental design, Figure 2.2, Figrue 2.3, Figure 2.4, Figure 2.5, Figure 2.6, Figure 2.7, Figure 2.8, Figure 2.9, Figure 2.10, Figure 2.11, Figure 2.12, Figure 2.13, Figure 2.14, Figure 2.15, Figure 2.16, Manuscript writing.

Dr. Beth A. Manhat

Figure 2.1, Manuscript writing

William J. I. DeBenedetti

Figure 2.1

Dr. Anna L. Brown

Figure 2.10

Dr. Katye Fichter

Figure 2.11, Experimental section writing (Live Cell Microscopy of Si NP Internalization)

Dr. Tania Vu

Manuscript revising

Micah Eastman

Figure 2.9

Dr. Jun Jiao

Manuscript revising

Dr. Andrea M. Goforth

Experimental design, Manuscript writing and revising

**2.9 Refereces**

1. Chiu, S. K.; Manhat, B. A.; DeBenedetti, W. J. I.; Brown, A. L.; Fichter, K.; Vu, T.; Eastman, M.; Jiao, J.; Goforth, A. M., Aqueous red-emitting silicon nanoparticles for cellular imaging: Consequences of protecting against surface passivation by hydroxide and water for stable red emission. *Journal of Materials Research* **2013,** 28, (2), 216-230.

2. Baxter, J. B.; Aydil, E. S., Nanowire-based dye-sensitized solar cells. *Appl. Phys. Lett.* **2005,** 86, (5), 053114.

3. Plass, R.; Pelet, S.; Krueger, J.; Gratzel, M.; Bach, U., Quantum dot sensitization of organic-inorganic hybrid solar cells. *J. Phys. Chem. B* **2002,** 106, (31), 7578-7580.

4. Gao, X. H.; Cui, Y. Y.; Levenson, R. M.; Chung, L. W. K.; Nie, S. M., In vivo cancer targeting and imaging with semiconductor quantum dots. *Nat. Biotechnol.* **2004,** 22, (8), 969-976.

5. Park, J. H.; Gu, L.; von Maltzahn, G.; Ruoslahti, E.; Bhatia, S. N.; Sailor, M. J., Biodegradable luminescent porous silicon nanoparticles for in vivo applications. *Nature Materials* **2009,** 8, (4), 331-336.

6. Canham, L. T., Silicon quantum wire array fabrication by electrochemical and chemical dissolution of wafers. *Appl. Phys. Lett.* **1990,** 57, (10), 1046-1048.

7. Alivisatos, A. P., Perspectives on the physical chemistry of semiconductor nanocrystals. *J. Phys. Chem.* **1996,** 100, (31), 13226-13239.

8. Belyakov, V. A.; Burdov, V. A.; Lockwood, R.; Meldrum, A., Silicon Nanocrystals: Fundamental Theory and Implications for Stimulated Emission. *Advances in Optical Technologies* **2008,** Article ID 279502, 1-32.

9. Green, M. A.; Zhao, J. H.; Wang, A. H.; Reece, P. J.; Gal, M., Efficient silicon light-emitting diodes. *Nature* **2001,** 412, (6849), 805-808.

10. Torres-Costa, V.; Martin-Palma, R. J.; Martinez-Duart, J. M., All-silicon color-sensitive photodetectors in the visible. *Materials Science & Engineering C-Biomimetic and Supramolecular Systems* **2007,** 27, (5-8), 954-956.

11. Walters, R. J.; Bourianoff, G. I.; Atwater, H. A., Field-effect electroluminescence in silicon nanocrystals. *Nature Materials* **2005,** 4, (2), 143-146.

12. Derfus, A. M.; Chan, W. C. W.; Bhatia, S. N., Probing the cytotoxicity of semiconductor quantum dots. *Nano Lett.* **2004,** 4, (1), 11-18.

13. Erogbogbo, F.; Yong, K.-T.; Roy, I.; Hu, R.; Law, W.-C.; Zhao, W.; Ding, H.; Wu, F.; Kumar, R.; Swihart, M. T.; Prasad, P. N., In vivo targeted cancer imaging, sentinel lymph node mapping and multi-channel imaging with biocompatible silicon nanocrystals. *ACS Nano* **2011,** 5, (1), 413-423.

14. Manhat, B. A.; Brown, A. L.; Black, L. A.; Ross, J. B. A.; Fichter, K.; Vu, T.; Richman, E.; Goforth, A. M., One-Step Melt Synthesis of Water-Soluble, Photoluminescent, Surface-Oxidized Silicon Nanoparticles for Cellular Imaging Applications. *Chem. Mater.* **2011,** 23, (9), 2407-2418.

15. Rosso-Vasic, M.; Spruijt, E.; Popovic, Z.; Overgaag, K.; van Lagen, B.; Grandidier, B.; Vanmaekelbergh, D.; Dominguez-Gutierrez, D.; De Cola, L.; Zuilhof, H., Amine-terminated silicon nanoparticles: synthesis, optical properties and their use in bioimaging. *J. Mater. Chem.* **2009,** 19, (33), 5926-5933.

16. Shiohara, A.; Hanada, S.; Prabakar, S.; Fujioka, K.; Lim, T. H.; Yamamoto, K.; Northcote, P. T.; Tilley, R. D., Chemical Reactions on Surface Molecules Attached to Silicon Quantum Dots. *J. Am. Chem. Soc.* **2010,** 132, (1), 248-253.

17. Warner, J. H.; Rubinsztein-Dunlop, H.; Tilley, R. D., Surface morphology dependent photoluminescence from colloidal silicon nanocrystals. *J. Phys. Chem. B* **2005,** 109, (41), 19064-19067.

18. Buriak, J. M., Organometallic chemistry on silicon surfaces: formation of functional monolayers bound through Si-C bonds. *Chem. Commun.* **1999**, (12), 1051-1060.

19. Aldana, J.; Wang, Y. A.; Peng, X. G., Photochemical instability of CdSe nanocrystals coated by hydrophilic thiols. *J. Am. Chem. Soc.* **2001,** 123, (36), 8844-8850.

20. Canham, L. T., Bioactive silicon structure fabrication through nanoetching techniques. *Adv. Mater.* **1995,** 7, (12), 1033-&.

21. Popplewell, J. F.; King, S. J.; Day, J. P.; Ackrill, P.; Fifield, L. K.; Cresswell, R. G.; Di Tada, M. L.; Liu, K., Kinetics of uptake and elimination of silicic acid by a human subject: A novel application of Si-32 and accelerator mass spectrometry. *J. Inorg. Biochem.* **1998,** 69, (3), 177-180.

22. He, Y.; Kang, Z. H.; Li, Q. S.; Tsang, C. H. A.; Fan, C. H.; Lee, S. T., Ultrastable, Highly Fluorescent, and Water-Dispersed Silicon-Based Nanospheres as Cellular Probes. *Angewandte Chemie-International Edition* **2009,** 48, (1), 128-132.

23. Hessel, C. M.; Henderson, E. J.; Kelly, J. A.; Cavell, R. G.; Sham, T. K.; Veinot, J. G. C., Origin of luminescence from silicon nanocrystals: a near edge X-ray absorption fine structure (NEXAFS) and X-ray excited optical luminescence (XEOL) study of oxide-embedded and free-standing systems. *Journal of Physical Chemistry C* **2008,** 112, (37), 14247-14254.

24. Bley, R. A.; Kauzlarich, S. M.; Davis, J. E.; Lee, H. W. H., Characterization of silicon nanoparticles prepared from porous silicon. *Chem. Mater.* **1996,** 8, (8), 1881-1888.

25. Tamura, H.; Ruckschloss, M.; Wirschem, T.; Veprek, S., Origin of the green-blue luminescence from nanocrystalline silicon. *Appl. Phys. Lett.* **1994,** 65, (12), 1537-1539.

26. Kanemitsu, Y., Luminescence Properties of Nanometer-sized Si Crystallites-Core and Surface-States. *Physical Review B* **1994,** 49, (23), 16845-16848.

27. Godefroo, S.; Hayne, M.; Jivanescu, M.; Stesmans, A.; Zacharias, M.; Lebedev, O. I.; Van Tendeloo, G.; Moshchalkov, V. V., Classification and control of the origin of photoluminescence from Si nanocrystals. *Nature Nanotechnology* **2008,** 3, (3), 174-178.

28. Yang, S.; Li, W.; Cao, B.; Zeng, H.; Cai, W., Origin of Blue Emission from Silicon Nanoparticles: Direct Transition and Interface Recombination. *Journal of Physical Chemistry C* **2011,** 115, (43), 21056-21062.

29. de Boer, W.; Timmerman, D.; Dohnalova, K.; Yassievich, I. N.; Zhang, H.; Buma, W. J.; Gregorkiewicz, T., Red spectral shift and enhanced quantum efficiency in phonon-free photoluminescence from silicon nanocrystals. *Nature Nanotechnology* **2010,** 5, (12), 878-884.

30. Vincent, J.; Maurice, V.; Paquez, X.; Sublemontier, O.; Leconte, Y.; Guillois, O.; Reynaud, C.; Herlin-Boime, N.; Raccurt, O.; Tardif, F., Effect of water and UV passivation on the luminescence of suspensions of silicon quantum dots. *J. Nanopart. Res.* **2010,** 12, (1), 39-46.

31. Coxon, P. R.; Wang, Q.; Chao, Y., An abrupt switch between the two photoluminescence bands within alkylated silicon nanocrystals. *Journal of Applied Physics D: Applied Physics* **2011,** 44, 495301.

32. Chao, Y.; Houlton, A.; Horrocks, B. R.; Hunt, M. R. C.; Poolton, N. R. J.; Yang, J.; Siller, L., Optical luminescence from alkyl-passivated Si nanocrystals under vacuum ultraviolet excitation: Origin and temperature dependence of the blue and orange emissions. *Appl. Phys. Lett.* **2006,** 88, (26), 263119.

33. Zhou, Z. Y.; Brus, L.; Friesner, R., Electronic structure and luminescence of 1.1- and 1.4-nm silicon nanocrystals: Oxide shell versus hydrogen passivation. *Nano Lett.* **2003,** 3, (2), 163-167.

34. Wang, X.; Zhang, R. Q.; Niehaus, T. A.; Frauenheim, T., Excited state properties of allylamine-capped silicon quantum dots. *Journal of Physical Chemistry C* **2007,** 111, (6), 2394-2400.

35. Liu, S. M., Luminescent silicon nanoparticles formed in solution. *Journal of Nanoscience and Nanotechnology* **2008,** 8, (3), 1110-1125.

36. Rosso-Vasic, M.; Spruijt, E.; van Lagen, B.; De Cola, L.; Zuilhof, H., Alkyl-Functionalized Oxide-Free Silicon Nanoparticles: Synthesis and Optical Properties. *Small* **2008,** 4, (10), 1835-1841.

37. Holmes, J. D.; Ziegler, K. J.; Doty, R. C.; Pell, L. E.; Johnston, K. P.; Korgel, B. A., Highly luminescent silicon nanocrystals with discrete optical transitions. *J. Am. Chem. Soc.* **2001,** 123, (16), 3743-3748.

38. Mangolini, L.; Jurbergs, D.; Rogojina, E.; Kortshagen, U., High efficiency photoluminescence from silicon nanocrystals prepared by plasma synthesis and organic surface passivation. *Phys. Status Solidi C* **2006,** 3, 3975-3978.

39. Jurbergs, D.; Rogojina, E.; Mangolini, L.; Kortshagen, U., Silicon nanocrystals with ensemble quantum yields exceeding 60%. *Appl. Phys. Lett.* **2006,** 88, (23), 233116

40. Kang, Z. H.; Liu, Y.; Tsang, C. H. A.; Ma, D. D. D.; Fan, X.; Wong, N. B.; Lee, S. T., Water-Soluble Silicon Quantum Dots with Wavelength-Tunable Photoluminescence. *Adv. Mater.* **2009,** 21, (6), 661-+.

41. Hessel, C. M.; Henderson, E. J.; Veinot, J. G. C., Hydrogen silsesquioxane: A molecular precursor for nanocrystalline Si-SiO2 composites and freestanding hydride-surface-terminated silicon nanoparticles. *Chem. Mater.* **2006,** 18, (26), 6139-6146.

42. Gupta, A.; Swihart, M. T.; Wiggers, H., Luminescent Colloidal Dispersion of Silicon Quantum Dots from Microwave Plasma Synthesis: Exploring the Photoluminescence Behavior Across the Visible Spectrum. *Adv. Funct. Mater.* **2009,** 19, (5), 696-703.

43. English, D. S.; Pell, L. E.; Yu, Z. H.; Barbara, P. F.; Korgel, B. A., Size tunable visible luminescence from individual organic monolayer stabilized silicon nanocrystal quantum dots. *Nano Lett.* **2002,** 2, (7), 681-685.

44. Hessel, C. M.; Reid, D.; Panthani, M. G.; Rasch, M. R.; Goodfellow, B. W.; Wei, J.; Fujii, H.; Akhavan, V.; Korgel, B. A., Synthesis of ligand-stabilized silicon nanocrystals with size-dependent photoluminescence spanning visible to near-infrared wavelengths. *Chem. Mater.* **2012,** 24, (2), 393-401.

45. Li, X. G.; He, Y. Q.; Talukdar, S. S.; Swihart, M. T., Process for preparing macroscopic quantities of brightly photoluminescent silicon nanoparticles with emission spanning the visible spectrum. *Langmuir* **2003,** 19, (20), 8490-8496.

46. Zhang, X. M.; Neiner, D.; Wang, S. Z.; Louie, A. Y.; Kauzlarich, S. M., A new solution route to hydrogen-terminated silicon nanoparticles: synthesis, functionalization and water stability. *Nanotechnology* **2007,** 18, (9), 095601.

47. Tilley, R. D.; Yamamoto, K., The microemulsion synthesis of hydrophobic and hydrophilic silicon nanocrystals. *Adv. Mater.* **2006,** 18, 2053-2056.

48. Lin, S. W.; Chen, D. H., Synthesis of Water-Soluble Blue Photoluminescent Silicon Nanocrystals with Oxide Surface Passivation. *Small* **2009,** 5, (1), 72-76.

49. Brewer, A.; Von Haeften, K., In-situ passivation and blue luminescence of silicon clusters using a cluster-beam/H2O co-deposition production method. *Appl. Phys. Lett.* **2009,** 94, 261102.

50. Tilley, R. D.; Warner, J. H.; Yamamoto, K.; Matsui, I.; Fujimori, H., Micro-emulsion synthesis of monodisperse surface stabilized silicon nanocrystals. *Chem. Commun.* **2005**, (14), 1833-1835.

51. Wilcoxon, J. P.; Samara, G. A.; Provencio, P. N., Optical and electronic properties of Si nanoclusters synthesized in inverse micelles. *Physical Review B* **1999,** 60, (4), 2704-2714.

52. Allan, G.; Delerue, C.; Lannoo, M., On the nature of luminescent surface states of semiconductor nanocrystallites. *Phys. Rev. Lett.* **1996,** 76, 2961.

53. Ray, M.; Sarkar, S.; Bandyopadhyay, N. R.; Hossain, S. M.; Pramanick, A. K., Silicon and silicon oxide core-shell nanoparticles: structural and photoluminescence characteristics. *J. Appl. Phys.* **2009,** 105, 074301.

54. Qin, G. G.; Song, H. Z.; Zhang, B. R.; Lin, J.; Duan, J. Q.; Yao, G. Q., Experimental evidence for luminescence from silicon oxide layers in oxidized porous silicon. *Physical Review B* **1996,** 54, (4), 2548-2555.

55. Li, Z. F.; Ruckenstein, E., Water-soluble poly(acrylic acid) grafted luminescent silicon nanoparticles and their use as fluorescent biological staining labels. *Nano Lett.* **2004,** 4, (8), 1463-1467.

56. Kravitz, K.; Kamyshny, A.; Gedanken, A.; Magdassi, S., Solid state synthesis of water-dispersible silicon nanoparticles from silica nanoparticles. *J. Solid State Chem.* **2010,** 183, (6), 1442-1447.

57. Henderson, E. J.; Kelly, J. A.; Veinot, J. C. G., Influence of HSiO1.5 Sol-Gel Polymer Structure and Composition on the Size and Luminescent Properties of Silicon Nanocrystals. *Chem. Mater.* **2009,** 21, 5426-5434.

58. *Operation Manual for Quanta-Phi Rev. C*; April 23, 2010.

59. Porres, L.; Holland, A.; Palsson, L.; Monkman, A. P.; Kemp, C.; Beeby, A., Absolute measurements of photoluminescence quantum yields of solutions using an integrating sphere. *J. Fluorescence* **2006,** 16, (2), 267-273.

60. NIH *Image J*, http://rsbweb.nih.gov/ij/.

61. Hessel, C.; Henderson, E. J.; Veinot, J. C. G., An investigation of the formation and growth of oxide-embedded silicon nanocrystals in hydrogen silsesquioxane-derived nanocomposites. *J. Phys. Chem. C* **2007,** 111, 6956-6961.

62. Veinot, J. C. G., Sol-gel precursors for Group 14 nanocrystals. *Chem. Commun.* **2010,** 46, 8404.

63. Higashi, G. S.; Chabal, Y. J.; Trucks, G. W.; Raghavachari, K., Ideal hydrogen termination of the Si(111) surface. *Appl. Phys. Lett.* **1990,** 56, (7), 656-658.

64. Michalak, D. J.; Amy, S. R.; Aureau, D.; Dai, M.; Esteve, A.; Chabal, Y. J., Nanopatterning Si(III) surfaces as selective surface-chemistry route. *Nature Materials* **2010,** 9, 266.

65. Pasternack, R. M.; Amy, S. R.; Chabal, Y. J., Attachment of 3-(Aminopropyl)triethoxysilane on silicon oxide surfaces: dependence on solution temperature. *Langmuir* **2008,** 24, 12963-12971.

66. Thissen, P.; Peixoto, T.; Longo, R. C.; Peng, W. G.; Cho, K.; Chabal, Y. J., Activation of Surface Hydroxyl Groups by Modification of H-Terminated Si(111) Surfaces. *J. Am. Chem. Soc.* **2012,** 134, 8869-8874.

67. Mazumder, S.; Dey, R.; Mitra, M. K.; Mukherjee, S.; Das, G. C., Review: Biofunctionalized Quantum Dots in Biology and Medicine. *Journal of Nanomaterials* **2009**.

68. Erogbogbo, F.; Yong, K. T.; Roy, I.; Xu, G. X.; Prasad, P. N.; Swihart, M. T., Biocompatible luminescent silicon quantum dots for imaging of cancer cells. *Acs Nano* **2008,** 2, (5), 873-878.

69. Shirahata, N.; Linford, M. R.; Furumi, S.; Pei, L.; Sakka, Y.; Gates, R. J.; Asplund, M. C., Laser-derived one-pot synthesis of silicon nanocrystals terminated with organic monolayers. *Chem. Commun.* **2009**, (31), 4684-4686..

70. Liu, J.; Du, X., pH- and competitor-driven nanovalves of cucurbit[7]uril pseudorotaxanes based on mesoporous silica supports for controlled release. *J. Mater. Chem.* **2010,** 20, 3642-3649.

**Chapter 3 Red-to-Blue Photoluminescence Conversion in Alcohol Dispersions of Alkyl-Capped Silicon Nanoparticles:** Insight into the origins of visible photoluminescence in colloidal nanocrystalline silicon

## 3.1 Abstract

Visibly emissive, hydride-terminated silicon nanoparticles (Si NPs) were obtained *via* high-temperature annealing of $(HSiO_{1.5})_n$ polymer, followed by chemical etching. The hydride-terminated Si NPs were surface-functionalized *via* thermal hydrosilylation with 1-decene and were subsequently re-dispersed in straight chain alcohols varying in carbon chain length (C1-C10). The initial red photoluminescence (PL) ($\lambda_{max,em}$ ~580 nm) observed from neat hexane dispersions of the decane-terminated Si NPs became weaker upon exposure to alcohols smaller than a certain minimum chain length, commensurate with appearance of strong, blue PL ($\lambda_{max,em}$ ~450 nm). A comprehensive suite of spectroscopic and microscopic techniques was employed to study and correlate the change in Si NP PL with composition and/or size changes to the Si NPs. The results of these studies support that the observed red-to-blue PL conversion originates from dangling bond defect passivation by small alcohol molecules, resulting in an enhanced blue/red PL ratio, and likely, an overall increase in PL quantum yield. We discuss these experimental results in light of current hypotheses about the origins of Si NP visible light emission, which we demonstrate is markedly influenced by the Si NP surface chemistry. A simple energy level diagram is proposed to account for the key spectral and dynamic features observed in our work, in which the role of surfaces states is highlighted.

## 3.2 Introduction

Semiconductor nanoparticles (NPs), also called quantum dots, have received widespread attention for their wavelength-tunable visible light emission, a property that is generally governed by a core size-dependent quantum confinement (QC) effect. This property has allowed photoluminescent (PL) semiconductor NPs to be used in many applications, such as in opto-electronic devices,[1] energy storage materials,[2] and biophotonics.[3-6] These and future commercial applications of visible light emitting NPs rely heavily on synthetic methods to produce desired particle sizes, with narrow size distributions and uniform morphologies. The NPs must furthermore be stable and resistant to aggregation, degradation, and detrimental redox chemistry, which is generally accomplished by NP surface passivation, *e.g.,* by inorganic shells, organic ligands, or both. With respect to degradation, light emission applications require both chemical (*e.g.,* oxidative) and photo-stability (*e.g.,* stability with respect to emission $\lambda_{max}$ and quantum yield (QY)) in variable or complex environments.

Elegant synthetic procedures have been developed for semiconductor NPs, particularly for II-VI semiconductor quantum dots (QDs), where QD size, size distribution, morphology, and surface stabilizing ligands are precisely controlled. This precise synthetic control has enabled production of size monodisperse, direct band gap, II-VI semiconductor QDs (*e.g.,* CdQ or PbQ QDs (Q = S, Se, or Te)) and core/shell II-VI semiconductor QDs (*e.g.,* CdSe/ZnS QDs) exhibiting size-dependent, narrow emission spectra, broad absorbance spectra, and high emission quantum yields.[7,8] Although II-VI semiconductor QDs often exhibit more favorable emission properties relative to molecular fluorophores, including tunable emission colors that can be excited with a

single wavelength of light, narrower emission spectra, higher QYs, and enhanced chemical and photo-stabilities,[6,9] their inherent biological toxicity renders them unfavorable for widespread use in biological and environmental applications.[10-13] Consequently, recent research has focused on the development of more benign photoluminescent NPs, *e.g.,* silicon NPs (Si NPs), which are also, in theory, capable of exhibiting QC-related emission in the nm-size regime.

Although photoluminescent Si NPs are considered biologically adventitious compared to II-VI QDs due to their lower cytotoxicity,[14] control over the emission characteristics of colloidal Si NPs is relatively challenging. Particularly, the emission $\lambda_{max}$ is not always well-correlated with particle size, an expectation of quantum confinement, and the emission $\lambda_{max}$ can furthermore change with respect to time and chemical environment.

The origin of light emission for nm-sized Si domains, whether in colloidal Si NPs (*i.e.,* free-standing) or in Si NPs embedded in solid hosts (*e.g.,* nanocrystalline Si domains in porous Si), has been the subject of intense debate since the observation of efficient, visible light emission from crystalline, nanometer-sized Si domains over two decades ago.[15,16] While Si NPs prepared by some methods have sample emission maxima that are reported to be well-correlated with particle size,[17-25] as expected for an emission process strictly governed by QC, other reports have shown particle size distributions and emission spectra that do not correlate with expectations of the QC theory.[26-29] Furthermore, many reports have suggested that localized luminescent centers (LCs), which may or may not be associated with Si(0) cores (*e.g.,* a self-trapped exciton in the oxidized shell of an Si nanocrystal),[30-32] are responsible for observed QC-inconsistent

PL.[28-30] Finally, several recent reports on the origins of Si NP PL have been in agreement that both core and surface states may give rise to visible light emission,[29, 33-38] although there is still variation in assignments of size-dependent core *vs.* (presumably) size-independent surface states

A quantum confinement/luminescence center (QC/LC) emission mechanism has been considered by numerous groups, [28,30,33,39,40] where QC/LC PL involves exciton formation in a quantum confined Si(0) core followed by radiative decay of the electron (or hole) at localized luminescent centers. This mechanism is often evoked for Si NP samples that show two or more distinct emission peaks, which may be attributed to multiple, possible radiative decay pathways available to the photogenerated Si NP excited state.

Though two other studies have observed photophysical property changes in nanocrystalline Si exposed to alcohols, such as increasing or decreasing quantum yield, neither of them reported the red-to-blue PL conversion that we describe herein.[41,42] In the latter, both blue- and red-emitting nanocrystalline Si were prepared electrochemically, and both samples were observed to undergo PL quenching without a change in $\lambda_{max}$ when exposed to methanol.[42] Another study comparing the photophysical properties of free-standing *vs.* oxide embedded nanocrystalline Si upon exposure to amines also reported quenching of initially red PL and did not report a change in emission $\lambda_{max}$.[43] These samples were also prepared by electrochemical etching of Si wafers.

We report herein observation of red-to-blue PL conversion when alkyl-terminated Si NPs prepared by thermal reduction of $(HSiO_{1.5})_n$ followed by hydrosilylations are re-dispersed in alcohol solvents smaller than a minimum steric volume. The composition

of the Si NPs was assessed using attenuated total reflectance Fourier transform infrared (ATR-FT-IR) spectroscopy and particle size was monitored by transmission electron microscopy (TEM) to determine structure/property relationships underlying the PL color change. Absorption, PL, and PL excitation (PLE) spectra were also measured. In addition, excited state dynamics associated with both the red and blue emissions have been studied using time resolved PL (TRPL) spectroscopy. Based on all the data collected and analyzed, in conjunction with previous literature, we propose that the solvent insensitive red emission likely originates from an intrinsic state and is an indirect bandgap transition, while the solvent sensitive blue emission results from a surface trap state associated with the direct bandgap transition. From these data and their analysis, a surface reaction mechanism and a simple energy diagram are constructed to explain the origins of the observed red and blue PL and associated dynamic processes concerning the excited electronic states.

### 3.3 Experimental

*Materials*: Synthetic preparations of the alkyl-terminated Si NPs were performed under inert (Ar) atmosphere using standard air-free techniques, unless otherwise noted. Alcohol dispersions of the alkyl-terminated Si NPs were prepared and handled under ambient atmosphere. The following analytical grade chemicals were purchased and used as received: trichlorosilane ($HSiCl_3$, Alfa Aesar, 97%), hydrofluoric acid (aqueous HF, Sigma Aldrich, 49 wt.%), ethanol ($C_2H_6O$, Sigma Aldrich, anhydrous), pentane ($C_5H_{12}$, Sigma Aldrich, anhydrous), and 1-decene ($C_{10}H_{20}$, Sigma Aldrich, 99%). Straight-

chained alcohols (Sigma Aldrich, 97-99%) with hydrocarbon chains ranging from C1-C10 were dried over activated 3 Å molecular sieves for 24 hours prior to use.[44]

*Synthesis of hydride-terminated Si NPs (H-Si NPs)*: A modified literature procedure[18] was used to synthesize free-standing H-Si NPs. In a typical reaction, 4.5 mL of $HSiCl_3$ (45 mmol) was placed in a two-necked round bottom flask equipped with two 16-gauge needles and a small PTFE-coated magnetic stir bar. The flask was cooled to $0^oC$ to prevent volatilization of $HSiCl_3$, and an aliquot (90 mmol) of nanopure water ($nH_2O$, 18 MOhm•cm resistivity) was rapidly injected to catalyze the hydrolysis and polycondensation of $HSiCl_3$. The reaction progress was qualitatively monitored at the exhaust vents for the cessation of $HCl_{(g)}$ using wet pH paper. The polymerization reaction resulted in the formation of a sol-gel hydridosilicate of putative stoichiometry $(HSiO_{1.5})_n$.[18] The resulting sol-gel hydridosilicate was dried *in vacuo* for 24 hrs to remove adsorbed water and $HCl_{(g)}$, placed in an alumina combustion boat (90 x 17x 11.5 mm), and loaded into a quartz flow through reactor (24 mm x 28 mm x 1 m). The reactor was situated in a tube furnace (Lindberg Blue M*, L = 30.5 cm, O.D. = 2.54 cm) and annealed at $1100^oC$ for 10 hrs under flowing industrial-grade $N_2$. Annealing resulted in an amorphous $SiO_2$ matrix encasing nanocrystalline Si (nc-Si) domains.[19,45] This binary phase material was ball-milled for 10 s in a tungsten carbide lined milling vial with two 1-cm tungsten carbide balls using a high energy mill mixer (Spex 8000M). After mechanical attrition, the nc-Si/$SiO_2$ nanocomposite was placed in a Teflon™ beaker and chemically etched according to a modified literature procedure.[19] Briefly, the chemical etch mixture was prepared by combining aqueous HF (49 wt.%), ethanol, and $nH_2O$ in a

1:1:1 volume ratio. The nc-Si/$SiO_2$ powder (~0.8g) was added to the chemical etch mixture (15 mL) and was vigorously stirred for 1 hr. The chemical etch was quenched by extracting the H-Si NPs into pentane. At the termination of a typical etch, 10-15 extractions were performed using 5 mL aliquots of pentane, which were subsequently combined to produce a stock solution of H-Si NPs.

*Synthesis of decane-terminated Si NPs (dec-Si NPs)*: The Si NPs were functionalized *via* thermal hydrosilylation reaction[46] of the H-Si NPs with 1-decene. In a typical thermal hydrosilylation reaction, a solution of pentane containing 15 mg of H-Si NPs (dried mass) was placed in a two-necked round bottom flask on a dual vacuum/gas manifold and 2.5 mL of degassed 1-decene was transferred to the reaction vessel under positive pressure of Ar *via* cannula. The solution was briefly sonicated and subsequently brought to reflux with vigorous stirring for 24 hrs under a heavy flow of Ar. After cooling to room temperature, the decane-terminated Si NP solution was transferred into an air-free scintillation vial and taken to dryness on a rotary evaporator to remove excess, unreacted 1-decene. The decane-terminated Si NPs (dec-Si NPs) were then re-dispersed in 5 mL of dry hexanes or toluene and stored under Ar for further use.

*Alcohol Dispersions of dec-Si NPs*: dec-Si NPs were re-dispersed after drying from hexane solution into straight chain alcohols of varying hydrocarbon chain lengths, from C1-C10 (methanol-decanol). A separate dispersion was made for each alcohol. To keep the Si NP concentration consistent from sample to sample, 2 mL aliquots of dec-Si NP stock solution in hexane were dried in separate vials *via* rotatory evaporation. Once dry,

2 mL of a straight-chained alcohol was added to each vial, so as to retain the approximate, original concentration of Si NPs. Individual dispersions were sonicated for 2 min prior to characterization.

*Analytical Characterization of Si NPs by Transmission Electron Microscopy (TEM), Fourier Transform Infrared (FT-IR) and Photoluminescence (PL) Spectroscopies*: Selected colloidal dispersions of the Si NPs were characterized by TEM and FT-IR spectroscopy before and after dispersion in alcohol. All colloidal dispersions of the Si NPs were characterized using steady-state PL spectroscopy. TEM measurements were performed on a Tecnai F-20 HR-TEM operating at 200 kV. Samples for TEM were prepared by drop casting diluted aliquots of the Si NPs onto 400-mesh holey carbon-coated copper grids (SPI), which were subsequently dried in air at 100ºC for two hours prior to imaging. FT-IR data were collected using a Nicolet iS10 spectrometer equipped with a diamond, single-bounce attenuated total reflectance (ATR) attachment. For these measurements, Si NP films were drop cast onto the ATR crystal and excess solvent was evaporated using a heat gun. IR absorbance spectra were corrected for atmospheric/background signal after 150 scans. Steady-state PL measurements were collected on a Shimadzu-RF5301PM spectrophotometer using standard 1 cm quartz cuvettes and excitation wavelengths ranging from 250-490 nm. While the exact concentration of the Si NP dispersions was not known, attempts to keep the relative Si NP concentration the same for each PL measurement, before and after dispersion in the alcohol solvents, were accomplished by drying (from hexanes) 2 mL aliquots of dec-Si NP stock solutions and dispersing them in an identical volume of alcohol.

*Time-resolved Photoluminescence (TRPL) Spectroscopy:* Prior to TRPL Spectroscopy measurements for representative red-, blue-, and dual red/blue-emitting alcohol-dispersed, dec-Si NPs, the steady-state PL spectra were re-measured using a Varian Cary Eclipse fluorescence spectrophotometer to verify the temporal stability of the PL wavelength maxima, at which excited state lifetimes were subsequently measured. The same was done for an as-prepared sample of dec-Si NPs in hexanes. For these samples, PL excitation (PLE) spectra were also collected on the same spectrophotometer, and electronic absorption spectra were collected at room temperature on a Hewlett Packard 845A diode array UV-Vis spectrometer. It should be noted that the peak of the red PL band was observed at different positions for the two instruments used to measure steady state PL due to differing detector sensitivities in the red-to-NIR spectral region, which we have discussed at length in our prior work.[45]

The PL lifetimes on the order of nanoseconds were measured using a time correlated single photon counting (TCSPC) system. A 5 W Coherent Verdi-V5 (532 nm) continuous wave laser was used to pump a tunable (790−820 nm), mode locked Ti:sapphire laser (Kapteyn-Murnane Laboratories, model: MTS Mini) operating at a repetition rate of 200 MHz. A wavelength of 800 nm was passed through a pulse picker (Conoptics, model 350−160) to increase the time between pulses to 50 ns. This 800 nm light was then frequency doubled to 400 nm using a bismuth borate (BiBO) crystal, which was used to excite Si NPs dispersed in different solvents. Light emitted from the Si NP samples was collected at a 90° angle and guided into a monochromator. The monochromatic photons were counted using an avalanche photodiode detector (ID Quantique SA id-100, Switzerland) operated in reverse start-stop mode. The instrument

response function was 50 ps. The decay spectrum was recorded at the blue PL lambda max of the Si NP colloids (445 nm for butanol and decanol colloids, 450 nm for ethanol colloid) using 390 nm excitation.

The PL lifetimes on the order of μs were measured using a Varian Cary Eclipse fluorescence spectrophotometer. The lifetime was monitored at the red PL lambda max of the Si NP colloids (645 nm for butanol and decanol colloids, 650 nm for hexane colloid) using 380 nm excitation. The decay and gate times were set at 0 and 0.001 ms, respectively.

### 3.4 Results

*Synthesis and Characterization of H- and dec-Si NPs*

The red-emitting Si NPs used in this study, which examines the effects of alcohol solvents on the emission wavelength, size, and composition of alkyl-terminated Si NPs, were prepared by modification of previously reported synthetic methods.[18] Briefly, the high temperature annealing of an $(HSiO_{1.5})_n$ polymer and subsequent aqueous HF chemical etch produced hydride-terminated Si NPs (H-Si NPs) that were extracted into an apolar solvent (pentane). While it has been reported that the emission wavelength of H-Si NP colloids may be controlled by varying the chemical etch time, as increasing the etch time should decrease the Si NP core size,[18] in this study, the chemical etch was quenched upon the initial observation of red emission (emission $\lambda_{max}$ at ~580 nm, $\lambda_{ex}$ = 375 nm). These H-Si NPs were subsequently functionalized using 1-decene *via* thermal hydrosilylation.

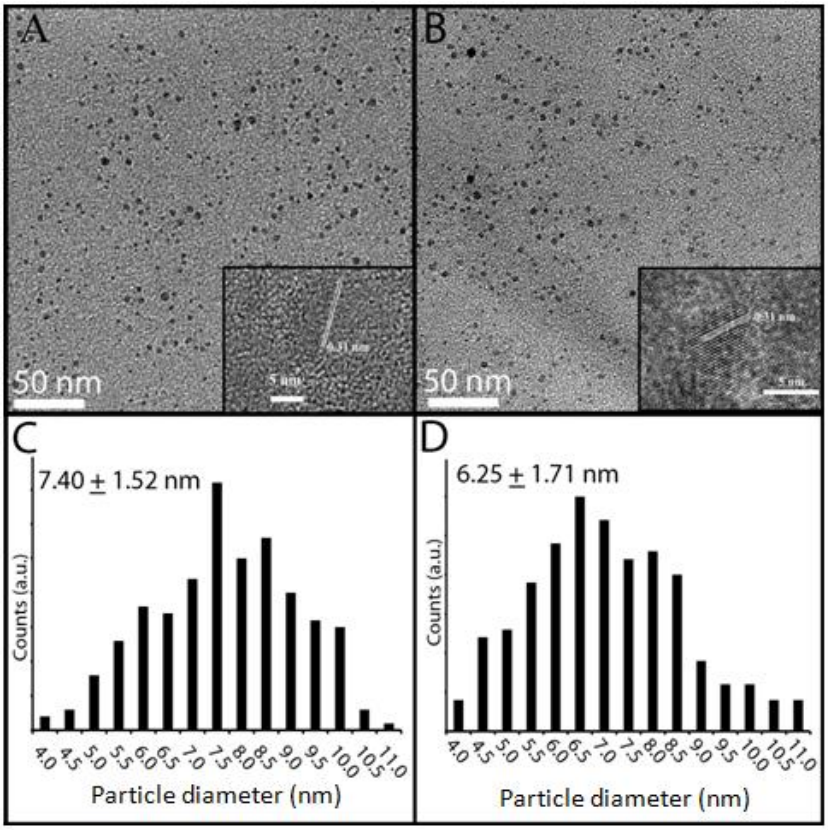


**Figure 3.1.** (A) TEM image of dec-Si NPs dispersed from hexane, scale bar 50 nm; (Inset A) HR-TEM image of the same, scale bar 5 nm. (C) Histogram corresponding to image A. (B) TEM image of dec-Si NPs dispersed from ethanol, scale bar 50 nm; (Inset B) HR-TEM image of the same, scale bar 5 nm. (D) Histogram corresponding to image B.

Our group and other groups have previously shown that the Si NPs obtained from the high-temperature annealing of $(HSiO_{1.5})_n$ polymer and functionalized with alkyl groups are composed of crystalline Si NP cores.[18,22,45] Consistent with this, representative TEM and HR-TEM images of the as-prepared decane-terminated Si NPs (dec-Si NPs) dispersed from hexane solution are shown in Figure 3.1A. In general, TEM images of the dec-Si NPs showed that the samples contain abundant, spherical, crystalline Si NPs that

are somewhat polydisperse. Representative of the typical size population produced by the high-temperature synthesis/etching/hydrosilylation method, measuring 300 NPs from various areas of the TEM grid, the dec-Si NPs were determined to have an average diameter of 7.4 ± 1.5 nm, as shown in the histogram in Figure 3.1C. From the HR-TEM image (inset, Figure 3.1A), lattice fringes with spacing of 0.31 nm are observed, supporting that the Si NP cores are composed of crystalline, diamond lattice $Si^0$ domains (<111> plane spacing = 0.31 nm).[47]

FT-IR was used to evaluate the success of the thermal hydrosilylation reaction of the H-Si NPs with neat 1-decene. The FT-IR spectra of H-Si NPs and dec-Si NPs, both dispersed from hexane, are shown in Figure 3.2 (lines a and e, respectively). After thermal hydrosilylation with 1-decene, the characteristic Si-H stretch at 2100 $cm^{-1}$ is no longer observed, and a Si-C stretch at 1260 $cm^{-1}$, indicative of covalent Si-C surface termination, appears. We note here that after hydrosilylation, there is some very weak absorption in the Si-O-Si region (1000-1100 $cm^{-1}$) that would indicate minor surface oxidation. Other features observed in the FT-IR spectrum of dec-Si NPs are assigned in Table 3.1 and further discussed below.

| Table 1. Features present in dec-Si NP colloid FT-IR spectra | | | | | |
|---|---|---|---|---|---|
| wavenumber (1/cm) | assignment | dec-Si NP samples dispersed in: | | | |
| | | hexane | ethanol | butanol | decanol |
| 3100 | C=**C-H** stretch | YES/weak | NO | NO | YES/weak |
| 2900-3000 | C-**C-H** stretch | YES | YES | YES | YES |
| 1650 | **C=C** stretch | YES/weak | NO | NO | YES/weak |
| 1460 | **C-H** methyl scissor | YES | YES | YES | YES |
| 1375 | **C-H** methyl rock | YES/weak | YES/weak | YES/weak | YES/weak |
| 1260 | **Si-C** | YES | YES | YES | YES |
| 1000-1100 | **Si-O-Si** (TO/LO modes) | Yes/v. weak | YES | YES/weak | YES/v. weak |
| 990 | C=**C-H** vinyl oop bend | YES | NO | YES/weak | YES |
| 915 | C=**C-H** vinyl oop bend | YES | NO | YES/weak | YES |
| 800 | **Si-C** | YES | YES | YES | YES |
| 740 | long chain methyl rock | YES/weak | YES/v. weak | YES/v. weak | YES/weak |
| | | Present | Weakly Present | Not Present | oop = out of plane |
| | | YES | weak | NO | |

**Table 3.1.** Features present in dec-Si NP colloid FT-IR spectra.

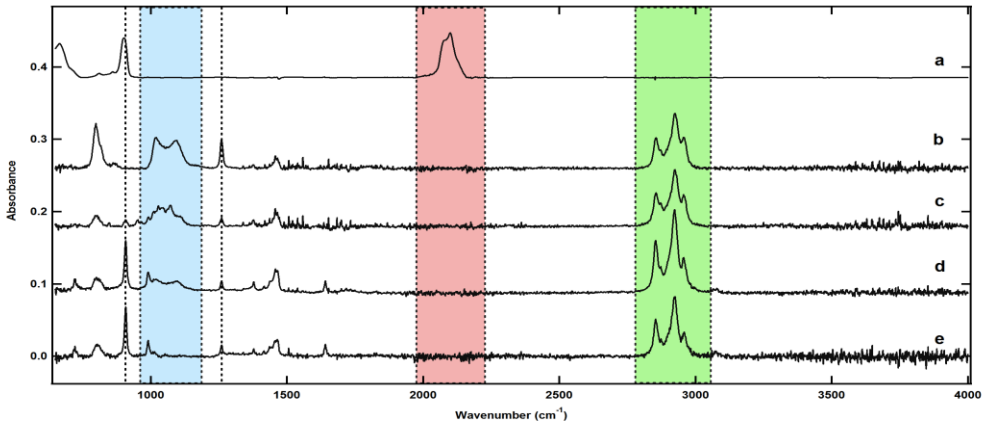


**Figure 3.2.** FT-IR spectra of (a) H-Si NPs in hexanes and (b)-(e) dec-Si NPs in EtOH (b), BuOH (c), DecOH (d), or hexane (e).

In the PL spectra of these crystalline core, dec-Si NPs (Fig. 3.3), no change in the emission wavelength *vs.* that of the H-Si NPs (data not shown) was observed after surface functionalization; the emission $\lambda_{max}$ remained ~580 nm with $\lambda_{ex}$ at 370 nm. Furthermore, these PL spectra show that the PL intensity changes with varying excitation wavelength (between 340 and 460 nm), while the emission $\lambda_{max}$ does not change. In general, the emitted red light intensity was maximal when the samples were excited at 370 nm. Thus, this excitation wavelength was used for the PL comparison of alkane- *vs.* alcohol-dispersed, dec-Si NPs discussed below. For the dec-Si NPs dispersed in hexane, the emitted visible light was observed to be red/orange under a handheld UV lamp ($\lambda_{ex}$ = 365 nm) and was visually observed to be relatively stable over time. To confirm the latter, PL spectroscopy measurements taken periodically on the same dec-Si NP sample over the course of several weeks of storage under ambient conditions were identical in emission $\lambda_{max}$ but were observed to diminish slightly in intensity (Fig. 3.4).

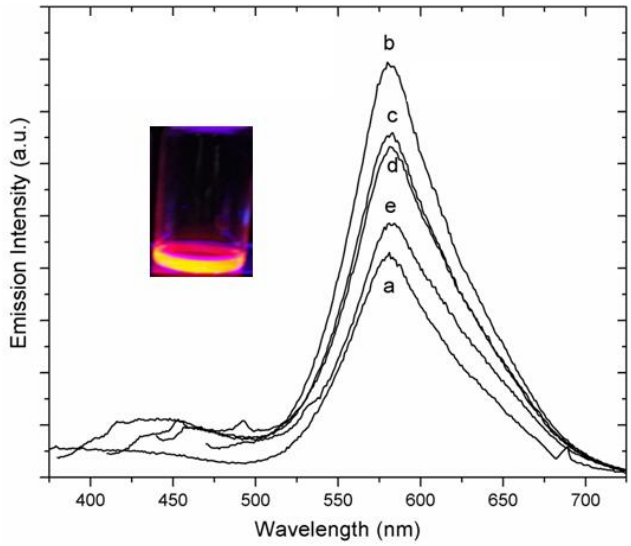


**Figure 3.3.** Emission spectra of dec-Si NPs dispersed in hexane using various excitation wavelengths: a, $\lambda_{ex}$ = 340 nm; b, $\lambda_{ex}$ = 370 nm; c, $\lambda_{ex}$ = 400 nm, d, $\lambda_{ex}$ = 430 nm; e, $\lambda_{ex}$ = 460 nm. Inset: Digital image of dec-Si NPs dispersed in hexane under 365 nm light.

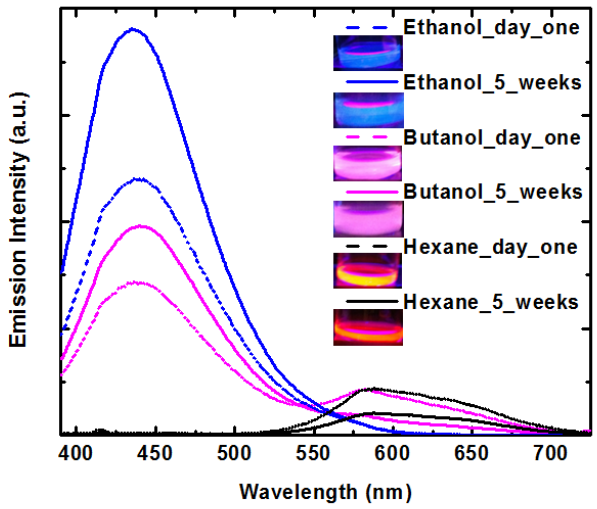


**Figure 3.4.** Dec-Si NPs in ethanol (blue curves), butanol (pink curves), and hexanes (black curves) after 1 day (dashed lines) or 5 weeks (solid lines) in air. Insets:

Photographs of colloids in the solvents indicated, at the time points indicated, under 365 nm light.

To examine the effects of exposure to potential surface passivants on the PL behavior, the dec-Si NPs were re-dispersed after drying from hexane solution into straight chain alcohols of varying chain lengths. For the straight chain alcohol dispersions, a series of potential surface passivants that varies in steric volume can be used to probe correlations between surface chemistry and PL properties, based on size-limited surface access, and therefore, reactivity.

*Comparison of Hexane vs. Primary Alcohol (C1-C10) Dispersions of dec-Si NPs*

When dispersed in the shortest-chained alcohols, *i.e.*, methanol (data not shown), ethanol (Fig. 3.5, line a), and propanol (Fig. 3.5, line b), the emission $\lambda_{max}$ of the dec-Si NPs dramatically blue-shifted to ~450 nm, *vs*. ~580 nm as-prepared and dispersed in hexane. After dispersion in these solvents, the samples were visually observed to emit blue light under a handheld UV lamp ($\lambda_{ex}$ = 365 nm), and dissimilar to the red emission intensity of Si NPs in hexane, the intensity of the blue emission of the Si NPs in short-chained alcohols was observed to increase with time (Fig. 3.4). Also unlike the original red emission, the blue emission $\lambda_{max}$ of these samples is observed to be dependent on the excitation wavelength, as shown for the ethanol-dispersed dec-Si NP PL spectra in Figure 3.6. Similar blue light emission that changes with varying excitation wavelength has often been reported,[48-52] and in general has been attributed to ultra-small (1-2 nm) Si NP cores with a polydisperse size distribution and therefore differentially excited quantum efficiencies. While this explanation is plausible, the excitation wavelength-dependent blue emission $\lambda_{max}$ can also be due to instrumental effects when the emission $\lambda_{max}$ is close

to $\lambda_{ex}$ (Fig. 3.6), which accounts for the absence of this observation for the red emission that is energetically well separated from the excitation wavelength.

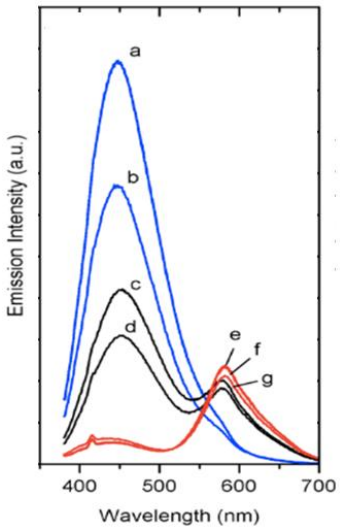


**Figure 3.5.** Emission spectra of dec-Si NPs excited at 370 nm dispersed in (a) ethanol, (b) propanol, (c) butanol, (d) pentanol, (e) hexanol, (f) octanol, and (g) decanol.

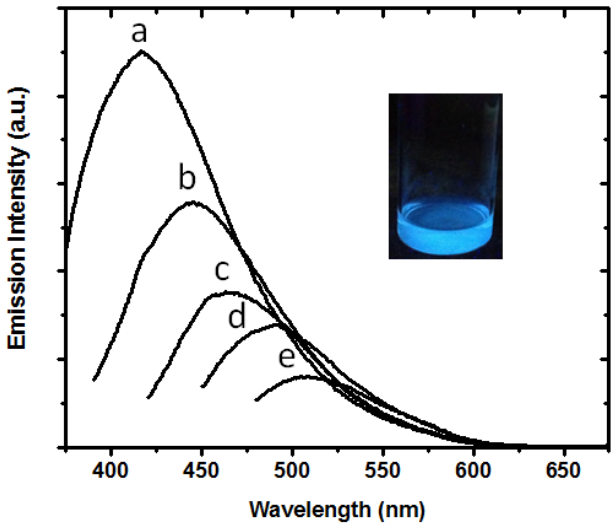


**Figure 3.6.** Emission spectra of dec-Si NPs dispersed in ethanol at various excitation wavelengths: a, $\lambda_{ex}$ = 340 nm; b, $\lambda_{ex}$ = 370 nm; c, $\lambda_{ex}$ = 400 nm; d, $\lambda_{ex}$ = 430 nm;

e, $\lambda_{ex}$ = 460 nm. Inset: Digital image of dec-Si NPs dispersed in ethanol under 365 nm light.

The same sample of dec-Si NPs was examined by TEM and FT-IR before (in hexanes) and after ethanol dispersion to survey for changes in size (by TEM) or composition (by FT-IR) that could be linked to the observed red-to-blue PL conversion. As shown in Figure 3.1, an approximately 1 nm decrease in the mean particle diameter was observed for the dec-Si NPs dispersed in ethanol (Fig. 3.1B, 3.1D) *vs.* those dispersed in hexane (Fig. 3.1A, 3.1C). The diameter distributions obtained were respectively 6.3 ± 1.7 nm (250 NPs measured) and 7.4 ± 1.5 nm (300 NPs measured). However, there are no obvious differences in the crystallinity or morphology of the particles as observed by HR-TEM (see insets to Figs. 3.1A and 3.1B). The difference in the population mean diameters is statistically significant ($p < 0.01$), but not consistent with the size change predicted using the effective mass approximation for such a large hypsochromic shift.[53-55]

While the small but significant change in the population mean diameters is inconsistent with quantum confinement expectations of the large blue shift, the FT-IR spectra of the dec-Si NPs in hexane *vs.* ethanol show marked differences. Though Si-C bonds are clearly still observed, compared to the spectrum of the hexane colloid (Fig. 3.2e), there is a notable increase in intensity in the Si-O-Si region (1000-1100 $cm^{-1}$) for the ethanol colloid (Fig. 3.2b), which is furthermore, better resolved into two distinct peaks. For oriented Si single crystals, these two peaks have been assigned as the TO (transverse optical) and LO (longitudinal optical) phonon modes of a surface oxide layer.[56] Additionally, for the ethanol colloid, there is not a sharp peak at 915 $cm^{-1}$, which

along with features at 3100, 1650, and 990 $cm^{-1}$, indicate the presence of 1-decene. Finally, both the blue-emitting ethanol colloid and the red-emitting hexane colloid have intensity in the feature observed at 800 $cm^{-1}$; this peak has been variably assigned in the literature as Si-OH deformation,[57, 58] Si-O-Si symmetric stretch,[59] or Si-C deformation.[49]

As supported by the additional FT-IR data discussed below, presence or absence of the 1000-1100 $cm^{-1}$ oxide and the 915 $cm^{-1}$ alkene modes are predictive of the steady state PL spectra: in general, presence of a strong, well developed oxide mode at 1000-1100 $cm^{-1}$ is associated with blue emission (~450 nm), presence of a strong peak at 915 $cm^{-1}$ is associated with red emission (~580 nm), and significant intensity in both the 1000-1100 $cm^{-1}$ and 915 $cm^{-1}$ peaks is associated with a sample exhibiting both red and blue PL emissions.

Prior to FT-IR measurements, we made our best effort to remove excess 1-decene remaining from the hydrosilylation capping step, and we discuss below that the 1-decene observed in the FT-IR spectra of the red-emitting samples is likely, at least in part, regenerated by heterolytic cleavage of the Si-C bond. We note also that the assignment of the 800 $cm^{-1}$ peak, which was observed for all dec-Si NP colloids, as Si-OH deformation, is inconsistent with the absence of O-H stretch modes (expected, ~3300 $cm^{-1}$). We suggest that the 800 $cm^{-1}$ feature corresponds to an Si-C mode, since its intensity scales with that of the putatively assigned 1260 $cm^{-1}$ Si-C stretch.

The TEM and FT-IR data together indicate that the red-to-blue PL conversion observed for the short chain alcohol dispersions of the dec-Si NPs is not due to substantial shrinkage or degradation of the crystalline Si NP cores, but is likely associated with changes in the surface-passivating layer. To further test this, we attempted to

correlate FT-IR features to the steady-state PL spectra for dec-Si NP dispersions in longer-chained alcohols, which would have less access to the Si NP surfaces.

Supporting that the red-to-blue PL conversion is associated with a change in the surface passivating layer, when dec-Si NPs were exposed to alcohols with linear steric volume greater than or equal to that of hexanol (Figure 3.5, hexanol, line e; octanol, line f; decanol, line g), the PL spectra show no appreciable shift in the emission $\lambda_{max}$ at ~580 nm when compared with the original hexane dispersion. These colloids continue to appear visually red/orange-emitting under 365 nm light. Additionally, the FT-IR spectrum of the dec-Si NPs in decanol (Figure 3.2, line d) reveals only modest growth in the 1000-1100 $cm^{-1}$ Si-O-Si feature when compared with that of the dec-Si NPs from the ethanol dispersion (Figure 3.2, line b). Furthermore, there is strong intensity in the 915 $cm^{-1}$ alkene mode in the decanol dispersion, as there also is for the hexane dispersion (Figure 3.2, line e). Thus, these data indicate that sufficiently long chain alcohols (*e.g.*, hexanol, octanol, decanol) cannot effectively intercalate the decane surface groups to interact with the Si NP surfaces, which suppresses surface oxidation and results in preservation of the alkene bonding features that are correlated with the red PL (*See Discussion*).

For butanol and pentanol, the alcohols with linear steric volume between those giving rise to predominantly blue PL (methanol, ethanol, and propanol) or predominantly red PL (hexanol, octanol, and decanol), both red and blue PL bands are observed (Fig. 3.5, butanol, line c; pentanol, line d), and these samples appear visually pink-emitting under 365 nm light. These PL data indicate that the blue and red emissions *are related* and that both transitions responsible for these PL bands are accessible in certain solvent

environments. Furthermore, when the butanol colloid was monitored spectroscopically over time (Fig. 3.4), the red PL band diminished in intensity and the blue PL band increased in intensity, analogous to the intensity changes observed for samples exhibiting only red (decreasing with time) or only blue PL bands (increasing with time). Although it seems as though the red emission intensity is decreased at the expense of the blue emission intensity, it is likely that the overall PL yield is increased by passivation of non-radiative defects (*See Discussion*), and that the blue PL yield increases faster than the red. Quantitative analysis of the red, blue, and overall PL yields is the subject of on-going studies, which requires careful control over the optical density of the samples. Nonetheless, the FT-IR spectrum of the butanol-dispersed dec-Si NPs (Figure 3.2, c) shows intensity in both the 915 $cm^{-1}$ alkene mode and the 1000-1100 $cm^{-1}$ Si-O-Si mode, and overall, the PL and FT-IR spectra of the dec-Si NP butanol dispersion are intermediate between those of the corresponding ethanol and decanol dispersions.

*Further optical characterization of dec-Si NPs*

In order to explore the nature of the blue and red emissions further, PL excitation (PLE, Fig. 3.7, grey lines), UV-visible absorption (Fig. 3.7, black lines), and time-resolved PL spectra (Fig. 3.8) were measured for dec-Si NPs dispersed in representative solvents (hexane, red PL only; ethanol, blue PL only; butanol, dual red and blue PL; decanol, red PL only). In Fig. 3.7, it can be seen that the PLE spectra corresponding to samples that are predominantly red-emitting are much broader in FWHM than those corresponding to samples with a blue emission band. The narrower PLE bands observed for the blue- or dual red/blue-emitting samples could be partly due to instrumental effects

resulting from partial distortion by the optical filter used for the long wavelength side. Nonetheless, regardless of the dispersion solvent, a fairly narrow excitation peak, centered between 360-390 nm, was observed in the PLE spectra *when monitoring at either the blue or the red emission maximum*. Thus, these data demonstrate that the same absorption results in both the blue and red emissions, further supporting that these emission transitions are related. Furthermore, the relatively narrow PLE spectra observed for the Si NP colloids are atypical for quantum confined nanoparticles and are indicative of absorption transitions involving electronic states that are localized or molecular in nature.

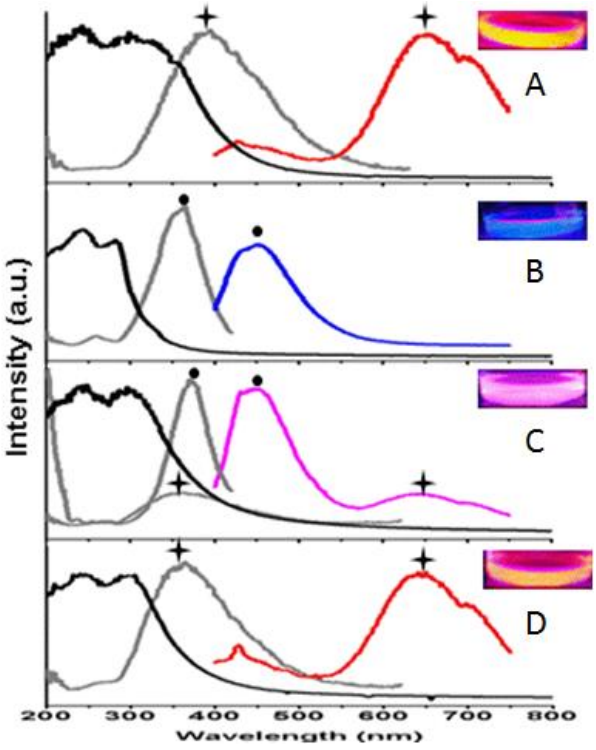


**Figure 3.7.** Absorption (black lines), PLE (grey lines) and PL (red, blue, or pink lines)

spectra of dec-Si NPs dispersed in (A) hexane, (B) ethanol, (C) butanol, and (D) decanol. (✚ and •) indicate corresponding PLE and PL spectra; that is the PLE is monitored at the correspondent PL $\lambda_{max}$ (excitation at 370 nm). Insets, show the color of the Si NP colloids under 365 nm excitation.

However, in the UV-Vis absorption spectra (Fig. 3.7, black lines), the broad absorbance with visible onset and increasing absorption cross-section at higher energies is as expected for quantum confined nanoparticles. Therefore, we propose that the PLE band observed is due to electronic transitions starting from the valance band and ending in a localized surface state, which subsequently leads to the blue and/or red PL. Additionally, because of the overlap of the PLE band with the absorption continuum, some of the localized states must be slightly higher in energy than the bottom of the conduction band corresponding to the direct band gap (*See Discussion*).

We further examined the PL lifetimes of the red- and blue-emissions of these colloids. Fig. 3.8 shows the time-resolved PL spectra of the Si NP colloids on two different time-scales. The intensity decay curves as a function of time (*I(t)*) were fit by the nonlinear least squares method to the double exponential decay function as given by the expression:

$$I(t) = I_0 + A_1 \exp(-t/\tau_1) + A_2 \exp(-t/\tau_2) \qquad (1),$$

where $A_1$ and $A_2$ are the amplitudes and $\tau_1$ and $\tau_2$ are the lifetimes of the two components, respectively, and $I_0$ is the y-axis offset.

For the alcohol colloids, the blue emission decays within several ns, as shown in Fig. 3.8A. However, the blue emission was only weakly observed for the red-emitting

hexane colloid and therefore reliable lifetime data from this sample could not be obtained at the blue $\lambda_{max}$. The excited state lifetime of the blue emission for the alcohol colloids follows the sequence $\tau_{EtOH} < \tau_{BuOH} < \tau_{DecOH,}$ as seen in Table 3.2. Thus, the blue PL lifetime was observed to be fastest in ethanol and slowest in decanol, and which is also correlated with the degree of surface oxidation observed for these samples by FT-IR, being faster with greater degrees of Si-O surface coverage.

Quite different from the blue emission, the red emission has a long lifetime of tens of ms (Fig. 3.8B), and the blue-emitting ethanol colloid does not show a measurable red component. For colloids with strong red components, the lifetime is less correlated with the identity of the dispersion solvent, and there is furthermore no clear lifetime trend paralleling the degree of Si-O surface coverage (see Table 3.2). This may indicate that the red emission is not strongly associated with the surface states, and is more related to the intrinsic states of the Si NPs. Table 3.2 gives the fits for the data shown in Fig. 3.8.

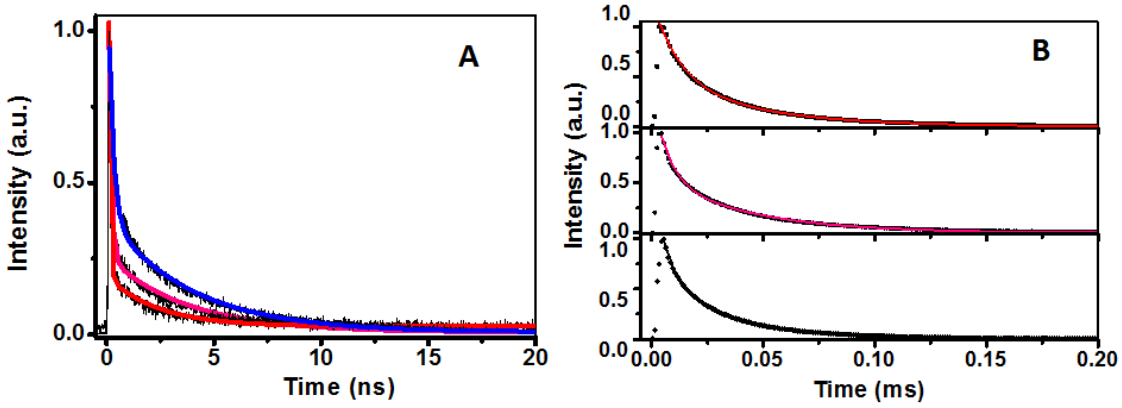


**Figure 3.8.** Photoluminescence intensity time decay of blue- (A) and red- (B) excited states for Si NP colloids dispersed in hexane (black lines), ethanol (blue lines), butanol (pink lines), and decanol (red lines) monitored at the PL $\lambda_{max}$.

Lifetime of blue emission

| | $I_0$ | $A_1$ | $\tau_1$ (ns) | $A_2$ | $\tau_2$ (ns) |
|---|---|---|---|---|---|
| EtOH | 0.008±0.0002 | 0.38±0.001 | 0.26±0.001 | 1.0±0.01 | 4.6±0.05 |
| BuOH | 0.008±0.0002 | 0.25±0.001 | 0.27±0.002 | 1.7±0.02 | 8.7±0.09 |
| DecOH | 0.027±0.0002 | 0.17±0.002 | 0.42±0.006 | 4.0±0.1 | 15.86±0.227 |

Lifetime of red emission

| | $I_0$ | $A_1$ | $\tau_1$ (ms) | $A_2$ | $\tau_2$ (ms) |
|---|---|---|---|---|---|
| BuOH | 0.001±0.0001 | 0.58±0.004 | 23.9±0.118 | 0.88±0.008 | 151±1.99 |
| DecOH | 0.001±0.0001 | 0.51±0.008 | 22.9±0.209 | 0.76±0.007 | 85.9±1.18 |
| Hexane | 0.001±0.00007 | 0.68±0.004 | 31.6±0.125 | 0.98±0.007 | 158±1.78 |

**Table 3.2.** Photoluminescence lifetimes of blue- and red-emitting Si NPs dispersed in hexane, ethanol (EtOH), butanol (BuOH), and decanol (DecOH). Time decay of the photoluminescence intensity (*I(t)*) was fit according to the double exponential decay function: $I(t) = I_0 + A_1 \exp(-t/\tau_1) + A_2 \exp(-t/\tau_2)$, where $I_0$ is the y-axis offset, $A_1$ and $A_2$ are the amplitudes and $\tau_1$ and $\tau_2$ are the lifetimes of the two components, respectively. The hexane sample shows very weak blue emission, with a low signal to noise ratio. The EtOH sample does not show the red emission.

### 3.5 Discussion

A proposed mechanism for the surface chemical reactions resulting in the red-to-blue PL conversion and consistent with the data presented herein is shown in Scheme 3.1. It is generally accepted that thermal hydrosilylation reactions are initiated and propagated *via* Si surface radicals formed by Si-H bond scission.[46] Thus, considering the bulky decyl capping ligands used in this study, after thermal hydrosilylation there are likely surface trap states associated with remaining dangling bonds (*i.e.*, surface radicals) on unpassivated or incompletely coordinated surface Si atoms, which is consistent with

recent reports of EPR active Si NPs.[28, 33] These remaining dangling bonds may further interact dynamically with the and alkene ligands in propagating surface radical reactions.

As shown in the propagation step of Scheme 3.1, Si surface radicals remaining after hydrosilylation may reversibly interact to some extent with surface bound hydrocarbon ligands in the absence of O-donor ligands, which would result in regeneration of the terminal alkene and give rise to the alkene features observed by FT-IR. Supportive of the radical reaction we propose, Veinot and co-workers have recently reported radical-mediated alkene polymerization accompanying surface hydrosilylation reactions to produce Si NPs with oligomerized alkane surfaces.[60] Thus, when the surface capping ligand is sufficiently bulky and unstable, it cannot fully remove the existent dangling bonds, which likely act as non-radiative recombination sites for the photogenerated carriers and thereby reduce the PL quantum yield.

However, when the Si NP surfaces are exposed to alcohols, more of the dangling bonds would be eliminated, since Si-O bonds are more stable (800 kJ/mol in the gas phase) *vs.* Si-H, Si-Si, or Si-C bonds (299, 327, and 452 kJ/mol, respectively, in the gas phase).[61-64] Thus, reaction with alcohols essentially terminates the surface radical reactions, since the Si NPs are stably Si-O passivated. Loss of alkene features in the FT-IR spectra of the short-chained alcohol dispersions with high levels of Si-O surface passivation is compatible with the combination of carbon radicals to produce stable alkanes as the surface radical reaction is terminated, a suggestion that we will further investigate in our future work. Surface alkoxylation, followed by hydrolysis and polycondensation, also accounts for the modest crystallite size change observed in the TEM study and the strong Si-O-Si modes observed in the FT-IR study for the blue-

emitting samples. As we discuss below, changes in the surface passivation as a result of surface radical reactions, accompanied by changes in available excited states, can account for the red-to-blue PL conversion.

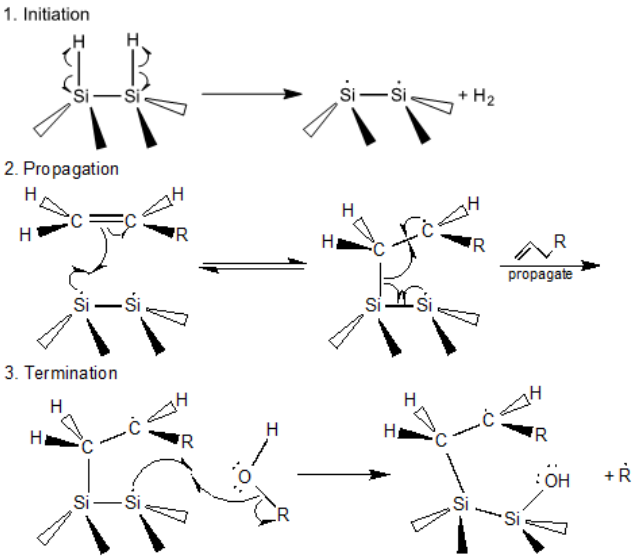


**Scheme 3.1.** Proposed surface reaction mechanism for H-Si NPs in the presence of alkene and/or alcohol (ROH, R = alkyl or H). Once the surface is initially alkylated, either reversal or propagation can occur. Termination of the dynamic radical reaction will occur upon formation of stronger (*vs*. Si-H and Si-C) Si-OH bonds. Hydrolysis and polycondensation following this step is likely (not shown), resulting in an oxidized surface.

Scheme 3.2 shows schematically the energy *vs.* k-space diagram of Si NPs within the first Brillouin zone along the (100) direction. The electronic transitions involved in both the photoexcitation and emission processes are illustrated as arrows, along with the key states and bands involved. While the indirect band gap of bulk Si is 1.1 eV (1100 nm) and the direct band gap is 3.4 eV,[52] quantum confined Si domains are expected to have

wider band gaps proportional to their length scale. We note that the size onset of the QCE effect for nanoscale Si has been discussed in the literature and that red emission is predicted for 4-5 nm diameter Si NPs,[53-55] while it has been experimentally observed for much larger particles, such as these we have studied herein.

For Si NPs with alkylated surfaces, we propose that there exists a large number of surface trap states that may be related to unpassivated sites, including the following two types: 1) dangling bonds (Si•) that would likely result in non-radiative de-excitation of the photogenerated carriers leading to emission intensity loss, and 2) surface reconstructions (*e.g.*, Si=Si), which are expected to be molecular (localized) in nature and may account for the narrow PLE absorptions. Other molecular surface species, such as silanone, have previously been implicated as involved in Si NP PL.[65]

When the red PL is relatively dominant, as in the cases of the dec-Si NPs in hexane or long-chained alcohols, where the surface bonds are primarily Si-C (Panel A), the overall PL yield is likely low and the density of trap states is likely high. In this scenario, following photoexcitation into a localized state, the electron quickly relaxes into the initial state for the red PL and produces the red PL observed. The initial state is likely the bottom of the conduction band, but could also be a localized deep trap state, and the final state is most likely the valance band. The initial state for the blue PL is either absent, or present but non-emissive (i.e., dark). The long lifetime of the red PL indicates that the emission is indirect bandgap in nature or dipole forbidden. The indirect nature of this transition *may differ quantitatively from* that of bulk Si, which has larger $\Delta k$ and PL that is usually very weak.

When the blue PL is dominant, as in the cases of the dec-Si NPs in short-chained alcohols, where the surface has a high degree of Si-O coverage (Panel B), following photoexcitation into a localized excited state, the electron can relax non-radiatively *via* trap states with a certain percentage reaching the initial state for the blue PL and subsequently, to a lesser degree, to the initial state for the red PL. The reduction in intensity or absence of red PL could be due to removal of the initial state responsible for the red PL due to surface passivation or to a relatively small population reaching the red-emitting state compared to the dominant blue-emitting state; nonetheless, the nature of the red PL is believed to be the same as in Panel A. The blue-emitting state, which could be absent or dark in the Si-C cases, now becomes more emissive due to the lower density of trap states as a result of overall better surface passivation. It is likely that the blue, trap state emission is more direct with respect to momentum (k) and does not require phonon assisted excitation and de-excitation, which accounts for the fairly short excited state lifetime of the blue emission (ns).

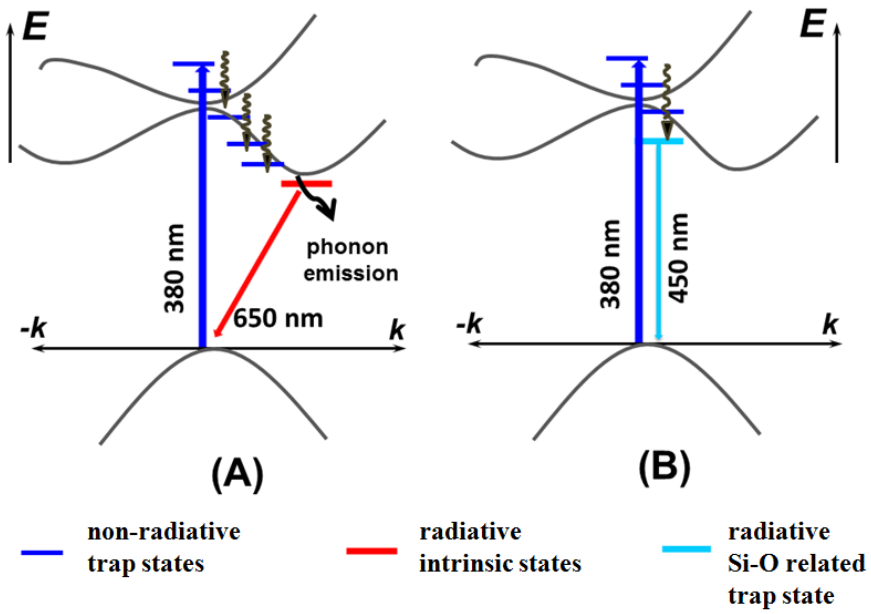


**Scheme 3.2.** E-k diagram of Si within the first Brillouin zone along the (100) direction and the proposed electron transitions in PL and PLE processes. (A) Si NPs with alkylated surface; (B) Si NPs with oxidized surface.

Briefly, we propose that the number of dangling bonds is decreased as the alkylated surface becomes increasingly oxidized. This results in a simultaneous increase in the possibility of radiative transition *via* newly available, Si-O emissive surface trap states, and thus an overall rise in the PL QY. In this scenario, surface dangling bonds act as the trip switch between intrinsic (red) and surface-trap (blue) emissions. Passivation of the surface dangling bonds by O atoms is expected to occur most efficiently in the smallest alcohol solvents. This hypothesis is supported in that the fastest radiative rate of the blue emission for Si NPs is observed in ethanol and in that the radiative rate becomes gradually slower with increasing size of the alcohol.

In general, the majority of Si NPs in water, alcohols and amine (polar) solvents have been reported to be blue-emitting, while the majority of Si NPs in hydrocarbon

(nonpolar) solvents have been reported to be red-emitting. Assignment of the blue PL as arising from the transition from a Si-O related surface trap state to the valence band is consistent with the data we present as well as with several recent literature reports, particularly the surface-oxide-related near-interface traps reported by Cai and co-workers.[28] Alternately, red-to-blue PL conversion has been attributed to the development of surface defects caused by N-donor ligands.[29] However, our work herein and trends reported in literature support that development of emissive trap states maybe a general effect of the formation of stable, highly polarized Si-X (X = N, O, for example) surface bonds.

### 3.6 Conclusion

In summary, visibly emissive Si NPs were synthesized from the high-temperature annealing of a $(HSiO_{1.5})_n$ polymer, followed by chemical etching that allowed for the liberation of Si NPs with hydride surface groups. The H-Si NPs were surface-functionalized *via* thermal hydrosilylation with 1-decene and were re-dispersed in straight chain alcohols varying in carbon chain lengths. The initial red PL band ($\lambda_{em}$ = ~580 nm) observed for the neat hexane dispersions of the alkyl-terminated Si NPs was found to decrease upon exposure to alcohols below a certain minimum chain length. The reduced red PL was also commensurate with an increase in blue PL ($\lambda_{em}$ = ~450 nm). Spectroscopic (FT-IR, steady state and time resolved PL, PLE and UV-visible) and microscopic (TEM) evidence supports that the observed red-to-blue PL conversion is

associated with passivation of the Si NP surfaces by alcohols small enough in steric volume to access the alkyl-passivated surfaces.

Furthermore, spectroscopic data indicate the existence of a localized excited state, as well as competitive emission pathways resulting from both intrinsic and surface states. Specifically, the red PL event can be attributed to emission from an intrinsic state, while the blue PL likely results from a transition between a surface trap state and either the valence band or another trap state. Relaxation from the blue-emitting state to the red emitting state is facilitated by other trap states associated with either defects or dangling bonds. When the red PL dominates, the overall PL yield is likely low and the total number of trap states is likely high. When the blue PL dominates, the overall PL yield is likely relatively higher and the total number of trap states is likely lower. It is possible that each of these emissive states may exist regardless of the observation of PL, as a high density of trap states can quench the PL. However, it is also feasible that the emissive states are directly associated with surface passivation, which we will further investigate in our ongoing work.

### 3.7 Contributions by author

Sheng-Kuei Chiu

Samples and experiments repetition, Figure 3.3, Figrue 3.3, Figure 3.4, Figure 3.6, Figure 3.7, manuscript writing.

Dr. Beth A. Manhat

Figure 3.1.

William J. I. DeBenedetti

Experimental design, Figure 3.2, Figure 3.5, Manuscript writing.

Christine Radlinger

Table 3.1, Figure 3.7, Scheme 3.1, Manuscript writing.

Dr. Jianying Shi

Figure 3.8, Table 3.2, Scheme 3.2, Manuscript writing.

Dr. Andrea M. Goforth, Dr. Jin Z. Zhang

Experimental design, Manuscript writing and revising

## 3.8 References

1. Eberl, K.; Lipinski, M. O.; Manz, Y. M.; Winter, W.; Jin-Phillipp, N. Y.; Schmidt, O. G., Self-assembling quantum dots for optoelectronic devices on Si and GaAs. *Physica E* **2001,** 9, (1), 164-174.

2. Das, A.; Han, Z. J.; Haghighi, M. G.; Eisenberg, R., Photogeneration of hydrogen from water using CdSe nanocrystals demonstrating the importance of surface exchange. *Proceedings of the National Academy of Sciences of the United States of America* **2013,** 110, (42), 16716-16723.

3. Choi, J.; Wang, N. S.; Reipa, V., Conjugation of the photoluminescent silicon nanoparticles to streptavidin. *Bioconjugate Chemistry* **2008,** 19, (3), 680-685.

4. Li, Z. F.; Ruckenstein, E., Water-soluble poly(acrylic acid) grafted luminescent silicon nanoparticles and their use as fluorescent biological staining labels. *Nano Letters* **2004,** 4, (8), 1463-1467.

5. Park, J. H.; Gu, L.; von Maltzahn, G.; Ruoslahti, E.; Bhatia, S. N.; Sailor, M. J., Biodegradable luminescent porous silicon nanoparticles for *in vivo* applications. *Nature Materials* **2009,** 8, (4), 331-336.

6. Mazumder, S.; Dey, R.; Mitra, M. K.; Mukherjee, S.; Das, G. C., Review: Biofunctionalized quantum dots in biology and medicine. *Journal of Nanomaterials* **2009**, 1-9

7. Dabbousi, B. O.; RodriguezViejo, J.; Mikulec, F. V.; Heine, J. R.; Mattoussi, H.; Ober, R.; Jensen, K. F.; Bawendi, M. G., (CdSe)ZnS core-shell quantum dots: Synthesis and characterization of a size series of highly luminescent nanocrystallites. *Journal of Physical Chemistry B* **1997,** 101, (46), 9463-9475.

8. Norris, D. J.; Bawendi, M. G., Measurement and assignment of the size-dependent optical spectrum in CdSe quantum dots. *Physical Review B* **1996,** 53, (24), 16338-16346.

9. Resch-Genger, U.; Grabolle, M.; Cavaliere-Jaricot, S.; Nitschke, R.; Nann, T., Quantum dots versus organic dyes as fluorescent labels. *Nature Methods* **2008,** 5, (9), 763-775.

10. Anas, A.; Akita, H.; Harashima, H.; Itoh, T.; Ishikawa, M.; Biju, V., Photosensitized breakage and damage of DNA by CdSe-ZnS quantum dots. *Journal of Physical Chemistry B* **2008,** 112, (32), 10005-10011.

11. Derfus, A. M.; Chan, W. C. W.; Bhatia, S. N., Probing the cytotoxicity of semiconductor quantum dots. *Nano Letters* **2004,** 4, (1), 11-18.

12. Bouldin, J. L.; Ingle, T. M.; Sengupta, A.; Alexander, R.; Hannigan, R. E.; Buchanan, R. A., Aqueous toxicity and food chain transfer of quantum dots (TM) in

freshwater algae and ceriodaphnia dubia. *Environmental Toxicology and Chemistry* **2008,** 27, (9), 1958-1963.

13. Tsay, J. M.; Michalet, X., New light on quantum dot cytotoxicity. *Chemistry & Biology* **2005,** 12, (11), 1159-1161.

14. Cheng, X. Y.; Lowe, S. B.; Reece, P. J.; Gooding, J. J., Colloidal silicon quantum dots: from preparation to the modification of self-assembled monolayers (SAMs) for bio-applications. *Chemical Society Reviews* **2014,** 43, (8), 2680-2700.

15. Cullis, A. G.; Canham, L. T., Visible-light emission due to quantum size effects in highly porous crystalline silicon. *Nature* **1991,** 353, (6342), 335-338.

16. Canham, L. T., Silicon quantum wire array fabrication by electrochemical and chemical dissolution of wafers. *Applied Physics Letters* **1990,** 57, (10), 1046.

17. Ledoux, G.; Gong, J.; Huisken, F.; Guillois, O.; Reynaud, C., Photoluminescence of size-separated silicon nanocrystals: Confirmation of quantum confinement. *Applied Physics Letters* **2002,** 80, (25), 4834-4836.

18. Henderson, E. J.; Kelly, J. A.; Veinot, J. G. C., Influence of $HSiO_{1.5}$ sol-gel polymer structure and composition on the size and luminescent properties of silicon Nanocrystals. *Chemistry of Materials* **2009,** 21, (22), 5426-5434.

19. Hessel, C. M.; Henderson, E. J.; Veinot, J. G. C., Hydrogen silsesquioxane: A molecular precursor for nanocrystalline Si-$SiO_2$ composites and freestanding hydride-surface-terminated silicon nanoparticles. *Chemistry of Materials* **2006,** 18, (26), 6139-6146.

20. Hua, F. J.; Swihart, M. T.; Ruckenstein, E., Efficient surface grafting of luminescent silicon quantum dots by photoinitiated hydrosilylation. *Langmuir* **2005,** 21, (13), 6054-6062.

21. Gupta, A.; Swihart, M. T.; Wiggers, H., Luminescent colloidal dispersion of silicon quantum dots from microwave plasma synthesis: Exploring the photoluminescence behavior across the visible spectrum. *Advanced Functional Materials* **2009,** 19, (5), 696-703.

22. Hessel, C. M.; Reid, D.; Panthani, M. G.; Rasch, M. R.; Goodfellow, B. W.; Wei, J. W.; Fujii, H.; Akhavan, V.; Korgel, B. A., Synthesis of ligand-stabilized silicon nanocrystals with size-dependent photoluminescence spanning visible to near-infrared wavelengths. *Chemistry of Materials* **2012,** 24, (2), 393-401.

23. Wolf, O.; Dasog, M.; Yang, Z.; Balberg, I.; Veinot, J. G. C.; Millo, O., Doping and quantum confinement effects in single Si nanocrystals observed by scanning tunneling spectroscopy. *Nano Letters* **2013,** 13, (6), 2516-2521.

24. Holmes, J. D.; Ziegler, K. J.; Doty, R. C.; Pell, L. E.; Johnston, K. P.; Korgel, B. A., Highly luminescent silicon nanocrystals with discrete optical transitions. *Journal of the American Chemical Society* **2001,** 123, (16), 3743-3748.

25. Shen, P.; Uesawa, N.; Inasawa, S.; Yamaguchi, Y., Stable and color-tunable fluorescence from silicon nanoparticles formed by single-step plasma assisted decomposition of SiBr4. *Journal of Materials Chemistry* **2010,** 20, (9), 1669-1675.

26. Manhat, B. A.; Brown, A. L.; Black, L. A.; Ross, J. B.; Fichter, K.; Vu, T.; Richman, E.; Goforth, A. M., One-step melt synthesis of water soluble,

photoluminescent, surface-oxidized silicon sanoparticles for cellular imaging applications. *Chemestry of Materials* **2011,** 23, (9), 2407-2418.

27. Dasog, M.; Veinot, J. G. C., Size independent blue luminescence in nitrogen passivated silicon nanocrystals. *Physica Status Solidi A - Applications and Materials Science* **2012,** 209, (10), 1844-1846.

28. Yang, S. K.; Li, W. Z.; Cao, B. Q.; Zeng, H. B.; Cai, W. P., Origin of blue emission from silicon nanoparticles: Direct transition and interface recombination. *Journal of Physical Chemistry C* **2011,** 115, (43), 21056-21062.

29. Dasog, M.; Yang, Z. Y.; Regli, S.; Atkins, T. M.; Faramus, A.; Singh, M. P.; Muthuswamy, E.; Kauzlarich, S. M.; Tilley, R. D.; Veinot, J. G. C., Chemical insight into the origin of red and blue photoluminescence arising from freestanding silicon nanocrystals. *ACS Nano* **2013,** 7, (3), 2676-2685.

30. Qin, G. G.; Song, H. Z.; Zhang, B. R.; Lin, J.; Duan, J. Q.; Yao, G. Q., Experimental evidence for luminescence from silicon oxide layers in oxidized porous silicon. *Physical Review B* **1996,** 54, (4), 2548-2555.

31. Trukhin, A. N.; Goldberg, M.; Jansons, J.; Fitting, H. J.; Tale, I. A., Silicon dioxide thin film luminescence in comparison with bulk silica. *Journal of Non-Crystalline Solids* **1998,** 223, (1-2), 114-122.

32. Shluger, A.; Stefanovich, E., Models of the self-trapped exciton and nearest-neighbor defect pair in $SiO_2$. *Physical Review B* **1990,** 42, (15), 9664-9673.

33. Godefroo, S.; Hayne, M.; Jivanescu, M.; Stesmans, A.; Zacharias, M.; Lebedev, O. I.; Van Tendeloo, G.; Moshchalkov, V. V., Classification and control of the origin of photoluminescence from Si nanocrystals. *Nature Nanotechnology* **2008,** 3, (3), 174-178.

34. de Boer, W.; Timmerman, D.; Dohnalova, K.; Yassievich, I. N.; Zhang, H.; Buma, W. J.; Gregorkiewicz, T., Red spectral shift and enhanced quantum efficiency in phonon-free photoluminescence from silicon nanocrystals. *Nature Nanotechnology* **2010,** 5, (12), 878-884.

35. Dohnalova, K.; Poddubny, A. N.; Prokofiev, A. A.; de Boer, W.; Umesh, C. P.; Paulusse, J. M. J.; Zuilhof, H.; Gregorkiewicz, T., Surface brightens up Si quantum dots: Direct bandgap-like size-tunable emission. *Light - Science & Applications* **2013**, 2, 1-6.

36. Kanemitsu, Y., Luminescence properties of nanometer-sized Si crystallites: Core and surface states. *Physical Review B* **1994,** 49, (23), 16845-16848.

37. Mariotti, D.; Mitra, S.; Svrcek, V., Surface-engineered silicon nanocrystals. *Nanoscale* **2013,** 5, (4), 1385-1398.

38. Liu, S. M., Luminescent silicon nanoparticles formed in solution. *Journal of Nanoscience and Nanotechnology* **2008,** 8, (3), 1110-1125.

39. Cooke, D. W.; Bennett, B. L.; Farnum, E. H.; Hults, W. L.; Sickafus, K. E.; Smith, J. F.; Smith, J. L.; Taylor, T. N.; Tiwari, P.; Portis, A. M., SiOx luminescence from light-emitting porous silicon: Support for the quantum confinement luminescence center model. *Applied Physics Letters* **1996,** 68, (12), 1663-1665.

40. Germanenko, I. N.; Li, S. T.; El-Shall, M. S., Decay dynamics and quenching of photoluminescence from silicon nanocrystals by aromatic nitro compounds. *Journal of Physical Chemistry B* **2001,** 105, (1), 59-66.

41. Sweryda-Krawiec, B.; Cassagneau, T.; Fendler, J. H., Surface modification of silicon nanocrystallites by alcohols. *Journal of Physical Chemistry B* **1999,** 103, (44), 9524-9529.

42. Rehm, J. M.; McLendon, G. L.; Tsybeskov, L.; Fauchet, P. M., How methanol affects the surface of blue and red emitting porous silicon. *Applied Physics Letters* **1995,** 66, (26), 3669-3671.

43. Sweryda-Krawiec, B.; Chandler-Henderson, R. R.; Coffer, J. L.; Rho, Y. G.; Pinizzotto, R. F., A comparison of porous silicon and silicon nanocrystallite photoluminescence quenching with amines. *Journal of Physical Chemistry* **1996,** 100, (32), 13776-13780.

44. Bradley, D.; Williams, G.; Lawton, M., Drying of organic solvents: Quantitative evaluation of the efficiency of several desiccants. *Journal of Organic Chemistry* **2010,** 75, (24), 8351-8354.

45. Chiu, S. K.; Manhat, B. A.; DeBenedetti, W. J. I.; Brown, A. L.; Fichter, K.; Vu, T.; Eastman, M.; Jiao, J.; Goforth, A. M., Aqueous red-emitting silicon nanoparticles for cellular imaging: Consequences of protecting against surface passivation by hydroxide and water for stable red emission. *Journal of Materials Research* **2013,** 28, (2), 216-230.

46. Buriak, J. M., Organometallic chemistry on silicon and germanium surfaces. *Chemical Reviews* **2002,** 102, (5), 1271-1308.

47. Satter, K., *Handbook of Thin Films Materials*. Nanomaterials and magnetic thin films, Academic Press ed., San Diego, USA, 2003.

48. Zhang, X. M.; Neiner, D.; Wang, S. Z.; Louie, A. Y.; Kauzlarich, S. M., A new solution route to hydrogen-terminated silicon nanoparticles: synthesis, functionalization and water stability. *Nanotechnology* **2007,** 18, (9), 1-6.

49. Heintz, A. S.; Fink, M. J.; Mitchell, B. S., Mechanochemical synthesis of blue luminescent alkyl/alkenyl-passivated silicon nanoparticles. *Advanced Materials* **2007,** 19, (22), 3984-3988.

50. Pettigrew, K. A.; Liu, Q.; Power, P. P.; Kauzlarich, S. M., Solution synthesis of alkyl- and alkyl/alkoxy-capped silicon nanoparticles *via* oxidation of $Mg_2Si$. *Chemistry of Materials* **2003,** 15, (21), 4005-4011.

51. Shiohara, A.; Hanada, S.; Prabakar, S.; Fujioka, K.; Lim, T. H.; Yamamoto, K.; Northcote, P. T.; Tilley, R. D., Chemical reactions on surface molecules attached to silicon quantum dots. *Journal of the American Chemical Society* **2010,** 132, (1), 248-253.

52. Warner, J. H.; Hoshino, A.; Yamamoto, K.; Tilley, R. D., Water-soluble photoluminescent silicon quantum dots. *Angewandte Chemie* **2005,** 117, (29), 4626-4630.

53. van Buuren, T.; Dinh, L. N.; Chase, L. L.; Siekhaus, W. J.; Terminello, L. J., Changes in the electronic properties of Si nanocrystals as a function of particle size. *Physical Review Letters* **1998,** 80, (17), 3803-3806.

54. Trwoga, P. F.; Kenyon, A. J.; Pitt, C. W., Modeling the contribution of quantum confinement to luminescence from silicon nanoclusters. *Journal of Applied Physics* **1998,** 83, (7), 3789-3794.

55. Barbagiovanni, E. G.; Lockwood, D. J.; Simpson, P. J.; Goncharova, L. V., Quantum confinement in Si and Ge nanostructures. *Journal of Applied Physics* **2012,** 111, 034307.

56. Pasternack, R. M.; Amy, S. R.; Chabal, Y. J., Attachment of 3-(aminopropyl)triethoxysilane on silicon oxide surfaces: Dependence on solution temperature. *Langmuir* **2008,** 24, (22), 12963-12971.

57. Michalak, D. J.; Amy, S. R.; Aureau, D.; Dai, M.; Esteve, A.; Chabal, Y. J., Nanopatterning Si(111) surfaces as a selective surface-chemistry route. *Nature Materials* **2010,** 9, (3), 266-271.

58. Thissen, P.; Peixoto, T.; Longo, R. C.; Peng, W. N.; Schmidt, W. G.; Cho, K. J.; Chabal, Y. J., Activation of surface hydroxyl groups by modification of H-terminated Si(111) surfaces. *Journal of the American Chemical Society* **2012,** 134, (21), 8869-8874.

59. Kusova, K.; Cibulka, O.; Dohnalova, K.; Pelant, I.; Valenta, J.; Fucikova, A.; Zidek, K.; Lang, J.; Englich, J.; Matejka, P.; Stepanek, P.; Bakardjieva, S., Brightly luminescent organically capped silicon nanocrystals fabricated at room temperature and atmospheric pressure. *ACS Nano* **2010,** 4, (8), 4495-4504.

60. Yang, Z. Y.; Iqbal, M.; Dobbie, A. R.; Veinot, J. G. C., Surface-induced alkene oligomerization: Does thermal hydrosilylation really lead to monolayer protected silicon nanocrystals? *Journal of the American Chemical Society* **2013,** 135, (46), 17595-17601.

61. Huber, K. P.; Herzberg, G., *Molecular Spectra and Molecular Structure Constants of Diatomic Molecules*. Van Nostand: New York, 1979.

62. Chatillon, C.; Allibert, M.; Pattoret, A., High-temperature knudsen cell mass-spectrometry-atomization energies determination of $Si_2$, $Si_3$, $Al_2$, AlSi, and $AlSi_2$ molecules. *Comptes Rendus Hebdomadaires Des Seances De L Academie Des Sciences Serie C* **1975,** 280, (25), 1505-1508.

63. Verhaegen, G.; Stafford, F. E.; Drowart, J., Mass spectromeric study of systems boron-carbon/ boron-carbon-silicon. *Physics* **1964,** 40, (6), 1622-1628.

64. Pedley, J. B.; Marshall, E. M., Thermochemical data for gaseous monoxides. *Journal of Physical and Chemical Reference Data* **1983,** 12, (4), 967-1031.

65. Luppi, E.; Iori, F.; Magri, R.; Pulci, O.; Ossicini, S.; Degoli, E.; Olevano, V., Excitons in silicon nanocrystallites: The nature of luminescence. *Physical Review B* **2007,** 75, 033303.

## Chapter 4

## Temporal and environmental effects on PL with changes of core size and surface chemistry in Si NP

### 4.1 Abstract

The motivation of this chapter is to test PL changes in H-Si NPs *via* acidic and basic treatments. Red-to-blue conversion in PL spectra was achieved by both acid/base additions and different etching time approaches, and that both etched products can be treated to look at size independent effect of oxidation.

### 4.2 Experimental

#### 4.2.1 Materials

A Schlenk line was utilized to maintain an air-free environment during the sol-gel polycondensation and thermal hydrosilylation reactions, with either $N_2$ or Ar as the inert gas. Other synthetic procedures, such as etching and solvent media switching, were done in air. Trichlorosilane ($HSiCl_{3(l)}$, ≤ 98%; Alfa Aesar), 1-decene ($CH_3(CH_2)_8CH_{2(l)}$, ≤ 97%; Aldrich), aqueous hydrofluoric acid ($HF_{(aq)}$, 48.0–51.0%, Fisher Scientific), aqueous hydrochloric acid ($HCl_{(aq)}$, 12N, Fisher Scientific), potassium hydroxide ($KOH_{(aq)}$, reagent grade, EMD chemicals), and ethanol (anhydrous $EtOH_{(l)}$, ACS grade, Pharmco-AAper) were purchased for syntheses and used without further purification.

### 4.2.2 Synthesis of nanocrystalline Si NPs encased in an oxide matrix by thermal reduction

5 mL of trichlorosilane was hydrolyzed and polycondensed to produce a sol-gel polymer hydrosilicate as previously reported.[1] A tube furnace was used to anneal approximately 0.9 g of the hydrosilicate polymer at 1100 °C for 10 h under flowing $N_2$ gas to yield nanocrystalline silicon encased in an oxide matrix (Si NC/$SiO_x$, $x \leq 2$).

### 4.2.3 Synthesis of H-Si NPs

The annealed Si NC/$SiO_x$ ($x \leq 2$) powders were ball-milled for 10 seconds in a tungsten carbide lined milling vial with two 1 cm tungsten carbide balls and a Spex 8000M mill mixer (SPEX SamplePrep, Metuchen, NJ). The milled Si NC/$SiO_x$ powder was subsequently etched in a chemical etching solution of 1:1:1 (by volume) ethanol/water/$HF_{(aq)}$ to liberate hydride-terminated Si NPs (H-Si NPs), and subsequently partitioned extracted into 50 mL of pentane by biphasic extraction. The influence of PL in H-Si NPs will be studied *via* pH changes in solution and the difference in etch time.

### 4.2.4 Acid-base Addition for Reversible Red and Blue Emission in H- Si NPs

Rotary evaporation was used to remove pentane or hexane from H-Si NP colloids prepared as described in previous Section 4.1.3. Approximately 20 mg of H-Si NPs were then re-dispersed in 3 mL of anhydrous ethanol in a reaction vial. 100 µL of a 2.5 M aqueous solution of $KOH_{(aq)}$ was added to the vial, with PL and FT-IR spectroscopy used to characterize the resulting colloid. Following bas addition, 200 µL of 12 N $HCl_{(aq)}$ was then injected into the vial, and the resulting colloid was also characterized by PL and

FT-IR spectroscopy. The base and acid additions to the ethanolic H-Si NP colloids were done in air.

### 4.2.5 Synthesis of dec-Si NPs and post-treatment of dec-Si NPs

A thermal hydrosilylation reaction was performed to functionalize Si NPs and generate decane-terminated Si NPs (dec-Si NPs). To accomplish this, 3 mL of 1-decene was degassed and transferred into a two-necked round-bottom flask containing 20 mg of H-Si NPs, followed by refluxing for 18 hrs under inert gas flow. After the thermal hydrosilylation reaction was completed, dec-Si NPs were re-dispersed in 5 mL of hexane and degassed to minimize oxygen exposure. As a control, sample of dec-Si NPs in 1-decene was heated at 160 °C in ambient air for 18 hrs. This treatment is referred to as the hot-air treatment (HA-treatment) from here on out.

### 4.2.6 Characterization of H-Si NP colloids

#### Photoluminescence (PL) and Photoluminescence Excitation (PLE) Spectroscopy

Emission spectra (i.e., PL spectra) were collected using a Shimadzu-RF5310 PC spectrophotometer in the 400 to 700 nm range with excitation at 370 nm. It should be mentioned that the instrument has an abated sensitivity over the red-to-NIR spectral region. PLE spectra were collected on the same instrument and were monitored at the corresponding PL $\lambda_{max}$.

#### ATR-FT-IR Spectroscopy

Si NP composition was examined using a ThermoFisher Nicolet iS10 infrared spectrometer in reflection geometry with a single bounce diamond attenuated total reflectance (ATR) accessory. Si NP samples were drop-cast onto the ATR crystal to form a thin film for FT-IR spectrum acquisition. A heat gun was used to evaporate excess solvents to avoid solvent interference during the measurement.

**Dynamic Light Scattering (DLS)**

Approximately 20 mg of H-Si NPs were re-dispersed into 3 mL of hexane, and the size distribution of the Si NPs was measured using a Horiba LB-550 DLS instrument with a 532 nm laser (Horiba, Edison, NJ). Measurements were taken on serially diluted samples to minimize multiple scattering effects.

**Transmission Electron Microscopy (TEM)**

The crystallinity, size, and morphology of H-Si NPs were studied on a FEI Tecnai F-20 TEM (North America NanoPort, Hillsboro, OR) operating at 200 kV. TEM samples were prepared by drop casting H-Si NP colloids onto 400 mesh holey carbon-coated Cu grids (Ted Pella, Redding, CA) prior to TEM measurement.

## 4.3 Results

### 4.3.1 Reversible red-to-blue PL conversion in ethanolic colloids of H-Si NPs *via* subsequent acid/base additions

To understand the effects of acidic and basic additions on the PL behavior and composition of H-Si NPs, $KOH_{(aq)}$ and $HCl_{(aq)}$ were added successively into ethanolic

colloids of H-Si NPs. The successive additions to the ethanolic H-Si NP colloids were monitored by PL and FT-IR spectroscopy.

Prior to the sequence of base and acid additions, the H-Si NPs, which were dispersed in pentane, had a red emission with $\lambda_{max}$ at 580 nm when excited with a wavelength of 370 nm (Figure 4.1, wine line). This red PL was quenched immediately after pentane removal upon re-dispersion of the H-Si NPs in anhydrous $EtOH_{(l)}$ (Figure 4.1, black line). Weak blue PL (Figure 4.1, blue dashed line) was observed after $KOH_{(aq)}$ addition to ethanolic colloids of H-Si NPs, and the intensity of the blue PL with $\lambda_{max}$ at 460 nm (excitation at 370 nm) was enhanced after 24 hrs (Figure 4.1, blue solid line). The $\lambda_{max}$ of 580 nm previously observed prior to the addition of $KOH_{(aq)}$ was re-established following addition of $HCl_{(aq)}$ (Figure 4.1, red line) to the $KOH_{(aq)}$-containing ethanolic colloids of H-Si NPs while the blue PL at 460 nm was again quenched.

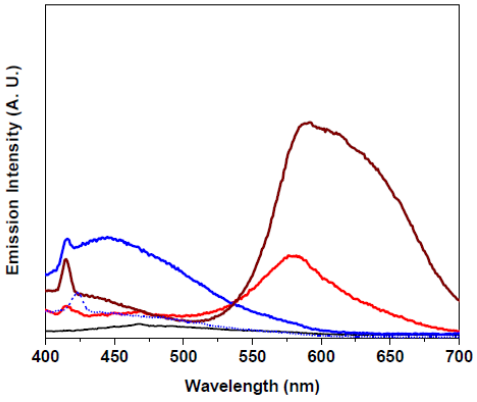


**Figure 4.1.** Emission spectra of H-Si NPs in pentane (wine line), $EtOH_{(l)}$ (black line), $EtOH/KOH_{(aq)}$ (blue dashed line), $EtOH/KOH_{(aq)}$ after aging 24 hrs (blue line), and in $EtOH/KOH_{(aq)}$ after $HCl_{(aq)}$ addition sufficient to neutralize $OH^-$ (red line).

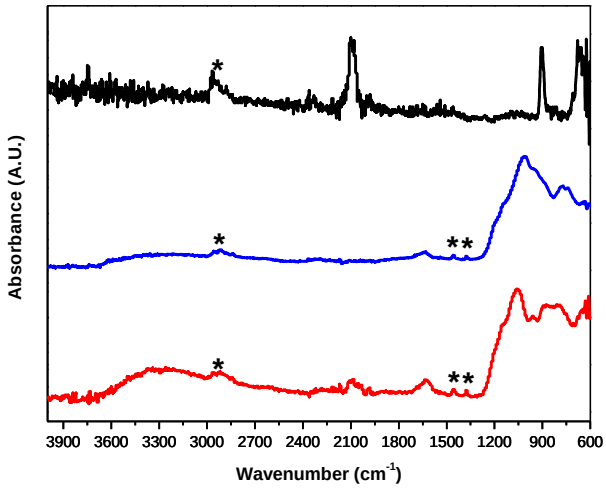


**Figure 4.2.** FT-IR spectra of H-Si NPs dispersed from pentane (black line), base (blue line), and acid (red line). * = alkane (solvent).

The FT-IR spectrum of H-Si NPs and dispersed from pentane following etching shows a Si-H stretching peak at 2083 $cm^{-1}$, a Si-$H_2$ scissor mode at 910 $cm^{-1}$ and a Si-$H_2$ bending mode at 665 $cm^{-1}$ (Figure 4.2, black line). No evidence of Si-O features is seen in the 1000-1100 $cm^{-1}$ range, indicatingthat the freshing etched H-Si NPs can be regarded as un-oxidized. However, after the addition of $KOH_{(aq)}$ to the ethanolic colloids of H-Si NPs, Si-H stretching modes were no longer observed, and a broad vibration in the approximately 700-1200 $cm^{-1}$ range was present, which may be attributed to Si-O surface modes arising from surface oxidation (Figure 4.2, blue line).[2] This result may suggest that the hydrogen passivation initially present on the Si NP surfaces has been replaced with an oxidized $SiO_x$-type shell upon dispersion in aqueous base. Subsequently after the addition of $HCl_{(aq)}$ to the $KOH_{(aq)}$-containing ethanolic colloids of Si NPs, the weak Si-H stretch at 2083 $cm^{-1}$ in the FT-IR spectrum was present again (Figure 4.2, red line), which suggests

that Si-H bonding was restored to some degree on the Si NP surfaces, in the acid treatment and that this restoration of the surface is correlated with the re-emergence of the red PL.

However, the strong Si-O-Si stretching indicative of surface oxidation remained after the acid treatment. Additionally, it should be noted that weak stretch at 1650 $cm^{-1}$ was observed in both the basic and acidic samples (Figure 4.2, blue and red lines), which may suggest a carbonyl stretch from acetaldehyde (the oxidation product of ethanol) in the presence of Si NPs under these conditions.[3]

### 4.3.2 Conversion from red to blue PL in H-Si NP colloids *via* HF etch control

Red-emitting H-Si NPs with a $\lambda_{max}$ at 580 nm (Figure 4.3 a, red line, excitation at 370 nm) were obtained *via* a 1 hour wet chemical etching of the annealed, ball-milled Si NC/$SiO_x$ powders; the nanoparticle size distribution after 1 hr of $HF_{(aq)}$ etching was 10.0 ± 2.2 nm by DLS measurement (Figure 4.3 b). In addition, lattice fringes with a 3.1 Å d-spacing were observed by HR-TEM (Figure 4.3 c), which corresponded to the (111) plane spacing of nanocrystalline silicon domains.

After a 2.5 h wet chemical etch of the annealed Si NC/$SiO_x$ powders, blue-emitting H-Si NPs with a $\lambda_{max}$ of 410 nm were obtained (Figure 4.3 d, blue line, excited of 370 nm), with an average particle size of 4.3 ± 1.0 nm as observed by DLS (Figure 4.3 e). Furthermore, lattice fringes with the same d-spacing as the red-emitting H-Si NPs were also observed (Figure 4.3 f) by HR-TEM. Though both red- and blue-emitting H-Si

NPs from the same annealed Si NC/$SiO_x$ powders contain crystalline $Si^0$ domains a blue shift (the conversion from red to blue emission) is observed in the PL emission spectra with the longer etch time, which the blue shift in the PL spectra of H-Si NPs is a core-related size effect, considering both red- and blue-emitting H-Si NPs can be presumed to have the same hydrogen surface passivation (Figure 4.2, black line for red-emitting H-Si NPs; FT-IR measurement of blue-emitting H-Si NPs was not shown because of sample's low concentration).

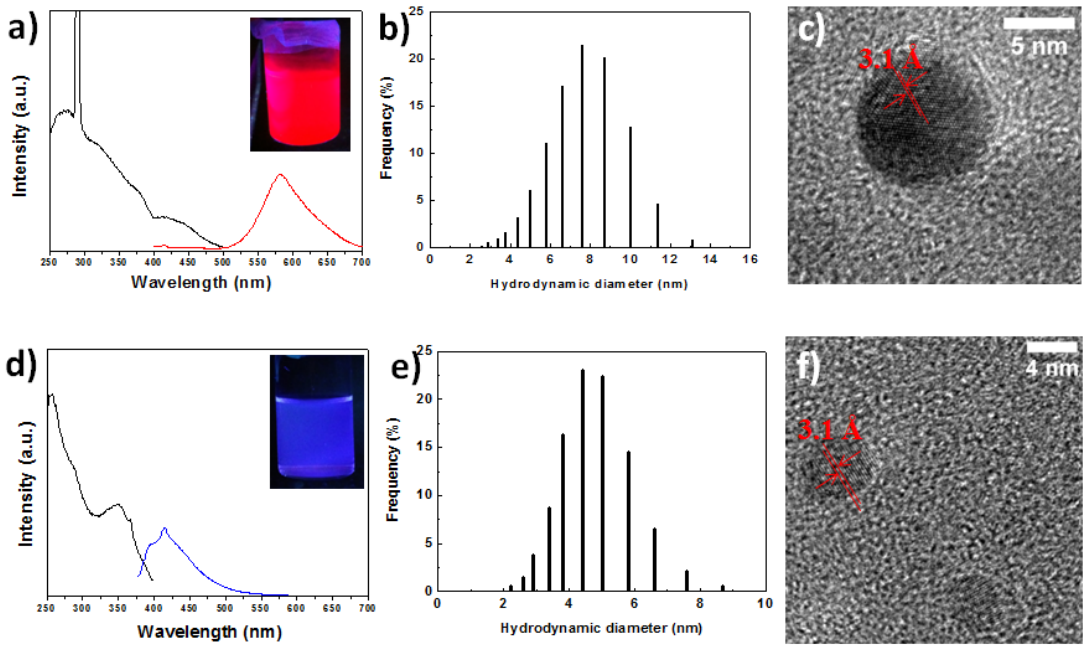


**Figure 4.3.** PLE (monitored at 410 nm and 580 nm) and PL (excitation at 370 nm) spectra (a), DLS size distribution (b), and HR-TEM image of H-Si NPs produced from a 1 hour etch (c). PLE (monitored at 410 nm and 580 nm) and PL (excitation at 370 nm) spectra (d), DLS size distribution (e), and HR-TEM image of H-Si NPs produced from a

2.5 hours etch (f). Insets: digital images of H-Si NPs colloids in hexane, under 365 nm UV-light irradiation.

### 4.3.3 Size-independent cyan-blue emission in Si NPs *via* surface thermal oxidation.

For the two differently size H-Si NP samples produced by varying the HF-etch time in Section 4.2.2, the PL $\lambda_{max}$ was not changed by the air-free thermal hydrosilylation of Si NPs with 1-decene , although FT-IR demonstrated that the hydrogen passivation was replaced by carbon passivation from 1-decene, as shown in Figures 4.3 and 4.4.

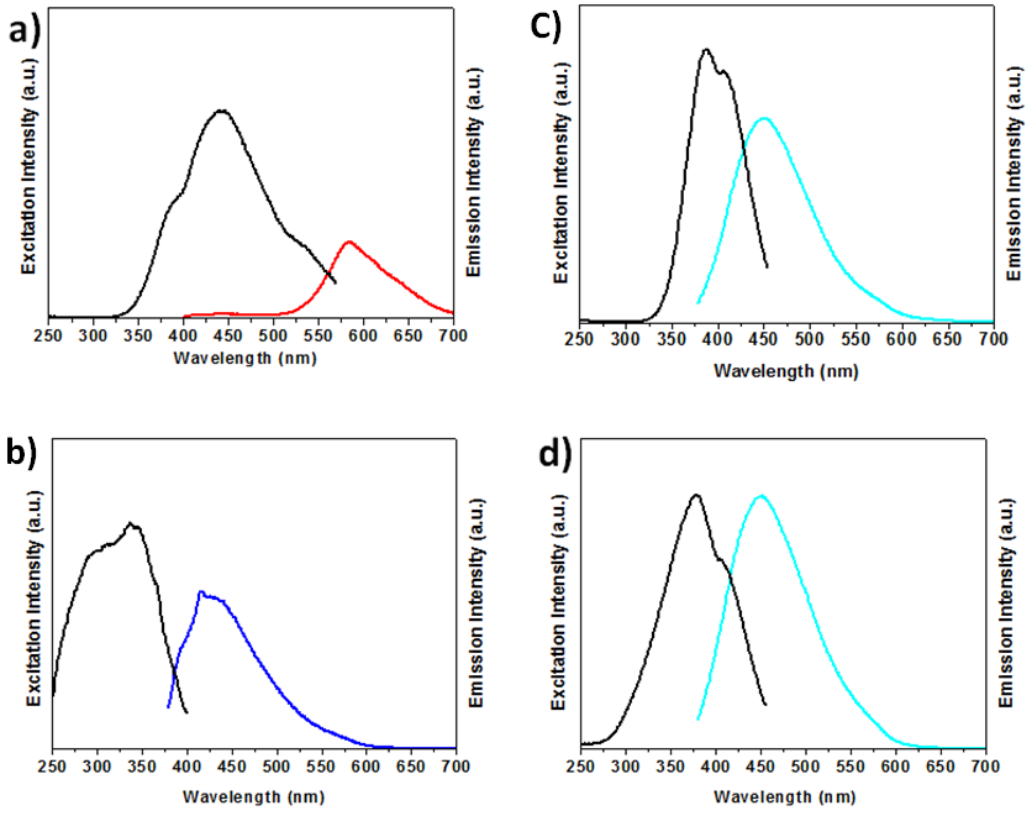


**Figure 4.4.** a) and c) are PLE (black lines) and PL (red and blue lines) spectra of dec-Si NPs; b) and d) are PLE (black lines) and PL (cyan-blue lines) spectra of dec-Si NPs after

underwent HA-treatment. The PLE is monitored at the corresponding PL emission at $\lambda_{max}$, and excitation wavelength at 370 nm for PL spectra.

However in comparing the PLE spectra before and after the HA-treatment reaction, it can be seen that the PLE absorption become narrorer after Si-C replaces Si-H for both Si NP size populations (as shown in Figure 4.3, a and d vs. Figure 4.4, a and b) Subsequently, regardless of the size population and initial PL $\lambda_{max}$, when Si NPs underwent the HA-treatment, the $\lambda_{max}$ of the PL emission shifted to 460 nm and the PLE spectra also become more similar. H-Si NP PLE spectrum look more like absorption continuing with visible onset expected for QDs, but dec-Si NP PLE spectra before and after HA-treatment are narrower, more resembling the absorption spectra of molecular fluorophore.

To monitor for compositional chages in the Si NPs after the HA-treatment, FT-IR spectroscopy was utilized. In Figure 4.5 (A), the FT-IR spectrum of neat 1-decene is also shown for comparison with the dec-Si NPs after thermal hydrosilylation. The internal RCH=CHR structure vibration at 730 $cm^{-1}$, RCH=$CH_2$ modes at 910-920 $cm^{-1}$ and 990-1000 $cm^{-1}$, C=C bond vibration at 1640-1680 $cm^{-1}$, and =C-H unsaturated vinyl modes vibration at 675 $cm^{-1}$ and 3020-3080 $cm^{-1}$ were assigned as alkene-related features in 1-decene. For alkane features, the CH methyl rock mode at 1375 $cm^{-1}$, CH methyl scissor mode at 1460 $cm^{-1}$, and C-C-H stretches at 2900 – 3000 $cm^{-1}$ were also observed in the FT-IR spectrum for 1-decene. The two signature Si-C bond vibration peaks found at 800 $cm^{-1}$ and 1260 $cm^{-1}$ in dec-Si NPs (as shown in Figure 4.5 (B)) suggests

passivation with decane on the Si NP surface. A weak surface oxidation was also observed after hydrosilylation with 1-decene; the Si-O-Si (TO/LO modes) modes seen at 1000-1100 $cm^{-1}$ in Figure 4.5 (B), indicate some degree of particle oxidation during the H-Si NP thermal hydrosilylation reaction with 1-decene.

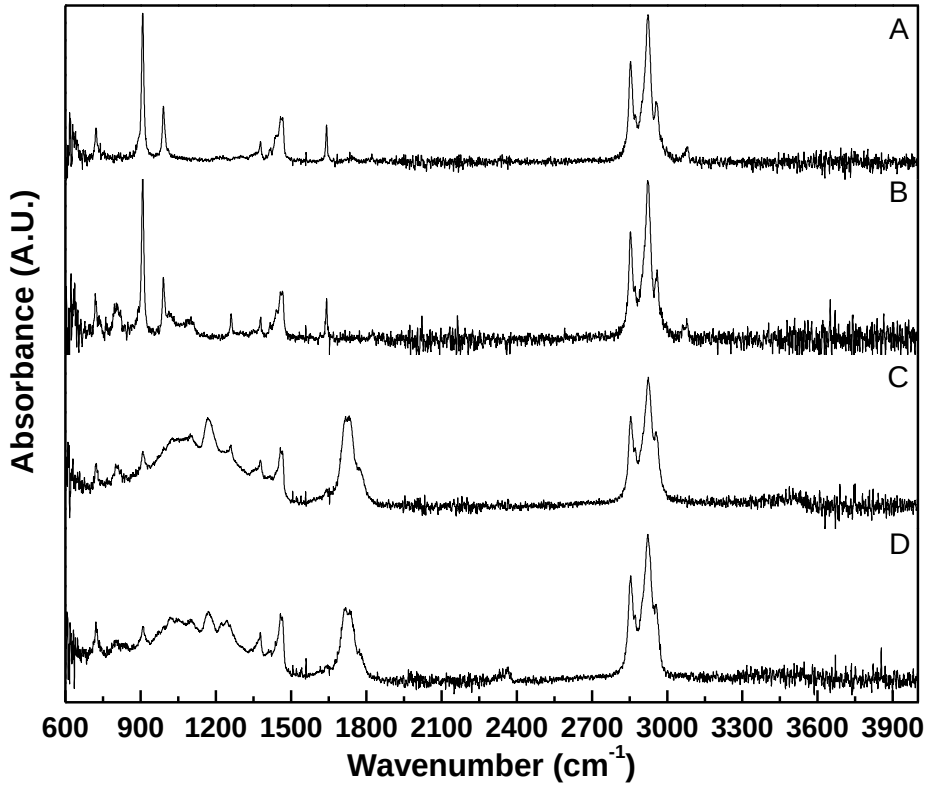


**Figure 4.5.** FT-IR spectra of (A) 1-decene, (B) red-emitting, dec-Si NPs dispersed from hexanes, (C) after HA-treatment, originally red-emitting, dec-Si NPs dispersed in excess 1-decene, and (D) after HA-treatment, originally blue-emitting, dec-Si NPs dispersed in excess 1-decene.

FT-IR analysis of the red-emitting dec-Si NPs that underwent the HA-treatment after air-free thermal hydrosilylation showed an increase in the level of surface oxidation, as seen in Figure 4.5 (C). Some alkene feature peaks disappeared, such as =C-H unsaturated vinyl structure vibration at 675 $cm^{-1}$ and 3020-3080 $cm^{-1}$, the C=C bond vibration at 1640-1680 $cm^{-1}$. Additionally, the RCH=CHR vinyl structure vibration at 730 $cm^{-1}$ and RCH=$CH_2$ vibration at 910-920 $cm^{-1}$ and 990-1000 $cm^{-1}$ became weaker, as shown in Figure 4.5 (C).

However, two new vibrations at 1150 $cm^{-1}$ and 1718 $cm^{-1}$ were observed,[3, 4] which is unexpected in Si NP after HA-treatment; further characterizations need to be measured to cyan-blue emitting Si NPs for identifying possible components for cyan-blue emission. Interestingly, a similar surface chemistry was observed in blue-emitting dec-Si NPs after undergoing the HA-treatment. This may suggest that the cyan-blue emission is related to the increase of surface oxidation in Si NPs, formed during the HA-treatment. It is worth noting that the two signature Si-C bond vibration peaks at 800 $cm^{-1}$ and 1260 $cm^{-1}$ remained in the FT-IR spectra (as shown in Figure 4.5 (C) and (D)), which suggests that surface may still contain some decane passivation after the HA-treatment.

## 4.4 Discussion

### Size-independent Photoluminescence in Si NPs *via* surface oxidation

As scheme 4.1 shows, when hydroxide ions were introduced to H-Si NPs, blue PL was observed from $KOH_{(aq)}$-containing ethanolic Si NPs colloids (which were originally

red-emitting H-Si NPs dispersed in pentane) and resulting in a broad $SiO_x$ (surface oxidation) peak from 700 to 1200 $cm^{-1}$, along with stretches corresponding to the presence of free hydroxide ions stretch seen from 3300 to 3600 $cm^{-1}$. Since the average diameter of base-containing, blue-emitting Si NPs was 7.1± 1.8 nm (measured by DLS, data not shown), which is not a typical quantum confinement-related blue PL event as Si NP size is below 4 nm,[5] this implies the blue PL event is a result of surface oxidation in Si NPs, which is surface-related PL event. The PL behavior was no longer dominated by this core state, but rather by surface oxidation.[6,7,8] Interestingly, the red PL event was reestablished in $KOH_{(aq)}$-containing ethanolic Si NP colloids after HCl addition. A weak Si-H stretch at 2083 $cm^{-1}$ appeared and a shoulder-like peak at 900 $cm^{-1}$ for $Si-H_2$ bending mode were found in the FT-IR spectrum, suggesting the red PL event is related to the partial removal of surface oxidization from the particles. Although the Si-O-Si stretch at 1000 to 1100 $cm^{-1}$ and free hydroxide stretches at 3300 to 3600 $cm^{-1}$ are still present in the FT-IR spectrum, this reveals the surface of Si NPs are still partial oxidized and passivated with hydroxide.

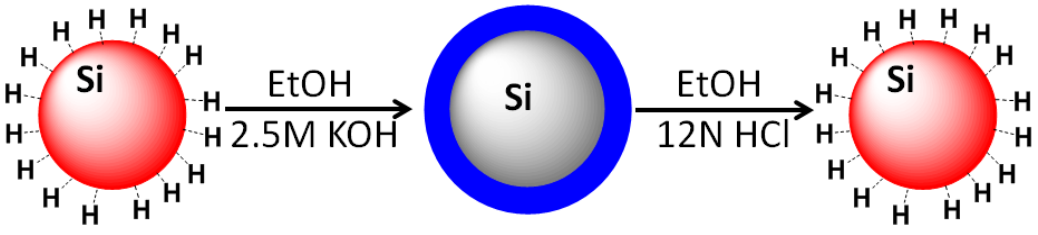


**Scheme 4.1.** Scheme showing the sequence of base and acid additions to ethanolic colloids of H-Si NP, which result in reversible red-to-blue luminescence conversion. As

described herein, red PL originates from the H-Si NP core (red circles), while blue PL is associated with the development of an oxidized surface (blue shell).

H-Si NPs have been reported that the emission wavelength is inversely proportional to the diameter of the nanoparticle.[9,5] Theoretical calculations predict that red- and blue-emitting particles should have ~4.5 nm and ~2.0 nm diameters, respectively.[10,11,12] In this work, the average diameter of red-emitting H-Si NP pentane colloids is 10 ± 2.2 nm, and blue-emitting H-Si NPs is 4 ± 1.0 nm. While these sizes are larger than those predicted with the theoretical calculations, DLS measurement to NP size is over estimated because the measured particle size is hydrodynamic diameter, instead of real nanoparticle diameter  This blue shift in the PL lambda max may be due to QC, corresponding to size reduction of H-Si NPs. Without further surface oxidation in H-Si NPs (examined by FT-IR), the PL emission suggests a size-related core state of $\lambda_{max}$, as demonstrated in the corresponding PL spectra and TEM data for H- and dec-Si NPs.

When dec-Si NPs with significantly different size distributions underwent HA-treatment, both were observed to emit the same cyan-blue. With very similar surface chemistry observed by FT-IR in Si NPs, cyan-blue emission may be related to surface effect. However, further size analysis by TEM or DLS for dec-Si NPs after the HA-treatment is necessary to confirm the assumption of that the size of dec-Si NPs does not change significantly to give a large emission shift in the PL spectra after the HA-treatment.

## 4.5 Conclusion

In this study, red-to-blue PL conversion was repeated by base ($KOH_{(aq)}$) and acid ($HCl_{(aq)}$) additions to H-Si NPs. Blue PL was consistently observed in Si NPs when the surface of the Si NP was hydroxide passivated and oxidized following the addition of $KOH_{(aq)}$ (wet oxidation). The hydroxide passivated surface acts as a deep surface trap and alters the excitonic radiative recombination pathway in $KOH_{(aq)}$-containing ethanolic Si NPs colloids, producing a short wavelength, high-energy, blue PL band. The acid ($HCl_{(aq)}$) addition to $KOH_{(aq)}$-containing ethanolic Si NPs colloids changed surface chemical components, and a weak Si-H stretch was observed again in the FT-IR spectrum, which was corresponding to a red PL band. Therefore, the red PL band may be related to hydrogen passivation along with surface oxidation removal while Si NP size is still larger than 4 nm. Since there is no significant change in Si NP size between acid and base additions, this suggests that the blue PL was related surface oxidation as deep surface traps in $KOH_{(aq)}$-containing ethanolic Si NPs. The size-independent, cyan-blue PL in dec-Si NPs was found and related to the increase of surface oxidation after the HA-treatment. Surface characterizations for cyan-blue-emitting dec-Si NPs will be the future work to investigate chemical compounds that responds to cyan-blue emission light.

## 4.6 References

1. Henderson, E. J.; Kelly, J. A.; Veinot, J. G. C., Influence of HSiO1.5 Sol-Gel Polymer Structure and Composition on the Size and Luminescent Properties of Silicon Nanocrystals. *Chemistry of Materials* **2009,** 21, (22), 5426-5434.

2. Kusova, K.; Cibulka, O.; Dohnalova, K.; Pelant, I.; Valenta, J.; Fucikova, A.; Zidek, K.; Lang, J.; Englich, J.; Matejka, P.; Stepanek, P.; Bakardjieva, S., Brightly Luminescent Organically Capped Silicon Nanocrystals Fabricated at Room Temperature and Atmospheric Pressure. *Acs Nano* **2010,** 4, (8), 4495-4504.

3. Wheeler, L. M.; Neale, N. R.; Chen, T.; Kortshagen, U. R., Hypervalent surface interactions for colloidal stability and doping of silicon nanocrystals. *Nature Communications* **2013,** 4.

4. Launer, P. J., Infrared analysis of organsilicon compounds: spectra-structure correlations. *Silicone Compounds Register and Review* **1987**, 4.

5. Chang, H.; Sun, S. Q., Silicon nanoparticles: Preparation, properties, and applications. *Chinese Physics B* **2014,** 23, (8).

6. Tsybeskov, L.; Vandyshev, J.; Fauchet, P., Blue emission in porous silicon: Oxygen-related photoluminescence. *Physical Review B* **1994,** 49, (11), 7821-7824.

7. Kanemitsu, Y., LUMINESCENCE PROPERTIES OF NANOMETER-SIZED SI CRYSTALLITES - CORE AND SURFACE-STATES. *Physical Review B* **1994,** 49, (23), 16845-16848.

8. Yang, S. K.; Li, W. Z.; Cao, B. Q.; Zeng, H. B.; Cai, W. P., Origin of Blue Emission from Silicon Nanoparticles: Direct Transition and Interface Recombination. *Journal of Physical Chemistry C* **2011,** 115, (43), 21056-21062.

9. Hessel, C. M.; Henderson, E. J.; Veinot, J. G. C., Hydrogen silsesquioxane: A molecular precursor for nanocrystalline Si-SiO2 composites and freestanding hydride-surface-terminated silicon nanoparticles. *Chemistry of Materials* **2006,** 18, (26), 6139-6146.

10. Wolkin, M. V.; Jorne, J.; Fauchet, P. M.; Allan, G.; Delerue, C., Electronic states and luminescence in porous silicon quantum dots: The role of oxygen. *Physical Review Letters* **1999,** 82, (1), 197-200.

11. Dohnalova, K.; Poddubny, A. N.; Prokofiev, A. A.; de Boer, W.; Umesh, C. P.; Paulusse, J. M. J.; Zuilhof, H.; Gregorkiewicz, T., Surface brightens up Si quantum dots: direct bandgap-like size-tunable emission. *Light-Science & Applications* **2013,** 2.

12. Nunez, J. R. R.; Kelly, J. A.; Henderson, E. J.; Veinot, J. G. C., Wavelength-Controlled Etching of Silicon Nanocrystals. *Chemistry of Materials* **2012,** 24, (2), 346-352.

## Chapter 5

## Diatomaceous earth as a new precursor for photoluminescent silicon nanoparticle fabrication

### 5.1 Abstract

We propose diatomaceous earth (DE) as an alternate precursor for photoluminescent silicon nanoparticles (Si NPs). DE (95% silica) was transformed to $SiO_x$-encapsulated ($x \leq 2$) nanocrystalline silicon *via* annealing at 1100°C. Following a wet chemical etch of the annealed matrix, blue luminescent (~400nm), free-standing hydride-terminated Si NPs (H-Si NPs) were obtained. SEM and TEM were used to characterize the $SiO_x$-encapsulated nanocrystalline silicon and H-Si NPs, respectively. Passivation of the H-Si NPs was accomplished by thermal hydrosilylation with 1-decene. Following passivation, a red shift (35 nm) in the emission spectrum was observed. DE is an inexpensive, non-toxic, and earth abundant natural silicon source, all of which make it a novel, low-cost, alternative precursor for synthesizing emissive Si NPs for both solid-state and solution-based luminescence applications.

### 5.2 Introduction

Silicon is an environmentally benign and earth abundant element. It has been extensively studied in past decades, with special attention being paid to its bulk electronic properties. Attention has been focused more recently, however, on the optical behavior of sub-10 nm crystallites. The optical properties of such Si NPs are attractive to researchers for their potential applications in various areas such as light-emitting devices,[1] energy

storage,[2-5] and biomedical imaging.[6] Photoluminescent Si NP fabrication has been studied extensively over the past two decades and some of the representative synthetic methods are summarized in Scheme 5.1 and briefly described below.

Commercially available chemical reagents, such as silicon tetrachloride ($SiCl_4$) and trichlorosilane ($HSiCl_3$), are widely used as precursors in solution reduction reactions in tandem with a variety of reducing agents to produce Si NPs. Zintl-phase reactions are another common subset of solution phase reactions that produce Si NPs, where these precursors are employed either exclusively, is solution oxidation reaction (using various oxidizing agents, such as $Br_2$), or in tandem with $SiCl_4$. For example, alkyl-terminated Si NPs have been made *via* reduction of $SiCl_{4(l)}$ by $Mg_2Si_{(s)}$ in ethylene glycol dimethyl ether solution.[7] $KSi_{(s)}$ has also been used to reduce $SiCl_{4(l)}$ in THF solvent.[8] A popular variation of these reactions involves oxidation of Zintl polyanions (e.g., $Si_4^{4-}$) of KSi or NaSi. For example, Zhang et al. fabricated Si NPs in a low temperature solution reaction by reacting sodium silicide ($NaSi_{(s)}$) with ammonium bromide ($NH_4Br_{(s)}$) in N,N-dimethylformamide ($DMF_{(l)}$).[9] The vast majority of the solution-phase fabrication routes utilize $SiCl_{4(l)}$, $SiH_{4(g)}$, or $NaSi_{(s)}$, all of which are extremely reactive and highly toxic materials.

Silane ($SiH_{4(g)}$) has also been heavily utilized as a precursor to prepare photoluminescent Si NPs. Si NP fabrication. In a method published by Kirkey, $SiH_{4(g)}$ was dissociated *via* $CO_2$ laser beam heating in an aerosol reactor to produce to produce red-emitting Si NPs.[10]

Shirahata et al. reported the use of a Nd:YAG pulsed laser to make Si NPs from a hydrogen-terminated silicon substrate.[11] However, such pulsed laser or electrochemical systems studied by Li[12] and Amoruso[13] are expensive and the syntheses are not scalable.

Another alternative method for fabricating Si NPs uses tetraethyl orthosilicate ($TEOS_{(l)}$). $TEOS_{(l)}$ is fairly inexpensive and non-toxic. Other studies have revealed that it is possible to fabricate crystalline Si domains at low temperatures by reducing $TEOS_{(l)}$ with sodium.[14] However, sodium is highly reactive, thus making it dangerous to use.

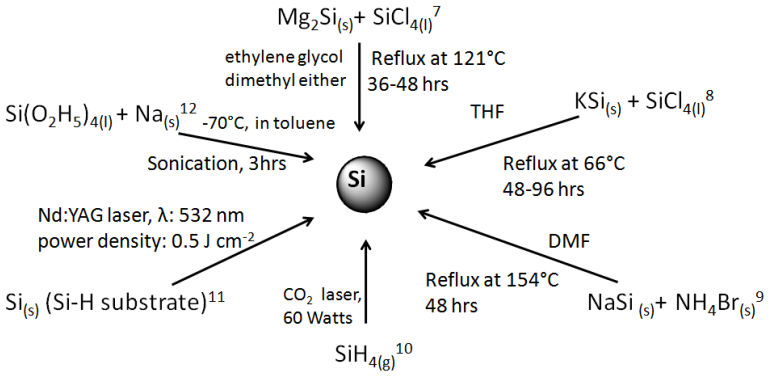


**Scheme 5.1** A summary of common Si NP synthesis methods from the literature.[7-12]

In order to avoid unstable chemical reagents and costly, unsalable synthesis apparatus, researchers have begun to study a solid state thermal reduction process that uses chemically stable and inexpensive materials, such as silicon monoxide ($SiO_{(s)}$) and silica ($SiO_{2(s)}$) as starting materials. For example, thermal annealing treatment of amorphous $SiO_{(s)}$ between 1000°C and 1300°C has been shown to generate elemental silicon nanoparticles.[15-18] Furthermore, it has been shown that DE can be used to obtain elemental silicon structures *via* a magnesiothermic reduction at 650°C.[21-24] DE is a

biosilica template comprised of micrometer-mesostructured intricate hierarchical porous structures.[20] These templates are inexpensive, earth abundant, produced naturally, and are environmentally friendly. $SiO_{2(s)}$ is found in abundance in various natural sources, such as rice hulls[19] and DE.

Herein we utilize DE as a novel precursor for Si NPs. The Si NPs prepared by annealing DE at 1100°C under Ar were confirmed to contain crystalline elemental were imaged using SEM and TEM, and crystalline $Si^0$ domains were confirmed by EDS and XRD. Blue-emitting H-Si NPs were liberated from the annealed DE matrix using an aqueous HF chemical etch. To avoid surface oxidation of the H-Si NPs, the air-free thermal hydrosilylation reaction with 1-decene was performed to generate dec-Si NPs. A red shift in the PL was observed following passivation of the surface with 1-decene vs. the H-Si NPs. In this chapter, we demonstrate that photoluminescent Si NPs can be fabricated using abundant, inexpensive, and naturally produced DE, without using toxic, highly reactive Si precursors, reactive reducing agents, or expensive specialty equipment.

## 5.3 Experimental Details

### Materials and methods

Celite 545 (diatomaceous earth, Fisher Scientific), 1-decene ($CH_3(CH_2)_7CH=CH_{2(l)}$, ≥ 97%, Sigma-Aldrich), and aqueous hydrofluoric acid ($HF_{(aq)}$, 48.0-51.0%, Fisher Scientific), were purchased and used as received. Electrophoretically pure water (nanopure water, 18 MΩ•cm resistivity) was used for the etching process. Hydrosilylation was performed under an inert argon atmosphere on a Schlenk line, using standard anaerobic techniques.

**Synthesis of decane-terminated silicon nanoparticles (dec-Si NPs)**

Celite 545 solid powder (1.5 g) was annealed at 1100°C under flowing $N_2$ gas in a horizontal tube furnace (Lindberg Blue, Model TF55035A) for 10 hrs to generate nanocrystalline silicon nanocrystal encapsulated in an $SiO_2$ matrix (Si NC/$SiO_2$). The Si NC/$SiO_2$ (~0.5g) powder was mixed with a 15 mL chemical etching solution of EtOH/$H_2O$/$HF_{(aq)}$ (1:1:1 (by volume)). The powder was etched for 60 min, and blue-emitting, H-Si NPs were extracted into pentane (~40 mL). dec-Si NPs were made by refluxing the H-Si NP in 3 mL of neat decene (b.p. = 172 °C) under Ar for 18 hrs. This process is shown in Scheme 5.2.

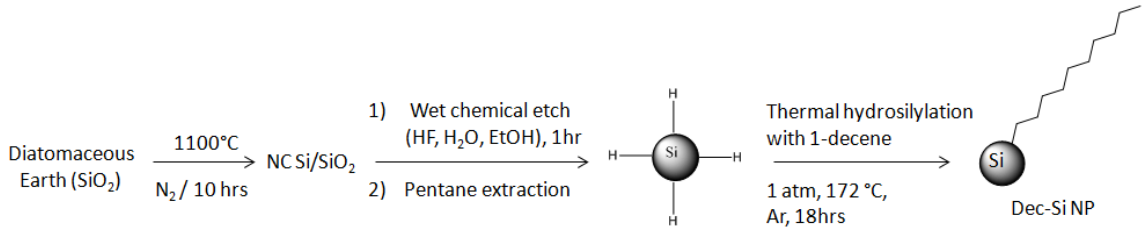


**Scheme 5.2** Outline of photoluminescent Si NP synthesis using diatomaceous earth as the silicon source.

**Characterization of DE, Si NC/$SiO_2$ and dec-Si NPs**

**Scanning Electron Microscopy (SEM) with Energy Dispersive Spectroscopy (EDS)**

DE and Si NC/$SiO_2$ samples were placed on carbon tape adhered to a pin type SEM mount (SPI) and sputter coated with gold (PELCO 91000 Sputter Coater) for 60 s prior to imaging. SEM and EDS were performed on an FEI Siron XL30 model SEM at an accelerating voltage of 5 kV.

**Transmission Electron Microscopy (TEM) with Energy Dispersive X-ray Spectroscopy (EDS)**

An FEI Technai F-20 TEM operating at 200kV was used to analyze the morphology and composition of Si NC/$SiO_2$ and dec-Si NPs. Samples were prepared by drop-casting concentrated solutions of dec-Si NPs onto 400 mesh holey carbon coated, Cu grids (Ted Pella) prior to imaging.

**Fourier Transform Infrared Spectroscopy (FT-IR) and Raman Spectroscopy**

FT-IR spectroscopy was performed on a ThermoFisher Nicolet iS10 infrared spectrometer in reflection geometry using a single bounce diamond attenuated total reflectance (ATR) accessory. Concentrated dec-Si NP solutions (in pentane) were drop-cast and evaporated onto the ATR crystal for analysis.

Raman spectroscopy was performed on a J-Y Lab RAM HR800 UV micro-Raman spectrometer using laser excitation at 532 nm. A concentrated dec-Si NP sample (in pentane) was prepared by drop-casting the solution onto carbon tape adhered to a glass slide.

**Dynamic Light Scattering (DLS)**

The dec-Si NP size distribution was analyzed by a Horiba LB-550 DLS instrument (Horiba, Edison, NJ). The dec-Si NP colloid was dispersed hexane and purified through a 25 nm sized syringe filter before measurement.

**UV-visible and Steady-state Photoluminescence (PL) Spectroscopies**

UV-visible absorption spectra were collected from 200 to 800 nm on a Shimadzu UV-2450 UV-vis spectrophotometer in a standard 1-cm quartz cuvette. The PL properties

of H-Si NPs and dec-Si NPs were examined using a Shimadzu-RF5310 PC spectrophotometer (Shimadzu Corporation, Kyoto, Japan). Steady state emission spectra were collected from 350 to 700 nm on an undiluted sample, with excitation wavelengths varying from 250 to 490 nm. The instrument is equipped with a standard photomultiplier tube detector (range 220-750 nm, wavelength accuracy ±1.5 nm), with diminished sensitivity over the red-to-NIR spectral region.

### 5.4 Morphology and composition analysis before and after high temperature annealing of DE

SEM with EDS was used to examine the effect of annealing. Before annealing, the morphology of the DE was similar to the porous structure of molecular sieves; it appears as a silica matrix with monodisperse pores (Figure 5.1 a). Annealing the porous silica matrix at 1100°C under $N_2$ caused it to fuse into a collapsed $SiO_x$ ($x \leq 2$) matrix with embedded $Si^0$ domains (circled in Figure 5.1 b).

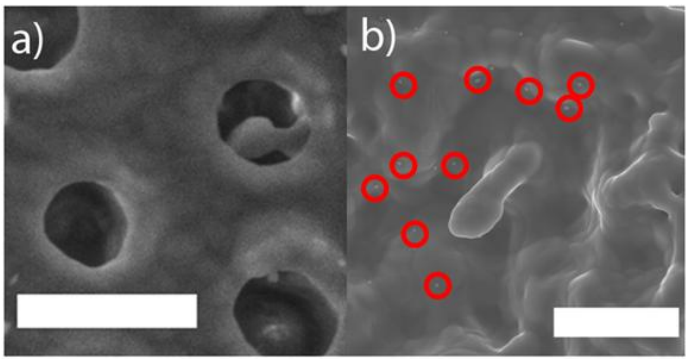


**Figure 5.1** SEM image of DE a) before the 1100 °C thermal reaction (scale bar 2 μm) and b) after the 1100 °C thermal reaction (scale bar 2 μm). Red circles areas are where Si is rich in composition.

SEM-EDX analysis supported the partial reduction of the highly oxidized matrix, resulting in the enrichment of Si in the material. In the EDX spectra shown in Figure 5.2, it can be seen that DE has an O: Si ratio of 2:1, which decreases to 0.7: 1 upon annealing.

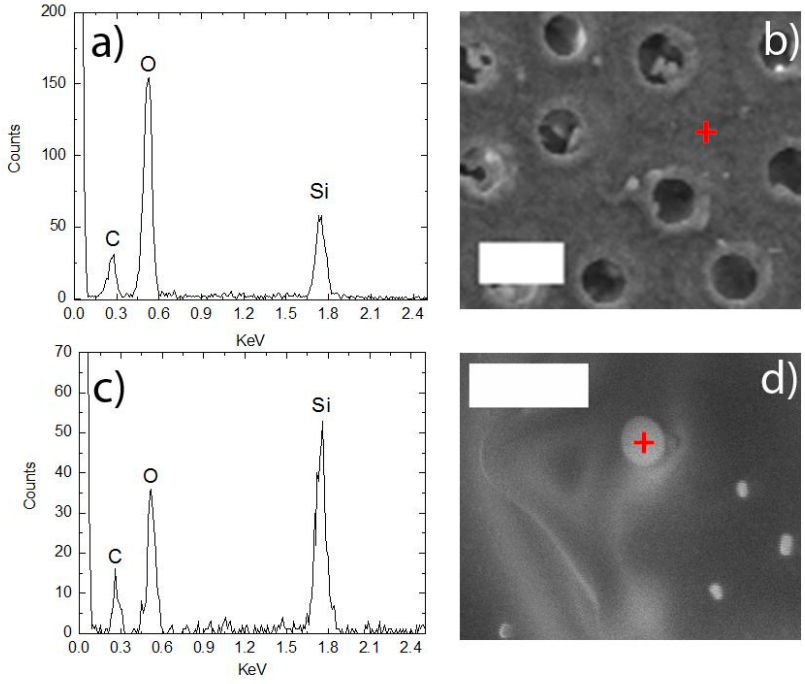


**Figure 5.2** Point energy dispersive X-ray spectra of DE a) before and c) after the 1100°C thermal reaction. SEM image of DE b) before (scale bar: 2 μm) and d) after annealing (scale bar: 150 nm). Red crosses indicate the position where the EDS spectrum shown was acquired.

TEM shows a high-resolution TEM image (HR-TEM) of annealed DE, where crystalline domains have a lattice d-spacing of ~3.1 Å, which is indicative of elemental silicon (111) plane (Figure 5.3 b, d).[6] This supports Si nanocrystals were formed in the annealed, Si-rich precursor in Figure 5.2 c. In addition, the variation of contrast along the

line in the image of annealed DE (Figure 5.3 d) showed a regular pattern, which indicated a high degree of crystallinity. For comparison, TEM and HRTEM images were also taken of DE before annealing. The variation of contrast along the line in the image is given of un-treated DE shows a lack of an ordered structure (Figure 5.3 c), TEM analysis strongly suggests the formation of crystalline silicon domains *via* thermal reduction of DE.

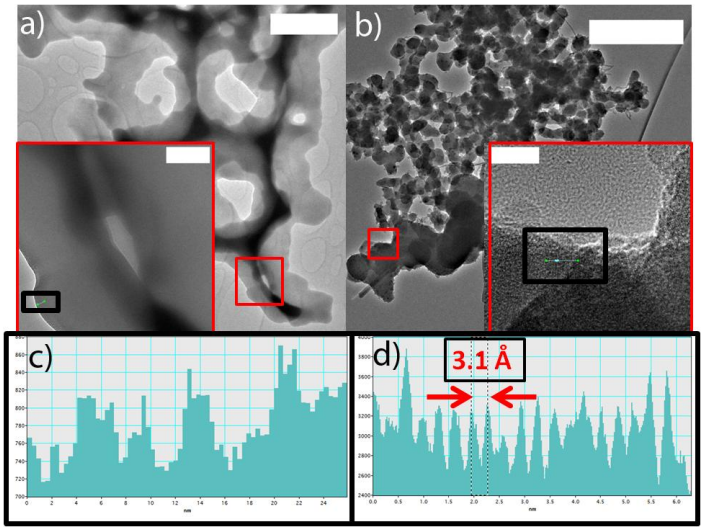


**Figure 5.3** TEM image of DE a) before annealing (scale bar 1µm), inset: HR-TEM image (scale bar 150 nm); b) after annealing (scale bar 500 nm), inset: HR-TEM image of nanocrystalline Si encapsulated in annealed diatomaceous earth (scale bar 5 nm); and The variation of contrast along the line in the inset image is given in c) before annealing, and d) after annealing.

**Liberation and Characterization of H-Si NPs from thermally reduced DE**

H-Si NPs were liberated from Si NC/$SiO_2$ *via* wet chemical etch, following thermal hydrosilylation with 1-decene to synthesize dec-Si NPs as showen in Figure 5.4;

Crystallinity of the Si NPs was present after passivation with 1-decene, as shown the presence of the Si (111) plane, as shown in lattice spacing of 3.11 Å in Figure 5.4 d. The size distribution of dec-Si NP was about 4.6 ± 1.7 nm as shown in Figure 5.5, b.

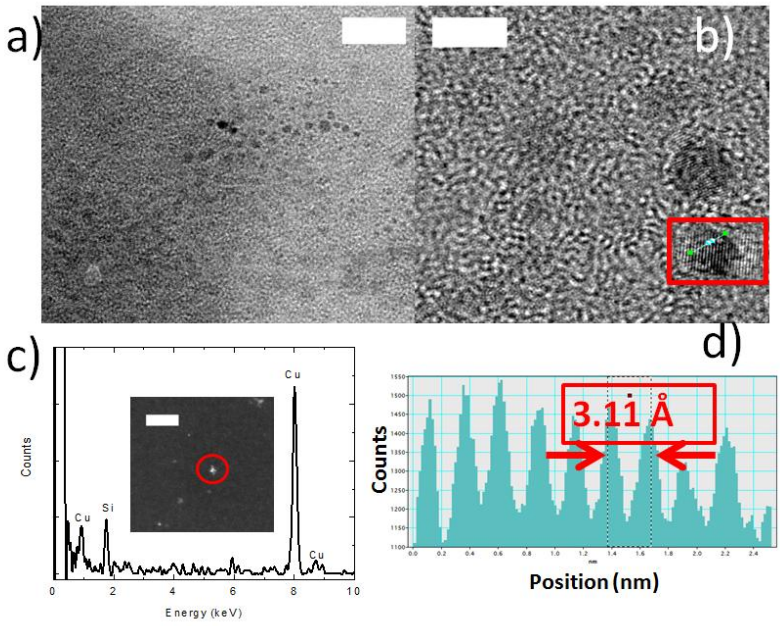


**Figure 5.4** a) TEM image of dec-Si NPs (scale bar 20 nm), b) HR-TEM image of dec-Si NPs (scale bar 5 nm), c) EDX point scan of dec-Si NPs (inset: a dark field STEM image of Si NPs) (scale bar 100 nm), and d) the variation of contrast along the line in the Figure 5.4 b image is given, represents a lattice d-spacing of 3.11 Å in dec-Si NP.

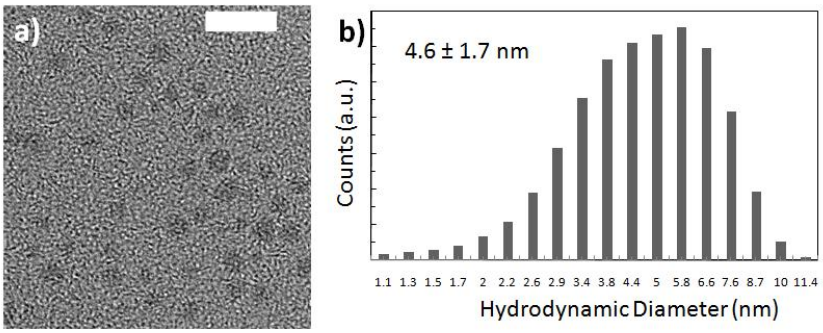


**Figure 5.5** a) TEM image of dec-Si NP with scale bar 8 nm, b) the dec-Si NP size distribution in hexane, the mean diameter is 4.6 ± 1.7 nm.

**UV-vis and steady-state Photoluminescence (PL) spectroscopies**

The optical properties of the Si NPs were studied by PL and UV-visible spectroscopies. As synthesized, ~4 nm H-Si NPs were found to emit 347 nm light with excitation wavelength at 310 nm (Figure 5.5). Thermal hydrosilylation was performed on H-Si NPs at178°C with 1-decene to prevent further oxidation on Si NP surface. Notice that the thermal hydrosilylation caused a red shift in the PL, which presented as a broad emission spanning from 350 nm to 600 nm (Figure 5, green line). The $\lambda_{max}$ at 484 nm could be the scattering effect in dec-Si NPs.

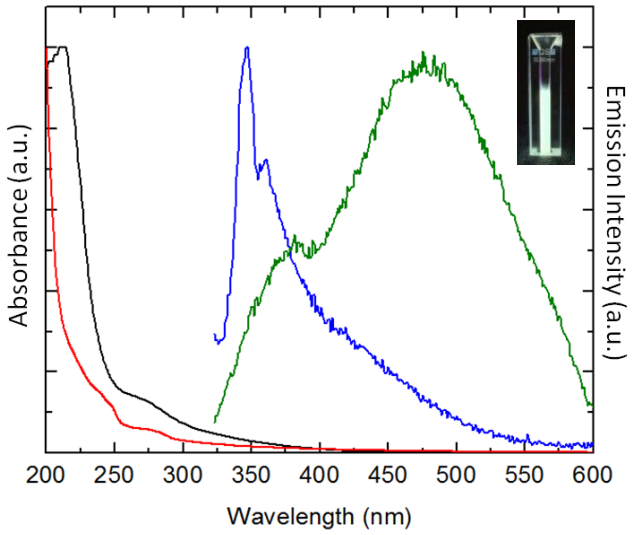


**Figure 5.6** Room temperature PL spectra (excitation wavelength 310 nm) of H-Si NPs (blue line) and dec-Si NPs (green line) and UV-Vis spectra of H-Si NPs (red line) and dec-Si NPs (black line). Inset image: Luminescent dec-Si NPs irradiated by UV-light at 365 nm.

In UV-Vis spectrum of H-Si NPs (Figure 5.5, red line), the absorption started to increase at around 350 nm and overlapped with H-Si NPs PL spectrum. The broad absorbance with PL band overlapping in H-Si NPs, may suggest photons are emitted for radiative recombination as core state, which is quantum confinement effect. Compared UV-Vis spectra between H-Si NPs and dec-Si NPs as shown in Figure 5.5, absorption was broader and started to rise at ~400 nm in dec-Si NPs' UV-Vis spectrum. This may suggest the surface passivation with 1-decene has provided a new surface trap that alters excitonic recombination pathway, resulting in red shift of PL spectrum in dec-Si NPs.

**Fourier Transform Infrared Spectroscopy (FT-IR), Raman Spectroscopy**

Thermal hydrosilylation was performed to passivate the surface of Si NP using 1-decene. The surface passivation in dec-Si NPs has been studied by FT-IR, and decane-terminated surface functionalization is confirmed by the presence of Si-C stretching vibrations at 1260 and 800 $cm^{-1}$ (as shown in Figure 5.7).[6,9,29]

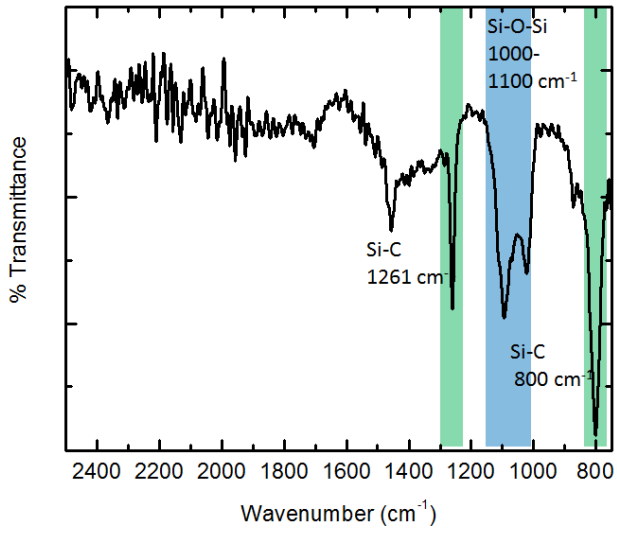


**Figure 5.7** Room temperature IR spectrum of dec-Si NP

Furthermore, there is no Si-H stretches observed at ~ 2100 $cm^{-1}$, which indicates the thermal hydrosilylation reactionof the H-Si NPs was successful. The 1000-1100 $cm^{-1}$ region was present in the FT-IR spectrum, which was attributed to Si-O-Si bonding on the surface.

Raman spectroscopy was also performed on a macroscopic sample of dec-Si NP, the maximum vibration band was found at 506 $cm^{-1}$ (Figure 5.8), which was assigned as the Si-Si vibration of elemental Si, consistent with the result of EDX analysis in TEM dark field. This value is blue-shifted by 10 $cm^{-1}$ from the Si-Si vibration of 516 $cm^{-1}$ in bulk crystalline silicon, [6, 30]and this blue shift has been attributed to the small domain size of the Si NPs (Figure 5.5). No Si-O vibration (~ 493 $cm^{-1}$)[6] was found in the Raman spectrum indicated that there were silicon-rich cores free of surface oxidization on Si NP surface.

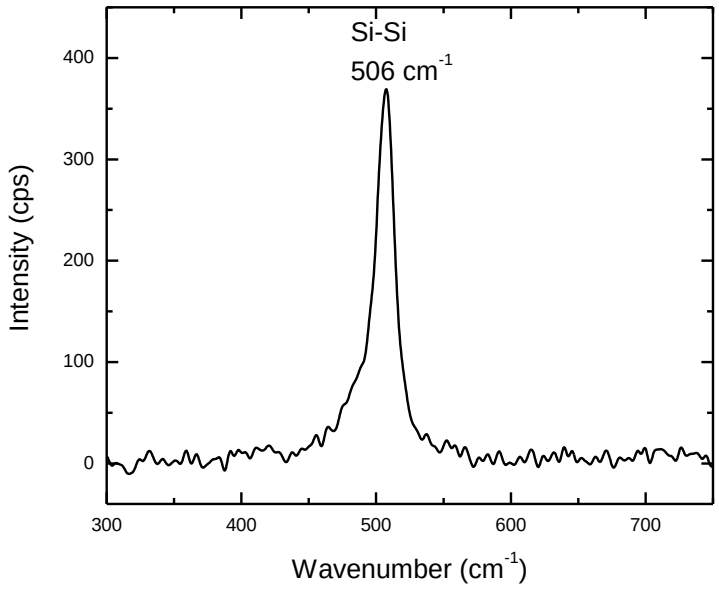


**Figure 5.8** Raman spectrum of dec-Si NP.

## 5.5 Discussion

### Nanocrystalline silicon encapsulated in silica

Diatom frustrules, which are composed of $SiO_2$ in the form of well-defined pores with a sieve-like structure, were converted into the Si NCs *via* magnesiothermic reduction at 650°C.[21,25] Chen and co-workers also reported silica-based materials were magnesiothermically converted into a matrix that contained microporous, nanocrystalline silicon-rich structures with Si NPs (size of 8 ± 1 nm). The composition was confirmed by EDX analysis and HR-TEM with the presence (111), (220), and (311) Si planes. In another study, Shen used magnesium to reduce DE, and was able to observe a change in morphology, but with the retention of the porous structure in DE.[23] Ordered, mesoporous silicon was made *via* magnesium reduction of silica polymer thin films, and produced 10 -17 nm Si nanocrystals, reported by Tolbert and coworkers.[22]

Si NPs can also be made *via* the thermal dynamic disproportionation of hydrogen silsesquioxane or other $SiO_x$ matrices by heating to temperatures above 1100°C under a reducing atmosphere ($N_2$ gas or 5% $H_2$/95% Ar gas). For example, Xie has made photoluminescent, periodic mesoporous nanocrystailline silicon encapsulated in silica by thermally disproportioning hydrosilica ($HSiO_{1.5}$) at 1100°C under 5% $H_2$/95% Ar flow. Their Raman data showed that the Si-Si vibration (515 $cm^{-1}$) peak was observed when the temperature reached 1100°C.[31] Colin reported a Raman peak position dependency with regards to Si NP size in freestanding and oxide-embedded Si NPs. As Si NP size decreased, a blue shift of the Si-Si peak was observed. [32]

In the study presented herein, the annealing of DE resulted in a formation of oxide-embedded Si NPs (process shown in Scheme 5.3). We propose that the annealing

procedure reduces the silicon, resulting in the evolution of oxygen. A collapsed structure formed after DE was annealed, and nanocrystalline silicon was generated, indicated as blue circles in collapsed structure.

A Si-Si vibration peak at 506 $cm^{-1}$ was observed in Raman spectrum of dec-Si NPs, which is blue shift from bulk silicon (520 $cm^{-1}$). Furthermore, the amorphous silicon Raman scattering peak at 480 $cm^{-1}$ was not found, which indicated that the dec-Si NP cores were crystalline.[32]

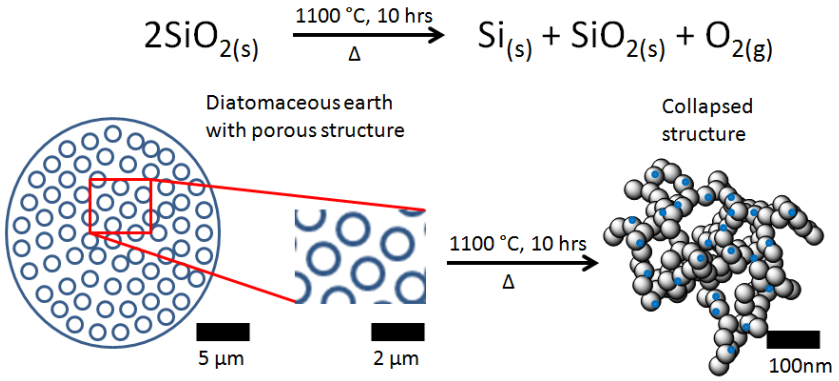


**Scheme 5.3** Proposed mechanism of the formation of Si NPs encapsulated in silica during the annealing the process. The blue dots indicate nanocrystalline silicon.

**Bathochromic shift (red shift) observed in the photoluminescence spectrum of Si NPs after surface passivaiton with 1-decence by thermal hydrosilylation**

This red-shift was also reported by Eckhoff and coworkers. Their ultra-small 1 nm H-Si NPs initially emitted 305 nm light, revealed red-shift emission after a stable Si-C covalent bond formed *via* thermal hydrosilylation reaction[27], which is consistent with the result presented in this study.

According to quantum confinement theory, the band gap of nanoscale silicon should increase as the NP's size decreases, along with red shift in PL emission wavelength.[28] This phenomenon is dictated by the quantum confinement (QC) effect. However, the red shift in PL was discovered in both our work and Eckhoff's after thermal hydrosilylation, without any size changed after hydrosilylation. In their system, the red shift occurred and emissions were shifted from 315nm to 350nm. Our red shift phenomenon was also revealed from the reaction of 1-decene insertion into a thermally activated H-Si bond to give dec-Si NP, which had emission shift from 347nm to 382nm and the maximum peak at 484nm could be the scattering effect.

In Wolkin's paper, a red shift was also found after H-Si NPs were transferred from an Ar environment into air. Wolkin suggested that the red shift was caused by surface passivation by oxygen.[34] Gole also stated that PL shifts correspond to changes in the surface chemistry of porous Si NP, and they were able to induce a red shift by adding ethylene glycol to their etching mixture.[35] Another similar observation was reported by Eckhoff. Methyl 4-pentenoate was capped on the H-Si NPs, which resulted in a red shift in the PL spectrum from 295-315 nm to 350-410nm, which could refer to surface defect or passivation by carbon.[27]

In our work, a red shift, from 347 nm to 382 nm in PL spectra was observed in Si NPs after surface passivation with 1-decene (Figure 5.5). A conclusion may be suggested that the 347 nm blue emission from H-Si NP is from quantum confinement,[36] and the red shift in PL emission along with another red shift in absorption spectrum (Figure 5, from red line to black line) were found in dec-Si NP after thermal hydrosilylation with 1-decene may refer surface passivation by carbon as Eckhoff reported.[27]

## 5.6 Conclusion

DE is an earth abundant and environmentally benign alternate precursor for fabricating photoluminescent Si NPs. Si NPs were synthesized *via* the thermal reduction of DE at 1100°C, without highly reactive metal reducing agents. SEM, TEM, EDS, and Raman data confirmed the presence nanocrystalline, $Si^0$ rich cores. A red-shift in PL was observed after thermal hydrosilylation of Si NPs with 1-decene.

## 5.7 References


1. Canham, L. T., Silicon quantum wire array fabrication by electrochemical and chemical dissolution of wafers. *Applied Physics Letters* **1990,** 57, (10), 1046.

2. Gribov, B. G.; Zinov'ev, K. V., Preparation of high-purity silicon for solar cells. *Inorganic Materials* **2003,** 39, (7), 653-662.

3. Won, C. W.; Nersisyan, H. H.; Won, H. I., Solar-grade silicon powder prepared by combining combustion synthesis with hydrometallurgy. *Solar Energy Materials and Solar Cells* **2011,** 95, (2), 745-750.

4. Park, S.; Cho, E.; Song, D. Y.; Conibeer, G.; Green, M. A., n-Type silicon quantum dots and p-type crystalline silicon heteroface solar cells. *Solar Energy Materials and Solar Cells* **2009,** 93, (6-7), 684-690.

5. Baxter, J. B.; Aydil, E. S., Nanowire-based dye-sensitized solar cells. *Applied Physics Letters* **2005,** 86, (5).

6. Chiu, S. K.; Manhat, B. A.; DeBenedetti, W. J. I.; Brown, A. L.; Fichter, K.; Vu, T.; Eastman, M.; Jiao, J.; Goforth, A. M., Aqueous red-emitting silicon nanoparticles for

cellular imaging: Consequences of protecting against surface passivation by hydroxide and water for stable red emission. *Journal of Materials Research* **2013,** 28, (2), 216-230.

7. Yang, C. S.; Bley, R. A.; Kauzlarich, S. M.; Lee, H. W. H.; Delgado, G. R., Synthesis of alkyl-terminated silicon nanoclusters by a solution route. *Journal of the American Chemical Society* **1999,** 121, (22), 5191-5195.

8. Bley, R. A.; Kauzlarich, S. M., A low-temperature solution phase route for the synthesis of silicon nanoclusters. *Journal of the American Chemical Society* **1996,** 118, (49), 12461-12462.

9. Zhang, X. M.; Neiner, D.; Wang, S. Z.; Louie, A. Y.; Kauzlarich, S. M., A new solution route to hydrogen-terminated silicon nanoparticles: synthesis, functionalization and water stability. *Nanotechnology* **2007,** 18, (9).

10. Kirkey, W. D.; Sahoo, Y.; Li, X. G.; He, Y. Q.; Swihart, M. T.; Cartwright, A. N.; Bruckenstein, S.; Prasad, P. N., Quasi-reversible photoluminescence quenching of stable dispersions of silicon nanoparticles. *Journal of Materials Chemistry* **2005,** 15, (20), 2028-2034.

11. Shirahata, N.; Linford, M. R.; Furumi, S.; Pei, L.; Sakka, Y.; Gates, R. J.; Asplund, M. C., Laser-derived one-pot synthesis of silicon nanocrystals terminated with organic monolayers. *Chemical Communications* **2009**, (31), 4684-4686.

12. Li, X. G.; He, Y. Q.; Talukdar, S. S.; Swihart, M. T., Process for preparing macroscopic quantities of brightly photoluminescent silicon nanoparticles with emission spanning the visible spectrum. *Langmuir* **2003,** 19, (20), 8490-8496.

13. Amoruso, S.; Bruzzese, R.; Spinelli, N.; Velotta, R.; Vitiello, M.; Wang, X.; Ausanio, G.; Iannotti, V.; Lanotte, L., Generation of silicon nanoparticles via

femtosecond laser ablation in vacuum. *Applied Physics Letters* **2004,** 84, (22), 4502-4504.

14. Dhas, N. A.; Raj, C. P.; Gedanken, A., Preparation of luminescent silicon nanoparticles: A novel sonochemical approach. *Chemistry of Materials* **1998,** 10, (11), 3278-+.

15. Mamiya, M.; Kikuchi, M.; Takei, H., Crystallization of fine silicon particles from silicon monoxide. *Journal of Crystal Growth* **2002,** 237, 1909-1914.

16. Mamiya, M.; Takei, H.; Kikuchi, M.; Uyeda, C., Preparation of fine silicon particles from amorphous silicon monoxide by the disproportionation reaction. *Journal of Crystal Growth* **2001,** 229, (1), 457-461.

17. Srivastava, S. K.; Singh, P. K.; Singh, V. N.; Sood, K. N.; Haranath, D.; Kumar, V., Large-scale synthesis, characterization and photoluminescence properties of amorphous silica nanowires by thermal evaporation of silicon monoxide. *Physica E-Low-Dimensional Systems & Nanostructures* **2009,** 41, (8), 1545-1549.

18. Lee, J. I.; Lee, K. T.; Cho, J.; Kim, J.; Choi, N. S.; Park, S., Chemical-assisted thermal disproportionation of porous silicon monoxide into silicon-based multicomponent systems. *Angewandte Chemie International Edition in English* **2012,** 51, (11), 2767-71.

19. Okutani, T., Utilization of silica in rice hulls as raw materials for silicon semiconductors. *Journal of Metals, Materials and Minerals* **2009,** 19, (2), 51-59.

20. Garcia, A. P.; Sen, D.; Buehler, M. J., Hierarchical silica nanostructures inspired by diatom algae yield superior deformability, toughness, and strength. *Metallurgical and*

*Materials Transactions a-Physical Metallurgy and Materials Science* **2011,** 42A, (13), 3889-3897.

21. Bao, Z. H.; Weatherspoon, M. R.; Shian, S.; Cai, Y.; Graham, P. D.; Allan, S. M.; Ahmad, G.; Dickerson, M. B.; Church, B. C.; Kang, Z. T.; Abernathy, H. W.; Summers, C. J.; Liu, M. L.; Sandhage, K. H., Chemical reduction of three-dimensional silica micro-assemblies into microporous silicon replicas. *Nature* **2007,** 446, (7132), 172-175.

22. Richman, E. K.; Kang, C. B.; Brezesinski, T.; Tolbert, S. H., Ordered mesoporous silicon through magnesium reduction of polymer templated silica thin films. *Nano Letters* **2008,** 8, (9), 3075-3079.

23. Shen, L.; Guo, X.; Fang, X.; Wang, Z.; Chen, L., Magnesiothermically reduced diatomaceous earth as a porous silicon anode material for lithium ion batteries. *Journal of Power Sources* **2012,** 213, 229-232.

24. Bao, Z. H.; Ernst, E. M.; Yoo, S.; Sandhage, K. H., Syntheses of porous self-supporting metal-nanoparticle assemblies with 3D morphologies inherited from biosilica templates (Diatom Frustules). *Advanced Materials* **2009,** 21, (4), 474-478.

25. Norris, D. J., Materials science - Silicon life forms. *Nature* **2007,** 446, (7132), 146-147.

26. Wang, W.; Martin, J. C.; Fan, X.; Han, A.; Luo, Z.; Sun, L., Silica nanoparticles and frameworks from rice husk biomass. *ACS Applied Materials & Interfaces* **2012,** 4, (2), 977-81.

27. Eckhoff, D. A.; Stuart, J. N.; Sutin, J. D. B.; Sweedler, J. V.; Gratton, E., Capillary electrophoresis of ultrasmall carboxylate functionalized silicon nanoparticles. *Journal of Chemical Physics* **2006,** 125, (8).

28. de Boer, W. D. A. M.; Timmerman, D.; Dohnalova, K.; Yassievich, I. N.; Zhang, H.; Buma, W. J.; Gregorkiewicz, T., Red spectral shift and enhanced quantum efficiency in phonon-free photoluminescence from silicon nanocrystals. *Nature Nanotechnology* **2010,** 5, (12), 878-884.

29. Hallmann, S.; Fink, M. J.; Mitchell, B. S., Mechanochemical synthesis of functionalized silicon nanoparticles with terminal chlorine groups. *Journal of Materials Research* **2011,** 26, (8), 1052-1060.

30. Meier, C.; Luttjohann, S.; Kravets, V. G.; Nienhaus, H.; Lorke, A.; Wiaers, H., Raman properties of silicon nanoparticles. *Physica E-Low-Dimensional Systems & Nanostructures* **2006,** 32, (1-2), 155-158.

31. Xie, Z.; Henderson, E. J.; Dag, O.; Wang, W.; Lofgreen, J. E.; Kubel, C.; Scherer, T.; Brodersen, P. M.; Gu, Z. Z.; Ozin, G. A., Periodic mesoporous hydridosilica-synthesis of an "impossible" material and its thermal transformation into brightly photoluminescent periodic mesoporous nanocrystal silicon-silica composite. *Journal of the American Chemical Society* **2011,** 133, (13), 5094-102.

32. Hessel, C. M.; Wei, J.; Reid, D.; Fujii, H.; Downer, M. C.; Korgel, B. A., Raman spectroscopy of oxide-embedded and ligand-stabilized silicon nanocrystals. *Journal of Physical Chemistry Letters* **2012,** 3, (9), 1089-1093.

33. Lewis, L. N.; Schattenmann, F. J.; Jordan, T. M.; Carnahan, J. C.; Flanagan, W. P.; Wroczynski, R. J.; Lemmon, J. P.; Anostario, J. M.; Othon, M. A., Reaction of silicate minerals to form tetramethoxysilane. *Inorganic Chemistry* **2002,** 41, (9), 2608-2615.

34. Wolkin, M. V.; Jorne, J.; Fauchet, P. M.; Allan, G.; Delerue, C., Electronic states and luminescence in porous silicon quantum dots: The role of oxygen. *Physical Review Letters* **1999,** 82, (1), 197-200.

35. Gole, J. L.; Dixon, D. A., Transformation, green to orange-red, of a porous silicon photoluminescent surface in solution. *Journal of Physical Chemistry B* **1998,** 102, (1), 33-39.

36. Kanemitsu, Y., Luminescence properties of nanometer-sized Si crystallites: Core and surface states. *Physical Review B* **1994,** 49, (23), 16845-16848.

## Terminal References

### Reference from Chapter 1


1. Valeur, B.; Berberan-Santos, M. N., A Brief History of Fluorescence and Phosphorescence before the Emergence of Quantum Theory. *Journal of Chemical Education* **2011,** 88, (6), 731-738.

2. Flückiger, F. A., Hanbury,Daniel., *Pharmacographia: A history of the principal drugs of vegetable origin, met with in Great Britain and British India*. Macmillan: London, UK, 1879.

3. Stokes, G. *G.*, On the change of refrangibility of light. *Philosophical Transcations of the Royal Society of London* **1852,** 142, 463-562.

4. Meyerm, R., *Zeitschrift fur Physikalische Chemie, Stochiometrie und Verwandtschaftslehre*. Leipzig, Verlag von Wilhelm Engelmann: 1887.

5. Jablonski, A., Efficiency of anti-stokes fluorescence in dyes. *Nature* **1933,** 131, 839-840.

6. Kricka, L. J.; Fortina, P., Analytical Ancestry: "Firsts" in Fluorescent Labeling of Nucleosides, Nucleotides, and Nucleic Acids. *Clinical Chemistry* **2009,** 55, (4), 670-683.

7. Musajo, L., Visentini, P., Bacchinetti, F., Razzi, M. A., Photoinactivation of Ehrlich ascites tumor cells in vitro obtained with skin-photosensitizing furocoumarins. *Experientia* **1967,** 23, (5).

8. Adams, L. R., Kamentsky, Louis A. Method for analysis of blood by optical analysis of living cells. 1972.

9. Einevoll, G. T., CONFINEMENT OF EXCITONS IN QUANTUM DOTS. *Physical Review B* **1992,** 45, (7), 3410-3417.

10. Alivisatos, A. P., Perspectives on the physical chemistry of semiconductor nanocrystals. *Journal of Physical Chemistry* **1996,** 100, (31), 13226-13239.

11. Bukowski, T. J.; Simmons, J. H., Quantum dot research: Current state and future prospects. *Critical Reviews in Solid State and Materials Sciences* **2002,** 27, (3-4), 119-142.

12. Donega, C. D., Synthesis and properties of colloidal heteronanocrystals. *Chemical Society Reviews* **2011,** 40, (3), 1512-1546.

13. Chan, W. C. W.; Nie, S. M., Quantum dot bioconjugates for ultrasensitive nonisotopic detection. *Science* **1998,** 281, (5385), 2016-2018.

14. Chen, N.; He, Y.; Su, Y. Y.; Li, X. M.; Huang, Q.; Wang, H. F.; Zhang, X. Z.; Tai, R. Z.; Fan, C. H., The cytotoxicity of cadmium-based quantum dots. *Biomaterials* **2012,** 33, (5), 1238-1244.

15. Derfus, A. M.; Chan, W. C. W.; Bhatia, S. N., Probing the cytotoxicity of semiconductor quantum dots. *Nano Letters* **2004,** 4, (1), 11-18.

16. Canham, L. T., Silicon quantum wire array fabrication by electrochemical and chemical dissolution of wafers. *Applied Physics Letters* **1990,** 57, (10), 1046.

17. Popplewell, J. F.; King, S. J.; Day, J. P.; Ackrill, P.; Fifield, L. K.; Cresswell, R. G.; Di Tada, M. L.; Liu, K., Kinetics of uptake and elimination of silicic acid by a human subject: A novel application of Si-32 and accelerator mass spectrometry. *Journal of Inorganic Biochemistry* **1998,** 69, (3), 177-180.

18. Li, Z. F.; Ruckenstein, E., Water-soluble poly(acrylic acid) grafted luminescent silicon nanoparticles and their use as fluorescent biological staining labels. *Nano Letters* **2004,** 4, (8), 1463-1467.

19. Aswathy, R. G.; Yoshida, Y.; Maekawa, T.; Kumar, D. S., Near-infrared quantum dots for deep tissue imaging. *Analytical and Bioanalytical Chemistry* **2010,** 397, (4), 1417-1435.

20. Hahn, M. A.; Singh, A. K.; Sharma, P.; Brown, S. C.; Moudgil, B. M., Nanoparticles as contrast agents for in-vivo bioimaging: current status and future perspectives. *Analytical and Bioanalytical Chemistry* **2011,** 399, (1), 3-27.

21. Michalet, X.; Pinaud, F. F.; Bentolila, L. A.; Tsay, J. M.; Doose, S.; Li, J. J.; Sundaresan, G.; Wu, A. M.; Gambhir, S. S.; Weiss, S., Quantum dots for live cells, in vivo imaging, and diagnostics. *Science* **2005,** 307, (5709), 538-544.

22. Hilderbrand, S. A.; Weissleder, R., Near-infrared fluorescence: application to in vivo molecular imaging. *Current Opinion in Chemical Biology* **2010,** 14, (1), 71-79.

23. Dasog, M.; Yang, Z. Y.; Regli, S.; Atkins, T. M.; Faramus, A.; Singh, M. P.; Muthuswamy, E.; Kauzlarich, S. M.; Tilley, R. D.; Veinot, J. G. C., Chemical Insight into the Origin of Red and Blue Photoluminescence Arising from Freestanding Silicon Nanocrystals. *Acs Nano* **2013,** 7, (3), 2676-2685.

24. Vincent, J.; Maurice, V.; Paquez, X.; Sublemontier, O.; Leconte, Y.; Guillois, O.; Reynaud, C.; Herlin-Boime, N.; Raccurt, O.; Tardif, F., Effect of water and UV passivation on the luminescence of suspensions of silicon quantum dots. *Journal of Nanoparticle Research* **2009,** 12, (1), 39-46.

25. Shiohara, A.; Hanada, S.; Prabakar, S.; Fujioka, K.; Lim, T. H.; Yamamoto, K.; Northcote, P. T.; Tilley, R. D., Chemical Reactions on Surface Molecules Attached to Silicon Quantum Dots. *Journal of the American Chemical Society* **2010,** 132, (1), 248-253.

26. Cullis, A. G.; Canham, L. T.; Calcott, P. D. J., The structural and luminescence properties of porous silicon. *Journal of Applied Physics* **1997,** 82, (3), 909.

27. Cullis, A. G.; Canham, L. T., VISIBLE-LIGHT EMISSION DUE TO QUANTUM SIZE EFFECTS IN HIGHLY POROUS CRYSTALLINE SILICON. *Nature* **1991,** 353, (6342), 335-338.

28. Holmes, J. D.; Ziegler, K. J.; Doty, R. C.; Pell, L. E.; Johnston, K. P.; Korgel, B. A., Highly luminescent silicon nanocrystals with discrete optical transitions. *Journal of the American Chemical Society* **2001,** 123, (16), 3743-3748.

29. Kang, Z. H.; Liu, Y.; Tsang, C. H. A.; Ma, D. D. D.; Fan, X.; Wong, N. B.; Lee, S. T., Water-Soluble Silicon Quantum Dots with Wavelength-Tunable Photoluminescence. *Advanced Materials* **2009,** 21, (6), 661-+.

30. Kim, T.-W.; Cho, C.-H.; Kim, B.-H.; Park, S.-J., Quantum confinement effect in crystalline silicon quantum dots in silicon nitride grown using SiH[sub 4] and NH[sub 3]. *Applied Physics Letters* **2006,** 88, (12), 123102.

31. Ledoux, G.; Gong, J.; Huisken, F.; Guillois, O.; Reynaud, C., Photoluminescence of size-separated silicon nanocrystals: Confirmation of quantum confinement. *Applied Physics Letters* **2002,** 80, (25), 4834-4836.

32. Hessel, C. M.; Henderson, E. J.; Veinot, J. G. C., Hydrogen silsesquioxane: A molecular precursor for nanocrystalline Si-SiO2 composites and freestanding hydride-

surface-terminated silicon nanoparticles. *Chemistry of Materials* **2006,** 18, (26), 6139-6146.

33. Ray, M.; Hossain, S. M.; Klie, R. F.; Banerjee, K.; Ghosh, S., Free standing luminescent silicon quantum dots: evidence of quantum confinement and defect related transitions. *Nanotechnology* **2010,** 21, (50), 505602.

34. Hapala, P.; Kůsová, K.; Pelant, I.; Jelínek, P., Theoretical analysis of electronic band structure of 2- to 3-nm Si nanocrystals. *Physical Review B* **2013,** 87, (19).

35. Trucks, G.; Raghavachari, K.; Higashi, G.; Chabal, Y., Mechanism of HF etching of silicon surfaces: A theoretical understanding of hydrogen passivation. *Physical Review Letters* **1990,** 65, (4), 504-507.

36. Wolkin, M. V.; Jorne, J.; Fauchet, P. M.; Allan, G.; Delerue, C., Electronic states and luminescence in porous silicon quantum dots: The role of oxygen. *Physical Review Letters* **1999,** 82, (1), 197-200.

37. Manhat, B. A.; Brown, A. L.; Black, L. A.; Ross, J. B.; Fichter, K.; Vu, T.; Richman, E.; Goforth, A. M., One-step Melt Synthesis of Water Soluble, Photoluminescent, Surface-Oxidized Silicon Nanoparticles for Cellular Imaging Applications. *Chem Mater* **2011,** 23, (9), 2407-2418.

38. Yang, S. K.; Li, W. Z.; Cao, B. Q.; Zeng, H. B.; Cai, W. P., Origin of Blue Emission from Silicon Nanoparticles: Direct Transition and Interface Recombination. *Journal of Physical Chemistry C* **2011,** 115, (43), 21056-21062.

39. Chiu, S. K.; Manhat, B. A.; DeBenedetti, W. J. I.; Brown, A. L.; Fichter, K.; Vu, T.; Eastman, M.; Jiao, J.; Goforth, A. M., Aqueous red-emitting silicon nanoparticles for

cellular imaging: Consequences of protecting against surface passivation by hydroxide and water for stable red emission. *Journal of Materials Research* **2013,** 28, (2), 216-230.

40. Kůsová, K. i.; Ondič, L. s.; Klimešová, E.; Herynková, K. i.; Pelant, I.; Daniš, S.; Valenta, J.; Gallart, M.; Ziegler, M.; Hönerlage, B.; Gilliot, P., Luminescence of free-standing versus matrix-embedded oxide-passivated silicon nanocrystals: The role of matrix-induced strain. *Applied Physics Letters* **2012,** 101, (14), 143101.

41. de Boer, W. D. A. M.; Timmerman, D.; Dohnalova, K.; Yassievich, I. N.; Zhang, H.; Buma, W. J.; Gregorkiewicz, T., Red spectral shift and enhanced quantum efficiency in phonon-free photoluminescence from silicon nanocrystals. *Nature Nanotechnology* **2010,** 5, (12), 878-884.

42. Godefroo, S.; Hayne, M.; Jivanescu, M.; Stesmans, A.; Zacharias, M.; Lebedev, O. I.; Van Tendeloo, G.; Moshchalkov, V. V., Classification and control of the origin of photoluminescence from Si nanocrystals. *Nat Nanotechnol* **2008,** 3, (3), 174-8.

43. Hua, F. J.; Swihart, M. T.; Ruckenstein, E., Efficient surface grafting of luminescent silicon quantum dots by photoinitiated hydrosilylation. *Langmuir* **2005,** 21, (13), 6054-6062.

44. Brewer, A.; von Haeften, K., In situ passivation and blue luminescence of silicon clusters using a cluster beam/H[sub 2]O codeposition production method. *Applied Physics Letters* **2009,** 94, (26), 261102.

45. Tilley, R. D.; Warner, J. H.; Yamamoto, K.; Matsui, I.; Fujimori, H., Micro-emulsion synthesis of monodisperse surface stabilized silicon nanocrystals. *Chemical Communications* **2005**, (14), 1833-1835.

46. Wilcoxon, J. P.; Samara, G. A.; Provencio, P. N., Optical and electronic properties of Si nanoclusters synthesized in inverse micelles. *Physical Review B* **1999,** 60, (4), 2704-2714.

**Reference from Chapter 2**

1. Chiu, S. K.; Manhat, B. A.; DeBenedetti, W. J. I.; Brown, A. L.; Fichter, K.; Vu, T.; Eastman, M.; Jiao, J.; Goforth, A. M., Aqueous red-emitting silicon nanoparticles for cellular imaging: Consequences of protecting against surface passivation by hydroxide and water for stable red emission. *Journal of Materials Research* **2013,** 28, (2), 216-230.

2. Baxter, J. B.; Aydil, E. S., Nanowire-based dye-sensitized solar cells. *Appl. Phys. Lett.* **2005,** 86, (5), 053114.

3. Plass, R.; Pelet, S.; Krueger, J.; Gratzel, M.; Bach, U., Quantum dot sensitization of organic-inorganic hybrid solar cells. *J. Phys. Chem. B* **2002,** 106, (31), 7578-7580.

4. Gao, X. H.; Cui, Y. Y.; Levenson, R. M.; Chung, L. W. K.; Nie, S. M., In vivo cancer targeting and imaging with semiconductor quantum dots. *Nat. Biotechnol.* **2004,** 22, (8), 969-976.

5. Park, J. H.; Gu, L.; von Maltzahn, G.; Ruoslahti, E.; Bhatia, S. N.; Sailor, M. J., Biodegradable luminescent porous silicon nanoparticles for in vivo applications. *Nature Materials* **2009,** 8, (4), 331-336.

6. Canham, L. T., Silicon quantum wire array fabrication by electrochemical and chemical dissolution of wafers. *Appl. Phys. Lett.* **1990,** 57, (10), 1046-1048.

7. Alivisatos, A. P., Perspectives on the physical chemistry of semiconductor nanocrystals. *J. Phys. Chem.* **1996,** 100, (31), 13226-13239.

8. Belyakov, V. A.; Burdov, V. A.; Lockwood, R.; Meldrum, A., Silicon Nanocrystals: Fundamental Theory and Implications for Stimulated Emission. *Advances in Optical Technologies* **2008,** Article ID 279502, 1-32.

9. Green, M. A.; Zhao, J. H.; Wang, A. H.; Reece, P. J.; Gal, M., Efficient silicon light-emitting diodes. *Nature* **2001,** 412, (6849), 805-808.

10. Torres-Costa, V.; Martin-Palma, R. J.; Martinez-Duart, J. M., All-silicon color-sensitive photodetectors in the visible. *Materials Science & Engineering C-Biomimetic and Supramolecular Systems* **2007,** 27, (5-8), 954-956.

11. Walters, R. J.; Bourianoff, G. I.; Atwater, H. A., Field-effect electroluminescence in silicon nanocrystals. *Nature Materials* **2005,** 4, (2), 143-146.

12. Derfus, A. M.; Chan, W. C. W.; Bhatia, S. N., Probing the cytotoxicity of semiconductor quantum dots. *Nano Lett.* **2004,** 4, (1), 11-18.

13. Erogbogbo, F.; Yong, K.-T.; Roy, I.; Hu, R.; Law, W.-C.; Zhao, W.; Ding, H.; Wu, F.; Kumar, R.; Swihart, M. T.; Prasad, P. N., In vivo targeted cancer imaging, sentinel lymph node mapping and multi-channel imaging with biocompatible silicon nanocrystals. *ACS Nano* **2011,** 5, (1), 413-423.

14. Manhat, B. A.; Brown, A. L.; Black, L. A.; Ross, J. B. A.; Fichter, K.; Vu, T.; Richman, E.; Goforth, A. M., One-Step Melt Synthesis of Water-Soluble,

Photoluminescent, Surface-Oxidized Silicon Nanoparticles for Cellular Imaging Applications. *Chem. Mater.* **2011,** 23, (9), 2407-2418.

15. Rosso-Vasic, M.; Spruijt, E.; Popovic, Z.; Overgaag, K.; van Lagen, B.; Grandidier, B.; Vanmaekelbergh, D.; Dominguez-Gutierrez, D.; De Cola, L.; Zuilhof, H., Amine-terminated silicon nanoparticles: synthesis, optical properties and their use in bioimaging. *J. Mater. Chem.* **2009,** 19, (33), 5926-5933.

16. Shiohara, A.; Hanada, S.; Prabakar, S.; Fujioka, K.; Lim, T. H.; Yamamoto, K.; Northcote, P. T.; Tilley, R. D., Chemical Reactions on Surface Molecules Attached to Silicon Quantum Dots. *J. Am. Chem. Soc.* **2010,** 132, (1), 248-253.

17. Warner, J. H.; Rubinsztein-Dunlop, H.; Tilley, R. D., Surface morphology dependent photoluminescence from colloidal silicon nanocrystals. *J. Phys. Chem. B* **2005,** 109, (41), 19064-19067.

18. Buriak, J. M., Organometallic chemistry on silicon surfaces: formation of functional monolayers bound through Si-C bonds. *Chem. Commun.* **1999**, (12), 1051-1060.

19. Aldana, J.; Wang, Y. A.; Peng, X. G., Photochemical instability of CdSe nanocrystals coated by hydrophilic thiols. *J. Am. Chem. Soc.* **2001,** 123, (36), 8844-8850.

20. Canham, L. T., Bioactive silicon structure fabrication through nanoetching techniques. *Adv. Mater.* **1995,** 7, (12), 1033-&.

21. Popplewell, J. F.; King, S. J.; Day, J. P.; Ackrill, P.; Fifield, L. K.; Cresswell, R. G.; Di Tada, M. L.; Liu, K., Kinetics of uptake and elimination of silicic acid by a human subject: A novel application of Si-32 and accelerator mass spectrometry. *J. Inorg. Biochem.* **1998,** 69, (3), 177-180.

22. He, Y.; Kang, Z. H.; Li, Q. S.; Tsang, C. H. A.; Fan, C. H.; Lee, S. T., Ultrastable, Highly Fluorescent, and Water-Dispersed Silicon-Based Nanospheres as Cellular Probes. *Angewandte Chemie-International Edition* **2009,** 48, (1), 128-132.

23. Hessel, C. M.; Henderson, E. J.; Kelly, J. A.; Cavell, R. G.; Sham, T. K.; Veinot, J. G. C., Origin of luminescence from silicon nanocrystals: a near edge X-ray absorption fine structure (NEXAFS) and X-ray excited optical luminescence (XEOL) study of oxide-embedded and free-standing systems. *Journal of Physical Chemistry C* **2008,** 112, (37), 14247-14254.

24. Bley, R. A.; Kauzlarich, S. M.; Davis, J. E.; Lee, H. W. H., Characterization of silicon nanoparticles prepared from porous silicon. *Chem. Mater.* **1996,** 8, (8), 1881-1888.

25. Tamura, H.; Ruckschloss, M.; Wirschem, T.; Veprek, S., Origin of the green-blue luminescence from nanocrystalline silicon. *Appl. Phys. Lett.* **1994,** 65, (12), 1537-1539.

26. Kanemitsu, Y., Luminescence Properties of Nanometer-sized Si Crystallites-Core and Surface-States. *Physical Review B* **1994,** 49, (23), 16845-16848.

27. Godefroo, S.; Hayne, M.; Jivanescu, M.; Stesmans, A.; Zacharias, M.; Lebedev, O. I.; Van Tendeloo, G.; Moshchalkov, V. V., Classification and control of the origin of photoluminescence from Si nanocrystals. *Nature Nanotechnology* **2008,** 3, (3), 174-178.

28. Yang, S.; Li, W.; Cao, B.; Zeng, H.; Cai, W., Origin of Blue Emission from Silicon Nanoparticles: Direct Transition and Interface Recombination. *Journal of Physical Chemistry C* **2011,** 115, (43), 21056-21062.

29. de Boer, W.; Timmerman, D.; Dohnalova, K.; Yassievich, I. N.; Zhang, H.; Buma, W. J.; Gregorkiewicz, T., Red spectral shift and enhanced quantum efficiency in phonon-free photoluminescence from silicon nanocrystals. *Nature Nanotechnology* **2010,** 5, (12), 878-884.

30. Vincent, J.; Maurice, V.; Paquez, X.; Sublemontier, O.; Leconte, Y.; Guillois, O.; Reynaud, C.; Herlin-Boime, N.; Raccurt, O.; Tardif, F., Effect of water and UV passivation on the luminescence of suspensions of silicon quantum dots. *J. Nanopart. Res.* **2010,** 12, (1), 39-46.

31. Coxon, P. R.; Wang, Q.; Chao, Y., An abrupt switch between the two photoluminescence bands within alkylated silicon nanocrystals. *Journal of Applied Physics D: Applied Physics* **2011,** 44, 495301.

32. Chao, Y.; Houlton, A.; Horrocks, B. R.; Hunt, M. R. C.; Poolton, N. R. J.; Yang, J.; Siller, L., Optical luminescence from alkyl-passivated Si nanocrystals under vacuum ultraviolet excitation: Origin and temperature dependence of the blue and orange emissions. *Appl. Phys. Lett.* **2006,** 88, (26), 263119.

33. Zhou, Z. Y.; Brus, L.; Friesner, R., Electronic structure and luminescence of 1.1- and 1.4-nm silicon nanocrystals: Oxide shell versus hydrogen passivation. *Nano Lett.* **2003,** 3, (2), 163-167.

34. Wang, X.; Zhang, R. Q.; Niehaus, T. A.; Frauenheim, T., Excited state properties of allylamine-capped silicon quantum dots. *Journal of Physical Chemistry C* **2007,** 111, (6), 2394-2400.

35. Liu, S. M., Luminescent silicon nanoparticles formed in solution. *Journal of Nanoscience and Nanotechnology* **2008,** 8, (3), 1110-1125.

36. Rosso-Vasic, M.; Spruijt, E.; van Lagen, B.; De Cola, L.; Zuilhof, H., Alkyl-Functionalized Oxide-Free Silicon Nanoparticles: Synthesis and Optical Properties. *Small* **2008,** 4, (10), 1835-1841.

37. Holmes, J. D.; Ziegler, K. J.; Doty, R. C.; Pell, L. E.; Johnston, K. P.; Korgel, B. A., Highly luminescent silicon nanocrystals with discrete optical transitions. *J. Am. Chem. Soc.* **2001,** 123, (16), 3743-3748.

38. Mangolini, L.; Jurbergs, D.; Rogojina, E.; Kortshagen, U., High efficiency photoluminescence from silicon nanocrystals prepared by plasma synthesis and organic surface passivation. *Phys. Status Solidi C* **2006,** 3, 3975-3978.

39. Jurbergs, D.; Rogojina, E.; Mangolini, L.; Kortshagen, U., Silicon nanocrystals with ensemble quantum yields exceeding 60%. *Appl. Phys. Lett.* **2006,** 88, (23), 233116

40. Kang, Z. H.; Liu, Y.; Tsang, C. H. A.; Ma, D. D. D.; Fan, X.; Wong, N. B.; Lee, S. T., Water-Soluble Silicon Quantum Dots with Wavelength-Tunable Photoluminescence. *Adv. Mater.* **2009,** 21, (6), 661-+.

41. Hessel, C. M.; Henderson, E. J.; Veinot, J. G. C., Hydrogen silsesquioxane: A molecular precursor for nanocrystalline Si-SiO2 composites and freestanding hydride-surface-terminated silicon nanoparticles. *Chem. Mater.* **2006,** 18, (26), 6139-6146.

42. Gupta, A.; Swihart, M. T.; Wiggers, H., Luminescent Colloidal Dispersion of Silicon Quantum Dots from Microwave Plasma Synthesis: Exploring the Photoluminescence Behavior Across the Visible Spectrum. *Adv. Funct. Mater.* **2009,** 19, (5), 696-703.

43. English, D. S.; Pell, L. E.; Yu, Z. H.; Barbara, P. F.; Korgel, B. A., Size tunable visible luminescence from individual organic monolayer stabilized silicon nanocrystal quantum dots. *Nano Lett.* **2002,** 2, (7), 681-685.

44. Hessel, C. M.; Reid, D.; Panthani, M. G.; Rasch, M. R.; Goodfellow, B. W.; Wei, J.; Fujii, H.; Akhavan, V.; Korgel, B. A., Synthesis of ligand-stabilized silicon nanocrystals with size-dependent photoluminescence spanning visible to near-infrared wavelengths. *Chem. Mater.* **2012,** 24, (2), 393-401.

45. Li, X. G.; He, Y. Q.; Talukdar, S. S.; Swihart, M. T., Process for preparing macroscopic quantities of brightly photoluminescent silicon nanoparticles with emission spanning the visible spectrum. *Langmuir* **2003,** 19, (20), 8490-8496.

46. Zhang, X. M.; Neiner, D.; Wang, S. Z.; Louie, A. Y.; Kauzlarich, S. M., A new solution route to hydrogen-terminated silicon nanoparticles: synthesis, functionalization and water stability. *Nanotechnology* **2007,** 18, (9), 095601.

47. Tilley, R. D.; Yamamoto, K., The microemulsion synthesis of hydrophobic and hydrophilic silicon nanocrystals. *Adv. Mater.* **2006,** 18, 2053-2056.

48. Lin, S. W.; Chen, D. H., Synthesis of Water-Soluble Blue Photoluminescent Silicon Nanocrystals with Oxide Surface Passivation. *Small* **2009,** 5, (1), 72-76.

49. Brewer, A.; Von Haeften, K., In-situ passivation and blue luminescence of silicon clusters using a cluster-beam/H2O co-deposition production method. *Appl. Phys. Lett.* **2009,** 94, 261102.

50. Tilley, R. D.; Warner, J. H.; Yamamoto, K.; Matsui, I.; Fujimori, H., Micro-emulsion synthesis of monodisperse surface stabilized silicon nanocrystals. *Chem. Commun.* **2005**, (14), 1833-1835.

51. Wilcoxon, J. P.; Samara, G. A.; Provencio, P. N., Optical and electronic properties of Si nanoclusters synthesized in inverse micelles. *Physical Review B* **1999,** 60, (4), 2704-2714.

52. Allan, G.; Delerue, C.; Lannoo, M., On the nature of luminescent surface states of semiconductor nanocrystallites. *Phys. Rev. Lett.* **1996,** 76, 2961.

53. Ray, M.; Sarkar, S.; Bandyopadhyay, N. R.; Hossain, S. M.; Pramanick, A. K., Silicon and silicon oxide core-shell nanoparticles: structural and photoluminescence characteristics. *J. Appl. Phys.* **2009,** 105, 074301.

54. Qin, G. G.; Song, H. Z.; Zhang, B. R.; Lin, J.; Duan, J. Q.; Yao, G. Q., Experimental evidence for luminescence from silicon oxide layers in oxidized porous silicon. *Physical Review B* **1996,** 54, (4), 2548-2555.

55. Li, Z. F.; Ruckenstein, E., Water-soluble poly(acrylic acid) grafted luminescent silicon nanoparticles and their use as fluorescent biological staining labels. *Nano Lett.* **2004,** 4, (8), 1463-1467.

56. Kravitz, K.; Kamyshny, A.; Gedanken, A.; Magdassi, S., Solid state synthesis of water-dispersible silicon nanoparticles from silica nanoparticles. *J. Solid State Chem.* **2010,** 183, (6), 1442-1447.

57. Henderson, E. J.; Kelly, J. A.; Veinot, J. C. G., Influence of HSiO1.5 Sol-Gel Polymer Structure and Composition on the Size and Luminescent Properties of Silicon Nanocrystals. *Chem. Mater.* **2009,** 21, 5426-5434.

58. *Operation Manual for Quanta-Phi Rev. C*; April 23, 2010.

59. Porres, L.; Holland, A.; Palsson, L.; Monkman, A. P.; Kemp, C.; Beeby, A., Absolute measurements of photoluminescence quantum yields of solutions using an integrating sphere. *J. Fluorescence* **2006,** 16, (2), 267-273.

60. NIH *Image J*, http://rsbweb.nih.gov/ij/.

61. Hessel, C.; Henderson, E. J.; Veinot, J. C. G., An investigation of the formation and growth of oxide-embedded silicon nanocrystals in hydrogen silsesquioxane-derived nanocomposites. *J. Phys. Chem. C* **2007,** 111, 6956-6961.

62. Veinot, J. C. G., Sol-gel precursors for Group 14 nanocrystals. *Chem. Commun.* **2010,** 46, 8404.

63. Higashi, G. S.; Chabal, Y. J.; Trucks, G. W.; Raghavachari, K., Ideal hydrogen termination of the Si(111) surface. *Appl. Phys. Lett.* **1990,** 56, (7), 656-658.

64. Michalak, D. J.; Amy, S. R.; Aureau, D.; Dai, M.; Esteve, A.; Chabal, Y. J., Nanopatterning Si(III) surfaces as selective surface-chemistry route. *Nature Materials* **2010,** 9, 266.

65. Pasternack, R. M.; Amy, S. R.; Chabal, Y. J., Attachment of 3-(Aminopropyl)triethoxysilane on silicon oxide surfaces: dependence on solution temperature. *Langmuir* **2008,** 24, 12963-12971.

66. Thissen, P.; Peixoto, T.; Longo, R. C.; Peng, W. G.; Cho, K.; Chabal, Y. J., Activation of Surface Hydroxyl Groups by Modification of H-Terminated Si(111) Surfaces. *J. Am. Chem. Soc.* **2012,** 134, 8869-8874.

67. Mazumder, S.; Dey, R.; Mitra, M. K.; Mukherjee, S.; Das, G. C., Review: Biofunctionalized Quantum Dots in Biology and Medicine. *Journal of Nanomaterials* **2009**.

68. Erogbogbo, F.; Yong, K. T.; Roy, I.; Xu, G. X.; Prasad, P. N.; Swihart, M. T., Biocompatible luminescent silicon quantum dots for imaging of cancer cells. *Acs Nano* **2008,** 2, (5), 873-878.

69. Shirahata, N.; Linford, M. R.; Furumi, S.; Pei, L.; Sakka, Y.; Gates, R. J.; Asplund, M. C., Laser-derived one-pot synthesis of silicon nanocrystals terminated with organic monolayers. *Chem. Commun.* **2009**, (31), 4684-4686..

70. Liu, J.; Du, X., pH- and competitor-driven nanovalves of cucurbit[7]uril pseudorotaxanes based on mesoporous silica supports for controlled release. *J. Mater. Chem.* **2010,** 20, 3642-3649.

**Reference from Chapter 3**

1. Eberl, K.; Lipinski, M. O.; Manz, Y. M.; Winter, W.; Jin-Phillipp, N. Y.; Schmidt, O. G., Self-assembling quantum dots for optoelectronic devices on Si and GaAs. *Physica E* **2001,** 9, (1), 164-174.

2. Das, A.; Han, Z. J.; Haghighi, M. G.; Eisenberg, R., Photogeneration of hydrogen from water using CdSe nanocrystals demonstrating the importance of surface exchange. *Proceedings of the National Academy of Sciences of the United States of America* **2013,** 110, (42), 16716-16723.

3. Choi, J.; Wang, N. S.; Reipa, V., Conjugation of the photoluminescent silicon nanoparticles to streptavidin. *Bioconjugate Chemistry* **2008,** 19, (3), 680-685.

4. Li, Z. F.; Ruckenstein, E., Water-soluble poly(acrylic acid) grafted luminescent silicon nanoparticles and their use as fluorescent biological staining labels. *Nano Letters* **2004,** 4, (8), 1463-1467.

5. Park, J. H.; Gu, L.; von Maltzahn, G.; Ruoslahti, E.; Bhatia, S. N.; Sailor, M. J., Biodegradable luminescent porous silicon nanoparticles for *in vivo* applications. *Nature Materials* **2009,** 8, (4), 331-336.

6. Mazumder, S.; Dey, R.; Mitra, M. K.; Mukherjee, S.; Das, G. C., Review: Biofunctionalized quantum dots in biology and medicine. *Journal of Nanomaterials* **2009**, 1-9

7. Dabbousi, B. O.; RodriguezViejo, J.; Mikulec, F. V.; Heine, J. R.; Mattoussi, H.; Ober, R.; Jensen, K. F.; Bawendi, M. G., (CdSe)ZnS core-shell quantum dots: Synthesis and characterization of a size series of highly luminescent nanocrystallites. *Journal of Physical Chemistry B* **1997,** 101, (46), 9463-9475.

8. Norris, D. J.; Bawendi, M. G., Measurement and assignment of the size-dependent optical spectrum in CdSe quantum dots. *Physical Review B* **1996,** 53, (24), 16338-16346.

9. Resch-Genger, U.; Grabolle, M.; Cavaliere-Jaricot, S.; Nitschke, R.; Nann, T., Quantum dots versus organic dyes as fluorescent labels. *Nature Methods* **2008,** 5, (9), 763-775.

10. Anas, A.; Akita, H.; Harashima, H.; Itoh, T.; Ishikawa, M.; Biju, V., Photosensitized breakage and damage of DNA by CdSe-ZnS quantum dots. *Journal of Physical Chemistry B* **2008,** 112, (32), 10005-10011.

11. Derfus, A. M.; Chan, W. C. W.; Bhatia, S. N., Probing the cytotoxicity of semiconductor quantum dots. *Nano Letters* **2004,** 4, (1), 11-18.

12. Bouldin, J. L.; Ingle, T. M.; Sengupta, A.; Alexander, R.; Hannigan, R. E.; Buchanan, R. A., Aqueous toxicity and food chain transfer of quantum dots (TM) in freshwater algae and ceriodaphnia dubia. *Environmental Toxicology and Chemistry* **2008,** 27, (9), 1958-1963.

13. Tsay, J. M.; Michalet, X., New light on quantum dot cytotoxicity. *Chemistry & Biology* **2005,** 12, (11), 1159-1161.

14. Cheng, X. Y.; Lowe, S. B.; Reece, P. J.; Gooding, J. J., Colloidal silicon quantum dots: from preparation to the modification of self-assembled monolayers (SAMs) for bio-applications. *Chemical Society Reviews* **2014,** 43, (8), 2680-2700.

15. Cullis, A. G.; Canham, L. T., Visible-light emission due to quantum size effects in highly porous crystalline silicon. *Nature* **1991,** 353, (6342), 335-338.

16. Canham, L. T., Silicon quantum wire array fabrication by electrochemical and chemical dissolution of wafers. *Applied Physics Letters* **1990,** 57, (10), 1046.

17. Ledoux, G.; Gong, J.; Huisken, F.; Guillois, O.; Reynaud, C., Photoluminescence of size-separated silicon nanocrystals: Confirmation of quantum confinement. *Applied Physics Letters* **2002,** 80, (25), 4834-4836.

18. Henderson, E. J.; Kelly, J. A.; Veinot, J. G. C., Influence of $HSiO_{1.5}$ sol-gel polymer structure and composition on the size and luminescent properties of silicon Nanocrystals. *Chemistry of Materials* **2009,** 21, (22), 5426-5434.

19. Hessel, C. M.; Henderson, E. J.; Veinot, J. G. C., Hydrogen silsesquioxane: A molecular precursor for nanocrystalline Si-$SiO_2$ composites and freestanding hydride-surface-terminated silicon nanoparticles. *Chemistry of Materials* **2006,** 18, (26), 6139-6146.

20. Hua, F. J.; Swihart, M. T.; Ruckenstein, E., Efficient surface grafting of luminescent silicon quantum dots by photoinitiated hydrosilylation. *Langmuir* **2005,** 21, (13), 6054-6062.

21. Gupta, A.; Swihart, M. T.; Wiggers, H., Luminescent colloidal dispersion of silicon quantum dots from microwave plasma synthesis: Exploring the photoluminescence behavior across the visible spectrum. *Advanced Functional Materials* **2009,** 19, (5), 696-703.

22. Hessel, C. M.; Reid, D.; Panthani, M. G.; Rasch, M. R.; Goodfellow, B. W.; Wei, J. W.; Fujii, H.; Akhavan, V.; Korgel, B. A., Synthesis of ligand-stabilized silicon nanocrystals with size-dependent photoluminescence spanning visible to near-infrared wavelengths. *Chemistry of Materials* **2012,** 24, (2), 393-401.

23. Wolf, O.; Dasog, M.; Yang, Z.; Balberg, I.; Veinot, J. G. C.; Millo, O., Doping and quantum confinement effects in single Si nanocrystals observed by scanning tunneling spectroscopy. *Nano Letters* **2013,** 13, (6), 2516-2521.

24. Holmes, J. D.; Ziegler, K. J.; Doty, R. C.; Pell, L. E.; Johnston, K. P.; Korgel, B. A., Highly luminescent silicon nanocrystals with discrete optical transitions. *Journal of the American Chemical Society* **2001,** 123, (16), 3743-3748.

25. Shen, P.; Uesawa, N.; Inasawa, S.; Yamaguchi, Y., Stable and color-tunable fluorescence from silicon nanoparticles formed by single-step plasma assisted decomposition of SiBr4. *Journal of Materials Chemistry* **2010,** 20, (9), 1669-1675.

26. Manhat, B. A.; Brown, A. L.; Black, L. A.; Ross, J. B.; Fichter, K.; Vu, T.; Richman, E.; Goforth, A. M., One-step melt synthesis of water soluble, photoluminescent, surface-oxidized silicon sanoparticles for cellular imaging applications. *Chemestry of Materials* **2011,** 23, (9), 2407-2418.

27. Dasog, M.; Veinot, J. G. C., Size independent blue luminescence in nitrogen passivated silicon nanocrystals. *Physica Status Solidi A - Applications and Materials Science* **2012,** 209, (10), 1844-1846.

28. Yang, S. K.; Li, W. Z.; Cao, B. Q.; Zeng, H. B.; Cai, W. P., Origin of blue emission from silicon nanoparticles: Direct transition and interface recombination. *Journal of Physical Chemistry C* **2011,** 115, (43), 21056-21062.

29. Dasog, M.; Yang, Z. Y.; Regli, S.; Atkins, T. M.; Faramus, A.; Singh, M. P.; Muthuswamy, E.; Kauzlarich, S. M.; Tilley, R. D.; Veinot, J. G. C., Chemical insight into the origin of red and blue photoluminescence arising from freestanding silicon nanocrystals. *ACS Nano* **2013,** 7, (3), 2676-2685.

30. Qin, G. G.; Song, H. Z.; Zhang, B. R.; Lin, J.; Duan, J. Q.; Yao, G. Q., Experimental evidence for luminescence from silicon oxide layers in oxidized porous silicon. *Physical Review B* **1996,** 54, (4), 2548-2555.

31. Trukhin, A. N.; Goldberg, M.; Jansons, J.; Fitting, H. J.; Tale, I. A., Silicon dioxide thin film luminescence in comparison with bulk silica. *Journal of Non-Crystalline Solids* **1998,** 223, (1-2), 114-122.

32. Shluger, A.; Stefanovich, E., Models of the self-trapped exciton and nearest-neighbor defect pair in $SiO_2$. *Physical Review B* **1990,** 42, (15), 9664-9673.

33. Godefroo, S.; Hayne, M.; Jivanescu, M.; Stesmans, A.; Zacharias, M.; Lebedev, O. I.; Van Tendeloo, G.; Moshchalkov, V. V., Classification and control of the origin of photoluminescence from Si nanocrystals. *Nature Nanotechnology* **2008,** 3, (3), 174-178.

34. de Boer, W.; Timmerman, D.; Dohnalova, K.; Yassievich, I. N.; Zhang, H.; Buma, W. J.; Gregorkiewicz, T., Red spectral shift and enhanced quantum efficiency in phonon-free photoluminescence from silicon nanocrystals. *Nature Nanotechnology* **2010,** 5, (12), 878-884.

35. Dohnalova, K.; Poddubny, A. N.; Prokofiev, A. A.; de Boer, W.; Umesh, C. P.; Paulusse, J. M. J.; Zuilhof, H.; Gregorkiewicz, T., Surface brightens up Si quantum dots: Direct bandgap-like size-tunable emission. *Light - Science & Applications* **2013**, 2, 1-6.

36. Kanemitsu, Y., Luminescence properties of nanometer-sized Si crystallites: Core and surface states. *Physical Review B* **1994,** 49, (23), 16845-16848.

37. Mariotti, D.; Mitra, S.; Svrcek, V., Surface-engineered silicon nanocrystals. *Nanoscale* **2013,** 5, (4), 1385-1398.

38. Liu, S. M., Luminescent silicon nanoparticles formed in solution. *Journal of Nanoscience and Nanotechnology* **2008,** 8, (3), 1110-1125.

39. Cooke, D. W.; Bennett, B. L.; Farnum, E. H.; Hults, W. L.; Sickafus, K. E.; Smith, J. F.; Smith, J. L.; Taylor, T. N.; Tiwari, P.; Portis, A. M., SiOx luminescence from light-emitting porous silicon: Support for the quantum confinement luminescence center model. *Applied Physics Letters* **1996,** 68, (12), 1663-1665.

40. Germanenko, I. N.; Li, S. T.; El-Shall, M. S., Decay dynamics and quenching of photoluminescence from silicon nanocrystals by aromatic nitro compounds. *Journal of Physical Chemistry B* **2001,** 105, (1), 59-66.

41. Sweryda-Krawiec, B.; Cassagneau, T.; Fendler, J. H., Surface modification of silicon nanocrystallites by alcohols. *Journal of Physical Chemistry B* **1999,** 103, (44), 9524-9529.

42. Rehm, J. M.; McLendon, G. L.; Tsybeskov, L.; Fauchet, P. M., How methanol affects the surface of blue and red emitting porous silicon. *Applied Physics Letters* **1995,** 66, (26), 3669-3671.

43. Sweryda-Krawiec, B.; Chandler-Henderson, R. R.; Coffer, J. L.; Rho, Y. G.; Pinizzotto, R. F., A comparison of porous silicon and silicon nanocrystallite photoluminescence quenching with amines. *Journal of Physical Chemistry* **1996,** 100, (32), 13776-13780.

44. Bradley, D.; Williams, G.; Lawton, M., Drying of organic solvents: Quantitative evaluation of the efficiency of several desiccants. *Journal of Organic Chemistry* **2010,** 75, (24), 8351-8354.

45. Chiu, S. K.; Manhat, B. A.; DeBenedetti, W. J. I.; Brown, A. L.; Fichter, K.; Vu, T.; Eastman, M.; Jiao, J.; Goforth, A. M., Aqueous red-emitting silicon nanoparticles for cellular imaging: Consequences of protecting against surface passivation by hydroxide and water for stable red emission. *Journal of Materials Research* **2013,** 28, (2), 216-230.

46. Buriak, J. M., Organometallic chemistry on silicon and germanium surfaces. *Chemical Reviews* **2002,** 102, (5), 1271-1308.

47. Satter, K., *Handbook of Thin Films Materials*. Nanomaterials and magnetic thin films, Academic Press ed., San Diego, USA, 2003.

48. Zhang, X. M.; Neiner, D.; Wang, S. Z.; Louie, A. Y.; Kauzlarich, S. M., A new solution route to hydrogen-terminated silicon nanoparticles: synthesis, functionalization and water stability. *Nanotechnology* **2007,** 18, (9), 1-6.

49. Heintz, A. S.; Fink, M. J.; Mitchell, B. S., Mechanochemical synthesis of blue luminescent alkyl/alkenyl-passivated silicon nanoparticles. *Advanced Materials* **2007,** 19, (22), 3984-3988.

50. Pettigrew, K. A.; Liu, Q.; Power, P. P.; Kauzlarich, S. M., Solution synthesis of alkyl- and alkyl/alkoxy-capped silicon nanoparticles *via* oxidation of $Mg_2Si$. *Chemistry of Materials* **2003,** 15, (21), 4005-4011.

51. Shiohara, A.; Hanada, S.; Prabakar, S.; Fujioka, K.; Lim, T. H.; Yamamoto, K.; Northcote, P. T.; Tilley, R. D., Chemical reactions on surface molecules attached to silicon quantum dots. *Journal of the American Chemical Society* **2010,** 132, (1), 248-253.

52. Warner, J. H.; Hoshino, A.; Yamamoto, K.; Tilley, R. D., Water-soluble photoluminescent silicon quantum dots. *Angewandte Chemie* **2005,** 117, (29), 4626-4630.

53. van Buuren, T.; Dinh, L. N.; Chase, L. L.; Siekhaus, W. J.; Terminello, L. J., Changes in the electronic properties of Si nanocrystals as a function of particle size. *Physical Review Letters* **1998,** 80, (17), 3803-3806.

54. Trwoga, P. F.; Kenyon, A. J.; Pitt, C. W., Modeling the contribution of quantum confinement to luminescence from silicon nanoclusters. *Journal of Applied Physics* **1998,** 83, (7), 3789-3794.

55. Barbagiovanni, E. G.; Lockwood, D. J.; Simpson, P. J.; Goncharova, L. V., Quantum confinement in Si and Ge nanostructures. *Journal of Applied Physics* **2012,** 111, 034307.

56. Pasternack, R. M.; Amy, S. R.; Chabal, Y. J., Attachment of 3-(aminopropyl)triethoxysilane on silicon oxide surfaces: Dependence on solution temperature. *Langmuir* **2008,** 24, (22), 12963-12971.

57. Michalak, D. J.; Amy, S. R.; Aureau, D.; Dai, M.; Esteve, A.; Chabal, Y. J., Nanopatterning Si(111) surfaces as a selective surface-chemistry route. *Nature Materials* **2010,** 9, (3), 266-271.

58. Thissen, P.; Peixoto, T.; Longo, R. C.; Peng, W. N.; Schmidt, W. G.; Cho, K. J.; Chabal, Y. J., Activation of surface hydroxyl groups by modification of H-terminated Si(111) surfaces. *Journal of the American Chemical Society* **2012,** 134, (21), 8869-8874.

59. Kusova, K.; Cibulka, O.; Dohnalova, K.; Pelant, I.; Valenta, J.; Fucikova, A.; Zidek, K.; Lang, J.; Englich, J.; Matejka, P.; Stepanek, P.; Bakardjieva, S., Brightly luminescent organically capped silicon nanocrystals fabricated at room temperature and atmospheric pressure. *ACS Nano* **2010,** 4, (8), 4495-4504.

60. Yang, Z. Y.; Iqbal, M.; Dobbie, A. R.; Veinot, J. G. C., Surface-induced alkene oligomerization: Does thermal hydrosilylation really lead to monolayer protected silicon nanocrystals? *Journal of the American Chemical Society* **2013,** 135, (46), 17595-17601.

61. Huber, K. P.; Herzberg, G., *Molecular Spectra and Molecular Structure Constants of Diatomic Molecules*. Van Nostand: New York, 1979.

62. Chatillon, C.; Allibert, M.; Pattoret, A., High-temperature knudsen cell mass-spectrometry-atomization energies determination of $Si_2$, $Si_3$, $Al_2$, AlSi, and $AlSi_2$ molecules. *Comptes Rendus Hebdomadaires Des Seances De L Academie Des Sciences Serie C* **1975,** 280, (25), 1505-1508.

63. Verhaegen, G.; Stafford, F. E.; Drowart, J., Mass spectromeric study of systems boron-carbon/ boron-carbon-silicon. *Physics* **1964,** 40, (6), 1622-1628.

64. Pedley, J. B.; Marshall, E. M., Thermochemical data for gaseous monoxides. *Journal of Physical and Chemical Reference Data* **1983,** 12, (4), 967-1031.

65. Luppi, E.; Iori, F.; Magri, R.; Pulci, O.; Ossicini, S.; Degoli, E.; Olevano, V., Excitons in silicon nanocrystallites: The nature of luminescence. *Physical Review B* **2007,** 75, 033303.

**Reference from Chapter 4**

1. Henderson, E. J.; Kelly, J. A.; Veinot, J. G. C., Influence of HSiO1.5 Sol-Gel Polymer Structure and Composition on the Size and Luminescent Properties of Silicon Nanocrystals. *Chemistry of Materials* **2009,** 21, (22), 5426-5434.

2. Kusova, K.; Cibulka, O.; Dohnalova, K.; Pelant, I.; Valenta, J.; Fucikova, A.; Zidek, K.; Lang, J.; Englich, J.; Matejka, P.; Stepanek, P.; Bakardjieva, S., Brightly Luminescent Organically Capped Silicon Nanocrystals Fabricated at Room Temperature and Atmospheric Pressure. *Acs Nano* **2010,** 4, (8), 4495-4504.

3. Wheeler, L. M.; Neale, N. R.; Chen, T.; Kortshagen, U. R., Hypervalent surface interactions for colloidal stability and doping of silicon nanocrystals. *Nature Communications* **2013,** 4.

4. Launer, P. J., Infrared analysis of organsilicon compounds: spectra-structure correlations. *Silicone Compounds Register and Review* **1987**, 4.

5. Chang, H.; Sun, S. Q., Silicon nanoparticles: Preparation, properties, and applications. *Chinese Physics B* **2014,** 23, (8).

6. Tsybeskov, L.; Vandyshev, J.; Fauchet, P., Blue emission in porous silicon: Oxygen-related photoluminescence. *Physical Review B* **1994,** 49, (11), 7821-7824.

7. Kanemitsu, Y., LUMINESCENCE PROPERTIES OF NANOMETER-SIZED SI CRYSTALLITES - CORE AND SURFACE-STATES. *Physical Review B* **1994,** 49, (23), 16845-16848.

8. Yang, S. K.; Li, W. Z.; Cao, B. Q.; Zeng, H. B.; Cai, W. P., Origin of Blue Emission from Silicon Nanoparticles: Direct Transition and Interface Recombination. *Journal of Physical Chemistry C* **2011,** 115, (43), 21056-21062.

9. Hessel, C. M.; Henderson, E. J.; Veinot, J. G. C., Hydrogen silsesquioxane: A molecular precursor for nanocrystalline Si-SiO2 composites and freestanding hydride-surface-terminated silicon nanoparticles. *Chemistry of Materials* **2006,** 18, (26), 6139-6146.

10. Wolkin, M. V.; Jorne, J.; Fauchet, P. M.; Allan, G.; Delerue, C., Electronic states and luminescence in porous silicon quantum dots: The role of oxygen. *Physical Review Letters* **1999,** 82, (1), 197-200.

11. Dohnalova, K.; Poddubny, A. N.; Prokofiev, A. A.; de Boer, W.; Umesh, C. P.; Paulusse, J. M. J.; Zuilhof, H.; Gregorkiewicz, T., Surface brightens up Si quantum dots: direct bandgap-like size-tunable emission. *Light-Science & Applications* **2013,** 2.

12. Nunez, J. R. R.; Kelly, J. A.; Henderson, E. J.; Veinot, J. G. C., Wavelength-Controlled Etching of Silicon Nanocrystals. *Chemistry of Materials* **2012,** 24, (2), 346-352.

**Reference from Chapter 5**

1. Canham, L. T., Silicon quantum wire array fabrication by electrochemical and chemical dissolution of wafers. *Applied Physics Letters* **1990,** 57, (10), 1046.

2. Gribov, B. G.; Zinov'ev, K. V., Preparation of high-purity silicon for solar cells. *Inorganic Materials* **2003,** 39, (7), 653-662.

3. Won, C. W.; Nersisyan, H. H.; Won, H. I., Solar-grade silicon powder prepared by combining combustion synthesis with hydrometallurgy. *Solar Energy Materials and Solar Cells* **2011,** 95, (2), 745-750.

4. Park, S.; Cho, E.; Song, D. Y.; Conibeer, G.; Green, M. A., n-Type silicon quantum dots and p-type crystalline silicon heteroface solar cells. *Solar Energy Materials and Solar Cells* **2009,** 93, (6-7), 684-690.

5. Baxter, J. B.; Aydil, E. S., Nanowire-based dye-sensitized solar cells. *Applied Physics Letters* **2005,** 86, (5).

6. Chiu, S. K.; Manhat, B. A.; DeBenedetti, W. J. I.; Brown, A. L.; Fichter, K.; Vu, T.; Eastman, M.; Jiao, J.; Goforth, A. M., Aqueous red-emitting silicon nanoparticles for cellular imaging: Consequences of protecting against surface passivation by hydroxide and water for stable red emission. *Journal of Materials Research* **2013,** 28, (2), 216-230.

7. Yang, C. S.; Bley, R. A.; Kauzlarich, S. M.; Lee, H. W. H.; Delgado, G. R., Synthesis of alkyl-terminated silicon nanoclusters by a solution route. *Journal of the American Chemical Society* **1999,** 121, (22), 5191-5195.

8. Bley, R. A.; Kauzlarich, S. M., A low-temperature solution phase route for the synthesis of silicon nanoclusters. *Journal of the American Chemical Society* **1996,** 118, (49), 12461-12462.

9. Zhang, X. M.; Neiner, D.; Wang, S. Z.; Louie, A. Y.; Kauzlarich, S. M., A new solution route to hydrogen-terminated silicon nanoparticles: synthesis, functionalization and water stability. *Nanotechnology* **2007,** 18, (9).

10. Kirkey, W. D.; Sahoo, Y.; Li, X. G.; He, Y. Q.; Swihart, M. T.; Cartwright, A. N.; Bruckenstein, S.; Prasad, P. N., Quasi-reversible photoluminescence quenching of stable dispersions of silicon nanoparticles. *Journal of Materials Chemistry* **2005,** 15, (20), 2028-2034.

11. Shirahata, N.; Linford, M. R.; Furumi, S.; Pei, L.; Sakka, Y.; Gates, R. J.; Asplund, M. C., Laser-derived one-pot synthesis of silicon nanocrystals terminated with organic monolayers. *Chemical Communications* **2009**, (31), 4684-4686.

12. Li, X. G.; He, Y. Q.; Talukdar, S. S.; Swihart, M. T., Process for preparing macroscopic quantities of brightly photoluminescent silicon nanoparticles with emission spanning the visible spectrum. *Langmuir* **2003,** 19, (20), 8490-8496.

13. Amoruso, S.; Bruzzese, R.; Spinelli, N.; Velotta, R.; Vitiello, M.; Wang, X.; Ausanio, G.; Iannotti, V.; Lanotte, L., Generation of silicon nanoparticles via femtosecond laser ablation in vacuum. *Applied Physics Letters* **2004,** 84, (22), 4502-4504.

14. Dhas, N. A.; Raj, C. P.; Gedanken, A., Preparation of luminescent silicon nanoparticles: A novel sonochemical approach. *Chemistry of Materials* **1998,** 10, (11), 3278-+.

15. Mamiya, M.; Kikuchi, M.; Takei, H., Crystallization of fine silicon particles from silicon monoxide. *Journal of Crystal Growth* **2002,** 237, 1909-1914.

16. Mamiya, M.; Takei, H.; Kikuchi, M.; Uyeda, C., Preparation of fine silicon particles from amorphous silicon monoxide by the disproportionation reaction. *Journal of Crystal Growth* **2001,** 229, (1), 457-461.

17. Srivastava, S. K.; Singh, P. K.; Singh, V. N.; Sood, K. N.; Haranath, D.; Kumar, V., Large-scale synthesis, characterization and photoluminescence properties of amorphous silica nanowires by thermal evaporation of silicon monoxide. *Physica E-Low-Dimensional Systems & Nanostructures* **2009,** 41, (8), 1545-1549.

18. Lee, J. I.; Lee, K. T.; Cho, J.; Kim, J.; Choi, N. S.; Park, S., Chemical-assisted thermal disproportionation of porous silicon monoxide into silicon-based multicomponent systems. *Angewandte Chemie International Edition in English* **2012,** 51, (11), 2767-71.

19. Okutani, T., Utilization of silica in rice hulls as raw materials for silicon semiconductors. *Journal of Metals, Materials and Minerals* **2009,** 19, (2), 51-59.

20. Garcia, A. P.; Sen, D.; Buehler, M. J., Hierarchical silica nanostructures inspired by diatom algae yield superior deformability, toughness, and strength. *Metallurgical and Materials Transactions a-Physical Metallurgy and Materials Science* **2011,** 42A, (13), 3889-3897.

21. Bao, Z. H.; Weatherspoon, M. R.; Shian, S.; Cai, Y.; Graham, P. D.; Allan, S. M.; Ahmad, G.; Dickerson, M. B.; Church, B. C.; Kang, Z. T.; Abernathy, H. W.; Summers, C. J.; Liu, M. L.; Sandhage, K. H., Chemical reduction of three-dimensional silica micro-assemblies into microporous silicon replicas. *Nature* **2007,** 446, (7132), 172-175.

22. Richman, E. K.; Kang, C. B.; Brezesinski, T.; Tolbert, S. H., Ordered mesoporous silicon through magnesium reduction of polymer templated silica thin films. *Nano Letters* **2008,** 8, (9), 3075-3079.

23. Shen, L.; Guo, X.; Fang, X.; Wang, Z.; Chen, L., Magnesiothermically reduced diatomaceous earth as a porous silicon anode material for lithium ion batteries. *Journal of Power Sources* **2012,** 213, 229-232.

24. Bao, Z. H.; Ernst, E. M.; Yoo, S.; Sandhage, K. H., Syntheses of porous self-supporting metal-nanoparticle assemblies with 3D morphologies inherited from biosilica templates (Diatom Frustules). *Advanced Materials* **2009,** 21, (4), 474-478.

25. Norris, D. J., Materials science - Silicon life forms. *Nature* **2007,** 446, (7132), 146-147.

26. Wang, W.; Martin, J. C.; Fan, X.; Han, A.; Luo, Z.; Sun, L., Silica nanoparticles and frameworks from rice husk biomass. *ACS Applied Materials & Interfaces* **2012,** 4, (2), 977-81.

27. Eckhoff, D. A.; Stuart, J. N.; Sutin, J. D. B.; Sweedler, J. V.; Gratton, E., Capillary electrophoresis of ultrasmall carboxylate functionalized silicon nanoparticles. *Journal of Chemical Physics* **2006,** 125, (8).

28. de Boer, W. D. A. M.; Timmerman, D.; Dohnalova, K.; Yassievich, I. N.; Zhang, H.; Buma, W. J.; Gregorkiewicz, T., Red spectral shift and enhanced quantum efficiency in phonon-free photoluminescence from silicon nanocrystals. *Nature Nanotechnology* **2010,** 5, (12), 878-884.

29. Hallmann, S.; Fink, M. J.; Mitchell, B. S., Mechanochemical synthesis of functionalized silicon nanoparticles with terminal chlorine groups. *Journal of Materials Research* **2011,** 26, (8), 1052-1060.

30. Meier, C.; Luttjohann, S.; Kravets, V. G.; Nienhaus, H.; Lorke, A.; Wiaers, H., Raman properties of silicon nanoparticles. *Physica E-Low-Dimensional Systems & Nanostructures* **2006,** 32, (1-2), 155-158.

31. Xie, Z.; Henderson, E. J.; Dag, O.; Wang, W.; Lofgreen, J. E.; Kubel, C.; Scherer, T.; Brodersen, P. M.; Gu, Z. Z.; Ozin, G. A., Periodic mesoporous hydridosilica-synthesis of an "impossible" material and its thermal transformation into brightly photoluminescent periodic mesoporous nanocrystal silicon-silica composite. *Journal of the American Chemical Society* **2011,** 133, (13), 5094-102.

32. Hessel, C. M.; Wei, J.; Reid, D.; Fujii, H.; Downer, M. C.; Korgel, B. A., Raman spectroscopy of oxide-embedded and ligand-stabilized silicon nanocrystals. *Journal of Physical Chemistry Letters* **2012,** 3, (9), 1089-1093.

33. Lewis, L. N.; Schattenmann, F. J.; Jordan, T. M.; Carnahan, J. C.; Flanagan, W. P.; Wroczynski, R. J.; Lemmon, J. P.; Anostario, J. M.; Othon, M. A., Reaction of silicate minerals to form tetramethoxysilane. *Inorganic Chemistry* **2002,** 41, (9), 2608-2615.

34. Wolkin, M. V.; Jorne, J.; Fauchet, P. M.; Allan, G.; Delerue, C., Electronic states and luminescence in porous silicon quantum dots: The role of oxygen. *Physical Review Letters* **1999,** 82, (1), 197-200.

35. Gole, J. L.; Dixon, D. A., Transformation, green to orange-red, of a porous silicon photoluminescent surface in solution. *Journal of Physical Chemistry B* **1998,** 102, (1), 33-39.

36. Kanemitsu, Y., Luminescence properties of nanometer-sized Si crystallites: Core and surface states. *Physical Review B* **1994,** 49, (23), 16845-16848.